THE EFFECTS OF VORTEX GENERATING FINS AND JETS ON THE CROSSFLOW SEPARATION OF A SUBMARINE IN A TURNING MANEUVER

by

Todd G. Wetzel

Thesis Submitted to the Faculty of the

Virginia Polytechnic Institute and State University

in partial fulfillment of the requirements for the degree of

Master of Science

in

Aerospace Engineering

APPROVED:

Dr. R. L. Simpson, Chairman

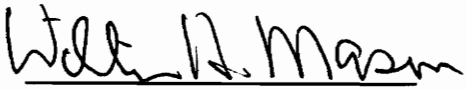

Dr. W. H. Mason

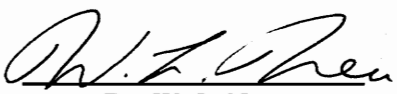

Dr. W. L. Neu

May, 1993

Blacksburg, Virginia

LD
5655
V855
1993
W479
C.2

C.2

Abstract

The effect of fin and jet vortex generators on the crossflow separation of a 688 class submarine in a turning maneuver was studied. The vortex generators are located on the top and bottom centerline of the submarine. The intent of the vortex generators is to improve turning performance by changing the hydrodynamic forces incurred from crossflow separation. Performance of the jets and the fins are compared. Oil flow visualization and force and moment measurements were used as the primary diagnostics in determining the effectiveness of various vortex generator configurations. The fins were found to be very effective in delaying crossflow separation, while the jets were less effective. In addition, the oil flows revealed the importance of locating vortex generators near the bow and the critical role the sail plays in the fluid dynamics near the submarine. Overall, the fins were found to be viable as a concept for flow control, while the jets were less attractive.

Acknowledgments

This work was supported by the National Science Foundation through a Graduate Fellowship and the Defense Advanced Research Projects Agency (Gary W. Jones, Program Manager) through the Office of Naval Research Grant N00014-91-J-1732 (James A. Fein, Program Manager).

We also thank Mr. S. Ha for performing the hot-wire measurements.

Table Of Contents

List Of Figures

List of Tables

Nomenclature

A_j	total jet exit area, parallel to jet direction
AR	rudder aspect ratio
c	submarine chord (length)
C	stability criteria
C^*	stability criteria for submarine with fins
C_D	rudder drag coefficient
C_{D0}	zero-lift rudder drag coefficient
C_l	roll moment coefficient, body axes, L/qc^3
$C_{L\alpha}$	rudder planform lift curve slope
C_m	pitching moment coefficient, body axes, M/qc^3
C_n	yaw moment coefficient, body axes, N/qc^3
C_{nr}	yaw moment - yaw rate derivative
$C_{nr}{}^*$	yaw moment - yaw rate derivative for submarine with fins
C_{nv}	yaw moment - v derivative
$C_{nv}{}^*$	yaw moment - v derivative for submarine with fins
$(C_{nv})_{body}$	body contribution to C_{nv} for naked submarine
$(C_{nv})_{body}{}^*$	body contribution to C_{nv} for submarine with fins
$C_{n\beta}$	yaw moment - sideslip derivative
$C_{n\delta}$	yaw moment - rudder deflection derivative
C_x	axial force coefficient, body axes, X/qc^2
ΔC_x	increase in axial force coefficient due to fins
C_{x0}	base line axial force coefficient
C_y	normal or side force coefficient, body axes, Y/qc^2

C_{yr}	side force - yaw rate derivative
C_{yv}	side force - v derivative
$C_{yv}{}^{*}$	side force - v derivative for submarine with fins
$(C_{yv})_{body}$	body contribution to C_{yv} for naked submarine
$(C_{yv})_{body}{}^{*}$	body contribution to C_{yv} for submarine with fins
$C_{y\beta}$	side force - sideslip derivative
$C_{y\delta}$	side force - rudder deflection derivative
C_z	vertical force coefficient, body axes, Z/qc^2
C_μ	jet momentum coefficient, $(VR)^2(A_j/S_{ref})$
d	submarine diameter
D	jet diameter
D_f	distance between fins
h	height of fins
L	roll moment, body axes
m	submarine mass
$\dot{m}$	jet mass flow rate
$\tilde{m}$	mass parameter, $m/\frac{1}{2}\rho c^3$
M	pitching moment, body axes
n	number of vortex generators
N	yaw moment, body axes
Δp	jet pressure rise
p	free-stream pressure
p_o	fan chamber pressure
q	dynamic pressure, $(1/2)\rho U_\infty{}^2$
r	submarine radius

r'	mean submarine radius
R	gas constant; or
	correlation coefficient
Re	chord Reynolds number, $\rho U_\infty c/\mu$
Re_θ	momentum thickness Reynolds number, $\rho U_\infty \theta/\mu$
R_1	primary reattachment
R_2	secondary reattachment
S_{ref}	reference area
S_1	primary separation
S_2	secondary separation
u	axial velocity, $U_\infty cos\beta$
U_∞	free-stream velocity
U'	non-dimensionalized jet speed parameter, $V_j \Big/ \sqrt{RT_j}$
v	axial velocity, $U_\infty sin\beta$
V	submarine volume
V_j	jet velocity
VR	velocity ratio, V_j/U_∞
$\dot{W}_{cruise}$	cruise power consumption
$\dot{W}_{fins}$	fin power consumption
$\dot{W}_{jets}$	jet power consumption
x	longitudinal distance along submarine from nose
x_{cg}	distance from submarine center of gravity to midships
X	axial force, body axes
Y	normal or side force, body axes
Z	vertical force, body axes

α	rudder local angle of attack
β	sideslip angle, or
	non-dimensionalized jet pressure, p_j/p_0
δ	boundary layer thickness
δ^*	displacement thickness
ε	rudder sidewash angle
ϕ	angular location around cross section measured from windward side
ϕ_i	inclination angle of jet to local surface
ϕ'	mean angular separation line location
γ	specific heat ratio
η	submarine shape factor
κ	linear jet speed/pressure slope
Λ	rudder quarter chord sweep angle
ρ	fluid density
ρ_{H_2O}	density of water
θ	skew angle vortex generators, referenced to model centerline; and
	momentum thickness
θ'	true skew angle of vortex generators, referenced to local flow direction
σ	vortex generator effect factor for C_{nr} (equation 47)
ζ	stability factor (equation 45)

Introduction

Turning maneuvers of submarines result in crossflow separation that generates large hydrodynamic forces and moments that substantially oppose the maneuver. Theoretically, flow control devices could be used to decrease this separation. Pearcey (1961) and Bragg and Gregorek (1987) have shown that strategically placed vortex generators can be used to control flow separation on wings at stall. It is therefore presumed that vortex generators can be used to control the crossflow separation on submarines in turning maneuvers.

Two concepts are pursued here. The first (Figure 1) calls for deployable fins as vortex generators that are free to move in both the amount of penetration into the flow and in the angle of attack to the local flow. The vortex generators should be deployable because the added drag of deployed vortex generators greatly detract from cruise performance. The variable orientation allows adaptation to any particular flow situation encountered. The second concept (Figure 2) involves jets with variable orientation. In either case, the vortex generators are placed along the top and bottom centerlines of the submarine from bow to stern in order to energize the crossflow of the boundary layer and move the crossflow separation further around the leeside of the submarine for either right or left turns.

This report supersedes Wetzel and Simpson (1992a, 1992b, 1993). The only information not contained in this report is some force and moment data from the first series of tests on Model 1, and the complete oil flow documentation from tests on Model 1 (Wetzel and Simpson, 1992a).

Previous Research

Axisymmetric bodies yawed to the freestream flow, like submarines in a turning maneuver, produce large amounts of vortical separation. Bushnell and Donaldson (1990) note that vortical flow affects acoustic and non-acoustic stealth, propulsion efficiency and body drag, control effectiveness, and maneuverability. The focus of this report is on maneuverability.

This separation is dominated by the crossflow component of the flow velocity. Figure 3 shows typical flow structures in such a crossflow separation (Ahn and Simpson, 1992). For circular cylindrical bodies at 15° sideslip, the crossflow usually separates near ϕ = 105° (Poll, 1985).

Bushnell and Donaldson (1990) also note that in the past it has been assumed that these vortical flows are largely insensitive to Reynolds number effects. However, Bushnell and Donaldson identify several aeronautical experiments that document Reynolds number effects for various vortical flows. Ahn and Simpson (1992) have studied the vortical flow on a prolate spheroid at angle of attack, which is similar to the submarine at yaw. In such a case, the primary separation location is largely dependent on the state of the boundary layer (laminar, transitional, or turbulent), which is a function of Reynolds number (Ahn and Simpson, 1992). For high Reynolds number flows or flows with boundary layer transition fixed such that the boundary layer is turbulent at separation, Ahn shows that the separation line dependency on Reynolds number is greatly reduced. The separation line no longer changes much circumferentially, but gradually extends upstream on the body with an increase in Reynolds number (Ahn and Simpson, 1992)

Ahn also studied the effects of angle of attack on the primary separation line. At increasing angle of attack, the separation line moves farther towards the leeside and farther upstream on the body (Ahn and Simpson, 1992).

It is desirable to attempt to reduce the magnitude of this flow separation. One device commonly used to reduce two-dimensional separation is the vortex generator. According to Pearcey (1961), as viscous friction and adverse pressure gradients slow the boundary layer, separation becomes imminent. The role of the vortex created by a vortex generator is to provide a mechanism whereby higher energy fluid outside the boundary layer can swirl with the near-surface, low-velocity fluid in order to re-energize the boundary layer and delay or prevent separation. This idea can be extended to the more complex, three-dimensional, vortical separation experienced by a yawed submarine.

While fins have been studied in detail, their high drag has prompted researchers to look more closely at jets. Compton and Johnston (1992) have concluded that the three-dimensional flow structure of a jet vortex is similar to weak vortices generated by a solid vortex generator, but different from the strong vortices of a large solid generator.

Bushnell and Donaldson (1990) identify several potential problems for these configurations. These include additional drag due to the fins or high energy consumption for the jets; constantly changing flow conditions; and control system complication. With these problems in mind, Bushnell and Donaldson (1990) recommend that a successful vortex generator system would need to be "active, dispersed, rapidly deployable, and triggered by distributed sensors." This configurational concept is compatible with double-hulled submarine design and is assumed in this paper.

Types and Configurations

Solid Vortex Generators

Half-delta wing type vortex generators consist of small plates mounted normal to the local body surface. Other types of vortex generators include ramps, wedges, notches, fences, and riblets (Pearcey, 1961).

Different configurations of the fins will offer different vortical structure and therefore various advantages and disadvantages. Co-rotating vanes produce several vortices that rotate in the same direction. Co-rotating systems offer relative insensitivity to spacing and local flow direction, and the vortical structure is relatively constant in the streamwise direction. These facts make the co-rotating vortex generators easiest to implement successfully. Also, the flow separation off the submarine is vortical in nature, so a unidirectional vortex is most suitable to counteract that separation. Other vortex generator systems include counter-rotating and biplane vortex generators(Pearcey, 1961).

Pneumatic Vortex Generators

Pneumatic vortex generators include blowing and suction slots, and jets. Most of the applications studied thus far have involved control of vortex lift of high performance aircraft (Huffman and Fox, 1978; Malcolm and Skow, 1986; Ng and Malcolm, 1991; Ziegler and Wooler, 1978).

Design and Considerations from Previous Work

Fins

According to Pearcey (1961), the most important consideration in designing a vortex generator system is not the boundary layer profile just upstream of the vortex generator but rather the range and severity of separation that needs to be controlled. Co-rotating vortex generators will dampen the effects of one another if spaced too closely, so Pearcey (1961) suggests that the fin separation (D_f) to height (h) ratio be kept above $D_f/h = 3$. Pearcey (1961) also notes that once above that minimum, vortex generator effectiveness drops off very slowly, so values of D_f/h often fall around 5 or 6.

Pearcey (1961) also stresses the importance of vortex generator uniformity. Non-uniform vortex generators create non-uniform vortices, which can result in "displacement of the vortices normal to the surface and relative to each other."

Another important factor is the local angle of attack, or skew, of the fin. While in 2-D studies the free-stream direction is constant and known, in 3-D flows the free-stream direction can vary and is more difficult to predict with certainty. Therefore, skew angle θ in these studies is referenced from the model centerline, and not from any local flow phenomenon. The true skew, θ', is referenced from an approximate local flow direction on the cylindrical midbody.

Pearcey (1961) points out that the vortices do not travel purely in the streamwise direction, but rather deviate through a curved path by up to 15° from the streamwise flow. This can alter control surface effectiveness aft of the vortex generators.

Often a given amount of separation can be controlled by one row of vortex generators if those generators are made large enough. However, one consequence of vortex

generators is increased drag in any normally unseparated flows, i.e., in the case of straight ahead cruise of the submarine. Larger vortex generators carry a larger drag penalty. Therefore, multiple rows of smaller vortex generators may be more effective than one row of large ones. Unfortunately, multiple rows are difficult to place. According to Pearcey (1961), the generators of the second row must be placed so that the vortices from the first row pass either in between the new vortex generators or over top of them. Otherwise, the new vortices will damp out the original ones and the system as a whole will be less effective than just the single row. The downstream deflection of co-rotating vortices makes multiple row placement even more difficult.

The fins are almost always low aspect-ratio rectangular plates, but more streamlined shapes can help alleviate drag penalties while retaining the original vortical effectiveness. Pearcey (1961) points out that the general goal in optimizing fin shape is to increase the lift-to-drag ratio of the fin, which results in the most vorticity for the least amount of drag. Airfoil shapes and camber may make vortex generators more efficient, but usually the scale involved in the tests is too small to account for such differences.

Vortex generators can make substantial improvements in the aerodynamic characteristics of objects. Bragg and Gregorek (1987) describe the effect of several different vortex generator systems on a laminar flow canard that in certain situations was experiencing premature stall. At the design lift coefficient, vortex generators returned almost all of the lost lift due to early separation, and delta-wing vortex generators were found to have the least drag penalty.

Jets

Vortex jets are simply streams of fluid that flow from a nozzle in the surface at some skew angle to the free stream flow, θ, and some inclination to the surface, ϕ_i (Figure 2). As with the fins, θ is measured relative to the model centerline.

The jet of fluid introduces velocity components normal to the freestream, which results in the formation of a vortex. Pearcey (1961) argues that a system of jets all pointing in the same direction is analogous to a co-rotating system of solid vortex generators. Pearcey thus suggests identical spacing criteria.

Several studies have focused attention on the inclination and skew angles. Lin et. al. (1990) studied two-dimensional separation and found the best inclination angle is between 15° and 25° and the best skew angle is between 60° and 120°. Morin et. al. (1992) used jets to control a three-dimensional separation and found optimal skew angles between 30° and 90°, but found no difference between inclination angles of 45° and 30°. The data of Morin et al (1992) suggests the jets are relatively ineffective.

Perhaps the most controversial and least intuitive parameter studied is the relative strength of the fluid jet. There are several schools of thought when it comes to non-dimensionalizing and scaling the jet strength. The simplest approach studies the velocity ratio of the jet to the freestream:

$$VR = V_j / U_\infty \quad (1)$$

Another approach non-dimensionalizes the jet speed and mass flow with a momentum coefficient, defined as:

$$C_\mu \equiv \dot{m} V_j / q S_{ref} \quad (2)$$

which reduces to

$$C_\mu = (VR)^2 (A_j / S_{ref}) \quad (3),$$

assuming incompressible flow (Lee et. al., 1989). These quantities are important not only for scaling the results from the model to full-size, but have also been used extensively for comparing the effectiveness of different pneumatic flow control devices. Ng and Malcolm (1991) argue that neither of these methods is appropriate. They argue that mass flow requirements are more intuitively correct for comparing and sizing pneumatic vortex generators. Using VR and C_μ as comparators, vortex jets were often found to be substantially less effective than suction slots or blowing slots. But when mass flow rate is used as a comparator, the jets are superior.

Regardless of the method used to non-dimensionalize the jet strength, the literature all concludes that stronger jets are more effective (Compton and Johnston, 1992; Malcolm and Skow, 1986; Lin et. al., 1989; Morin et. al., 1992; Johnston and Nishi, 1990).

Experimental Apparatus

The Wind Tunnel

All tests were performed in the VPI&SU Stability Wind Tunnel. This continuous, closed return, subsonic wind tunnel has a 25 ft. long, 6 x 6 ft. square interchangeable test section. The tunnel has a flow speed range of 0-220 ft/s and a maximum unit Reynolds number of 1.33×10^6 per foot. The tunnel is powered by a 600 hp DC motor which turns a 14 ft diameter prop. The flow is directed through screens and a 9:1 contraction with a very low-turbulence intensity of around 0.03%. The tunnel allows force and moment measurements to be taken from either a strut or sting mounted strain gauge balance. The sting was selected for its lower interference with the flow and its higher ranges of force and moment measurements.

The Submarine Models

Two 1/48 scale Los Angeles class (688) submarine models (Scale Shipyard, 1991) were built (Figure 6). The models are nominally 90.25" long and have a nominal 8.25" maximum diameter. The model structures consist of a fiberglass skin mated to an aluminum skeleton. On Model 1, built in 1991, the rear 5" of the model was removed, while on Model 2, built in 1992, the rear 7" was removed in order to grant access for the sting. Because the propeller was not modeled and the major crossflow separation flow phenomena occur closer to the bow, none of the rear control surfaces were modeled. The towed array housing, sail diving planes and sail were all modeled. The black body surface was marked with a white grid spaced every 4" in the longitudinal direction and every 45°

in the circumferential direction. When the model was in the tunnel, all mounting holes were filled with red vacuum wax and/or plaster.

To trip the flow, posts 21 mils high, 0.1" center to center, and 0.05" in diameter were placed around the nose at x/c=0.044 and along the length of the model at +/-45° from the windward side of the model to act as trip strips (Smith, 1989) (see Figure 5). The trip strips were placed on the nose to guarantee tripped boundary layers at low angles of sideslip, while the longitudinal trips were effective for higher angles of sideslip. The posts were made by first laying up 3 layers of 3M brand 7 mil black electrical tape onto a metallic data tape backing. This tape was then run through a computer paper tape punching machine which punched out a continuous string of evenly spaced holes (10 holes per inch) of the same diameter (0.05 inches). The tape was pealed off its backing and applied to the model. Then, a polyester filler (Akemi #7, 1991) was forced into the holes and allowed to cure. Finally, the tape was removed and the 21 mil posts remained. Tests on Model 1 indicated little Re dependence from Re = 4.6 million to 8.8 million, so the trip strips were effective.

To simulate a turning maneuver, the model was placed in a sideslip. The model was mounted in the tunnel on its side in order to utilize the adjustable angle of attack feature of the strut-mounted sting (Figure 6). The towed array was placed on the windward side, so a left turn was modeled. Sideslip angles of up to 15° were simulated.

There were several differences between the two models that must be kept in mind when interpreting the data. On Model 1, the fins were glued directly to the model surface, which made it inconvenient to vary skew angle settings, and were mounted with the fin trailing edges at ϕ=+/-90°. Model 2, on the other hand, was fitted with mounting disks (Figure 7) every 4" on the top and bottom centerline of the model in order to provide variable skew settings for the vortex generators. The disks were 0.5" thick, 1.25" diameter

aluminum round stock and provided a base for either jets or fins. The disks were mounted to spacers and then individual electronic servos (Figure 8). Originally, the servos were to be controlled by radio from outside the tunnel, but the electronics failed, so a hand tool was constructed. The electronics failure was due to cross-frequency interference in the custom built radios and could not be corrected by the manufacturer. The skew setting was accurate to within +/-1°. When the fins were mounted on the disk, the fin root chord was centered at ϕ=+/-90°. Figures 9 through 11 show the basic configurational layout for Model 2. Also, on Model 2 a fin was placed at x=20" on the sail side, which is just ahead of the sail leading edge. On Model 1, this fin was omitted. Finally, vortex generators were included at x = 80" on Model 1 but omitted on Model 2. The fin and jet configurations for each model are shown in Figure 12.

Vortex Generators

It is difficult to transform Pearcey's sizing and spacing guidelines for vortex generators in two-dimensional flow to a three-dimensional problem. The vortex generators were spaced 4" apart.

Half-delta wings were used for the fins. The fins were made of sheet aluminum, were 1" long, 1/2" high, and 1/16" thick, and had leading and trailing edges that were rounded with a radius half the thickness of the sheet aluminum. On Model 1, the vortex generators were glued to the model skin directly at 55° off the centerline, which is about 15° to the local flow based on wall skin-friction lines of the midbody at 15° sideslip. A jig that held a generator in the proper position and orientation was used to mount the delta wings. "Superglue" was used to tack the fins into place, and then a bead of 5-minute epoxy was

applied to secure the fin (Figure 13). On Model 2, the fins were glued to paper labels (Figure 14) which were then stuck to the mounting disks on the model (Figure 15).

For the jets, the air intake consists of two 1/8"x8" slots located at peripheral angles of 90° and 270° and spanning from x/c=9% to x/c=18% (see Figure 12). Fine mesh screen was installed in the slots in order to make the intake flow more uniform over its area. It was very difficult to find a motor that could provide enough volumetric flow rate and pressure rise to produce the very high speeds required. Compressed air could not be used because the heavy hose would need to cross over the balance, potentially interfering with force and moment measurements. A Sears Model 113.177460 Wet/Dry Shop Vac motor was mounted just under the sail (Figure 16). The fan provides up to 50"H_2O pressure at 10 CFM. The fan exhaust was distributed via a 1" ID Tygon tubing manifold, to 1/8" ID Tygon tubing, through a tapered 1/8" ID brass fitting, and finally to 24 jets, each 0.065" ID at 30° inclination. The total system could provide jets speeds of over 300 ft/s. Jets were spaced every 4" from behind the sail aft.

Instrumentation and Experimental Techniques

Forces and Moments

A six-component strain gauge balance made by the Transducer Systems Division of Modern Machine and Tool, Inc., of Newport News, Virginia, was used for the force and moment measurements. All data were collected with a Hewlett-Packard Model 3052 data acquisition unit. Each reading was the average of 50 values. The data are reported in body axes with the moments taken about the quarter chord of the sail (Figure 18). Notice that all the forces and moments are non-dimensionalized by c^2 and c^3, respectively, and not with span or area terms as is the convention in aeronautics (Goodman, 1960). Runs were made for wind tunnel speeds of 100 to 200 ft/s (Reynolds numbers of 4.60 million to 8.77 million) to examine Reynolds number dependence, and at sideslip angles of 0 to 15°. The uncertainties were estimated at 20:1 odds to be δC_x=+/-0.0002, δC_y=+/-0.0004, δC_z=+/-0.0005, δC_l=+/-0.00002, δC_m=+/-0.0001, and δC_n=+/-0.0002.

Oil Flows

A primary diagnostic for these tests was surface oil flow visualization. The oil flow mixture consisted of titanium dioxide (TiO_2) as a pigment, kerosene for the solvent, and oleic acid to prevent coagulation or lumping of the TiO_2. The mixture is made by adding 40 ml of sifted, unpacked TiO_2 to a 100 ml graduated cylinder. Kerosene is added up to the 100 ml mark, and 5 ml of Oleic acid is added on top of that. Several variations of this mixture were tried during the first couple runs, and the quality of the runs was found to be relatively insensitive to small changes from this recipe. The mixtures are then thoroughly

stirred and transferred to a pail. A sponge brush is used to apply a coat of the mixture to the model. Brush strokes are made normal to the expected flow direction so that brush marks are not later misinterpreted as skin friction lines.

After the tunnel is turned on and the oil mixture is almost entirely dry, the tunnel is turned off. The oil flows are recorded by photographing the model in sections and from different peripheral orientations. Also, separation locations are directly measured off the model surface and recorded. After carefully recording the flow separation location, the dried mixture is then cleaned off with kerosene.

Lines of separation are indicated by converging surface skin friction line patterns. The peripheral angle separation location ϕ is measured from the windward side, counter-clockwise facing the model (Figure 18). The indicated ϕ is probably premature for two reasons. The oil flow mixture is drawn down (towards the windward side) due to gravitational effects, and the oil flow mixture itself initiates separation earlier then would occur on a clean surface. Simpson et. al. (1992) have shown that these effects can add errors of up to -5° for a similar flow at 30° angle of attack to the free-stream flow. No attempts were made to correct any of the present data.

It can be very difficult to determine exactly the streamwise location where separation begins. Separation lines are located at converging skin friction lines in the oil flow pattern. Simpson et al. (1992) have proposed, as a rule of thumb, that the point where the angle of incidence of converging skin friction lines is smallest but positive be interpreted as the start of open separation. For most of the runs, this location was still difficult to pick out with any degree of certainty, so no numerical results are presented. Downstream of this location the skin friction lines on each side of the separation line intersect the separation line at a sharp finite angle.

Separation lines are characterized numerically by a mean separation location, ϕ'. This parameter is defined by integrating the separation line to find the separation area. This separation area is then non-dimensionalized by the separation length and the average radius r' in the separation region. This value is the mean separation location ϕ', which is geometrically the straight separation line location for the equivalent separation area on a cylinder of radius r':

$$r' = \frac{1}{x_f - x_i} \int_{x_i}^{x_f} r(x)dx \quad (4)$$

$$\phi' = \pi - \frac{1}{(x_f - x_i)r'} \int_{x_i}^{x_f} (\pi - \phi(x))r(x)dx \quad (5)$$

where x_i and x_f bound the separation zone, $\phi(x)$ is the separation line location at x, and $r(x)$ is the radius at station x.

Boundary Layer Measurements

Hot-wire anemometer measurements were made in order to get an approximate boundary layer thickness at the location of the vortex generators. A custom hot-wire rake with sixteen logarithmically-spaced gold-plated sensors was used to measure the u component of velocity simultaneously throughout the boundary layer. However, only fourteen of the sensors were used because two were broken. A detailed description of the probe, hot-wire electronics, and data acquisition are found in Ha (1993).

The probe was calibrated against the tunnel's pitot tube and pressure transducer. A least squares fit resulted in regression coefficients of at least 0.999 for all but two of the sensors, and it was better than 0.998 for the two exceptions. The rake was mounted normal to the body and aligned so that the rake was approximately normal to the free-

stream velocity at 15° sideslip (Figure 19). At other angles of sideslip, the measurements were corrected using a cosine law and ignoring the cooling effect on the sensors due to the tangential component of velocity which is small at small angles of misalignment.

The rake was positioned as close to the body as possible at x/c=0.43 and ϕ=90°. With the aid of feeler gauges, the height of the bottom sensor off the model surface was measured to be 0.047". It was therefore necessary to extend the measured profile down to the sub-layer by fitting additional points calculated by assuming the law of the wall for 2-D boundary layers.

Vortex Jets Data Acquisition

The pressure and temperature inside the fan canister were used to calculate the jet speed. The pressure was measured with a National Semiconductors LX1601A pressure transducer that was calibrated against the wind tunnel's dynamic pressure transducer. The temperature was measured with an Omega Type K Thermocouple and TAC80 Thermocouple-to-Analog Converter.

In the literature (Huffman and Fox, 1978; Lee et. al., 1989; Ziegler and Wooler, 1978) the velocity has usually been calculated using isentropic relations:

$$Vj = \sqrt{2RT_j \frac{\gamma}{\gamma - 1}\left(1 - \left(\frac{p_o}{p}\right)^{\frac{1-\gamma}{\gamma}}\right)} \quad (6)$$

This method tends to predict very high jet speeds because it ignores pressure losses due to friction and jet expansion. Hansen (1967) offers an empirical method for estimating these losses. Because the losses vary with the local dynamic pressure, which varies directly with the square of the velocity. Accordingly, it can be shown that the pressure loss is inversely proportional to the fourth power of jet diameter:

$$\Delta p \propto q \propto V_j^2 \quad (7)$$

$$V_j \propto 1/A_j \propto 1/D^2 \quad (mass\ continuity) \quad (8)$$

$$\therefore \Delta p \propto 1/D^4 \quad (9)$$

Therefore, only losses in the smallest diameter of the circuit, namely the end jet, are significant. The total pressure loss due to friction and expansion varies with the square of velocity:

$$\Delta p_{loss} = \overbrace{\frac{4f}{D/l}\frac{1}{2}\rho_j V_j^2}^{friction} + \overbrace{\frac{1}{2}\rho_j V_j^2}^{expansion} = kV_j^2 \frac{p_o}{RT_j} \quad (10),$$

where $4f$ is a friction factor (about 0.045) and D/l is the diameter-to-length ratio of the jet (about 0.065). Introducing this correction into the isentropic relations gives:

$$V_j = \sqrt{2RT_j \frac{\gamma}{\gamma - 1}\left(1 - \left(\frac{p_o - kV_j^2 \frac{p_o}{RT_j}}{p}\right)^{\frac{1-\gamma}{\gamma}}\right)} \quad (11),$$

which can not be solved explicitly for Vj. However, if the following substitutions are made:

$$U' = \frac{V_j}{\sqrt{RT_j}},\ and\ \beta = \frac{p_o}{p} \quad (12),$$

then the temperature dependence is eliminated and the equation is reduced to a relation between two non-dimensionalized quantities:

$$U' = \sqrt{2\frac{\gamma}{\gamma - 1}\left(1 - (\beta(1 - kU'^2))^{\frac{1-\gamma}{\gamma}}\right)} \quad (13)$$

This relation was solved numerically, assuming γ=7/5, and the resulting data were fit with a curve using polynomial regression in order to get a more workable form. A parabolic fit works very well (R^2=0.999), so that the following relation is obtained for U':

$$U' = \kappa\sqrt{\beta - 1},\ \kappa = 0.774. \quad (14)$$

Finally, the jet speed is obtained from

$$Vj = \kappa\sqrt{RT_j(\frac{p_o}{p} - 1)}, (15)$$

which gives much more realistic results for the jet speed.

There are errors introduced in this new approximation, especially in the friction term 4f and in the exact modeling of the pressure losses. Therefore, the jet speed was calibrated with a rotameter placed on the suction of the vacuum motor. The volumetric flow rate gives jet speed directly from the mass continuity equation.

Figure 20 shows a linearized jet speed/pressure plot (U' *vs.* $\sqrt{\beta - 1}$). First, this plot visually verifies that the parabola is a good model for both the isentropic relations and the corrected equation. The only discrepancy is the line slope. Second, actual measured data from the flow meter fall somewhere in between the original corrected relation and the isentropic relations. Finally, the measured data were fit with a regressed line in order to calculate the actual slope κ (0.913), and this relation was used to calculate all jet speeds.

Experimental Results

Boundary Layer Measurements

Boundary layer profiles were taken at 0° to 15° sideslip and *Re*=4.6 million, and at 15° sideslip for *Re*=4.6 to 9.7 million. The results are listed in Table 1. It is important to note that the boundary layer thickness at 15° sideslip and Re = 6.8 million, the most common test case, is on the order of 0.3". This verifies that the 0.5" high fins are scaled properly to the boundary layer thickness.

Forces and Moments-Fins

Figure 21 shows the variation of the force and moment coefficients with respect to sideslip β for both the naked submarine and the submarine with fins over the entire submarine at different θ.

The fins drastically change the forces and moments. Examination of the axial force (C_x) plot reveals the huge drag penalties of these fins as the axial force is doubled and sometimes tripled in the worst case. On the other hand, both the normal force C_y and yaw moment C_n experience a decrease in magnitude and more importantly, a decrease in curve slope. C_y decreases by as much as 50%, while C_n decreases by as much as 35%.

Surprisingly, the out-of-plane forces and moments are affected by the fins as well. The roll moment C_l is unchanged, but both the pitching moment C_m and vertical force C_z increase by several orders of magnitude with the addition of the fins.

It is important to know whether the changes in the forces and moments by the fins are due to the additional forces and moments on each fin or the separation delay by the vortex

generator system. Polhamus' method was used to estimate the forces acting on the fins (Bertin and Smith, 1989). Despite, the fact that the fins are mostly submerged in the boundary layer, the approach velocity distribution was conservatively approximated as uniform, free-stream velocity. At 15° sideslip and θ=55°, it was found that about 25% of the axial force C_x is due to the fins directly, while the contribution to the normal force C_y was about 1% and the contribution to the yaw moment C_n was about 5%.

Effect of Skew Angle

Figure 22 shows the forces and moments plotted against θ for different β. θ is the skew angle referenced from the model centerline. The axial force plot (C_x) shows the drag penalty at higher skew angles. This penalty is finite and peaks out at about 45° for the lower sideslip angles, or 60° for higher sideslip. *Cy* and *Cn* both bottom out at 30° to 45° skew. Yaw moment tends to vary more subtly than axial or normal force.

Although the roll moment C_l is unaffected, pitching moment C_m and especially vertical force C_z vary significantly with skew angle. In fact, the vertical force becomes as large or larger than the side force and the axial force at some skew angles. The generation of a vertical force is most likely due to the configurational asymmetries of the sail. Such large vertical forces must be accounted for in any actual design.

Figure 22 shows the same data plotted against θ′, the skew angle referenced from the local flow direction. While it was convenient from a vehicle design standpoint to reference the skew angle from the model centerline, from a fluid dynamics point of view the skew angle should be referenced to the local flow direction. Due to flow three-dimensionality, the local flow direction is different at different points of the model. Therefore, the flow direction is characterized by an estimated flow direction at some station along the

cylindrical midbody. The local flow direction was estimated by measuring the skin friction line direction from oil flow photos for different sideslip angles. The following curve approximates this variation of θ' with sideslip angle:

$$\theta' = \theta - 1.31\beta - 0.09\beta^2, \quad (16)$$

with all angles in degrees. The trends are similar to those in Figure 22, but an important trend is notable in the C_y and C_n curves. For each series on these two plots, there is some true skew angle θ' for which C_y or C_n is a minimum, and this true skew angle increases with sideslip. At higher sideslip angles, there is more separation to control, so the fins need to be steeper relative to the local flow. The plots also point out that beyond this point, higher skew actually hampers the vortex generator effectiveness.

Effect of Number of Fins

A series of tests was run on each model to determine the variation of the forces and moments with the number of vortex generators at β=15°, θ=55°, and *Re*=6.8 million. These series began with all of the vortex generators on the submarine. For each run, a pair of fins (one on the top, one on the bottom) was removed and forces and moments were measured. Series 1 (Model 1) involved removing the fins from the nose rearward, while Series 2 (Model 2) involved removing the fins from the rear forward. This series of tests in effect measured the effect of starting or ending location of the fins on the forces and moments. It is important to note that there were several rows at the sail (3 for Model 1, 2 for Model 2) where only one vortex generator was removed per run. This is because on the sail side, no vortex generators could be placed in the vicinity of the sail (see Figure 12).

The results of these series are presented in Figure 23. Both series are plotted on the same graphs, but due to the geometrical differences between the two models, the end data points will not exactly match. The presence of the sail relative to the fin system plays an important role in the force and moment trends. For Series 1, the sail is at the front of the vortex generating system for n=26 fins, while for Series 2 the sail is behind the fin system for n=10.

The axial force varies linearly with the number of fins in both cases, which suggests that the drag can be broken down by the individual contribution per fin. Using linear regression on this data, the average contribution per fin to the axial force C_x was found to be 6.3×10^{-5}, or 6% of the baseline drag. The normal force C_y varies somewhat linearly, with an inflection point in both series at the sail region. This indicates that the fins forward of the sail do not play as important a role in the normal force as those aft of the sail. The yaw moment C_n follows a similar trend, but this time it's the rear 10 or 15 fins that don't contribute much to the change in yaw moment.

The out-of-plane forces and moments (C_z, C_l, and C_m) follow interesting trends as well. As before, the roll moment is unchanged with or without fins. There's a huge inflection in the pitching moment and vertical force for Series 1 in the sail region. A similar trend is more subtle in Series 2.

All of these inflection points in the sail region are due to the fact that the presence of the sail forces the separation line just aft of the sail down to the sail trailing edge regardless of the fin configuration employed. Therefore, the effectiveness of the fins on the top of the submarine in the vicinity of the sail is less than that of the mirrored fin on the bottom of the submarine or a fin on the top far aft of the sail.

Forces and Moments-Jets

The jets were much less effective in changing the forces and moments. Figure 25 shows the variation of each of the forces and moments with β for a skew angle of 90° and velocity ratios from 0 to 3.54. It is quite clear that the changes due to the jets are on the order of a few percent, rather than orders of magnitude as experienced with the fins.

The jets' fluid momentum alone contributed about 50% of the change in axial force C_x, 40% of the change in normal force C_y, and 20% of the change in yaw moment C_n. Therefore, the jets are relatively ineffective in changing the forces and moments by delaying separation.

Effect of Velocity Ratio

Figure 26 shows the variation of the forces and moments with *VR* at 15° sideslip and a skew angle of 90°. The jets don't have the huge drag penalty that fins do. In fact, axial force C_x drops off a little with increasing *VR*. This is very possibly due to the pure jet momentum. However, the effect on C_y and C_n are much more subtle than for the fins. C_y drops about 15% while C_n drops about 5%. There are no discernible trends in the out-of-plane forces and moments.

Effect of Skew Angle

Figure 27 shows the variation of the forces and moments with skew angle for 15° sideslip and *VR*=3.54. These skew angles, as previously mentioned, are measured relative to the centerline of the submarine and range from 45° to 135°. The local flow angle along

the cylindrical midbody is about 40° off horizontal, so the true skew angle, referenced to the local surface velocity direction, is 85° to 175°. The forces and moments seem to vary in an oscillatory manner with skew angle, with peak to peak variations on the order of 10-20% for *Cx* and *Cy*.

Oil Flows

Submarine Without Vortex Generators

After determining experimentally the best oil flow mixture, runs were made without vortex generators (naked submarine) at Reynolds numbers of $Re = 4.60 \times 10^6$ to $Re = 6.77 \times 10^6$ for sideslip angles of 0°, 5°, 10°, and 15°. Most of this discussion will focus on cases with 15° of sideslip at $Re = 6.77 \times 10^6$.

Figure 27 shows the bottom of the submarine from x = 52" to x = 68" from the nose. This run was made at 15° sideslip and $Re = 6.78 \times 10^6$. Primary separation (indicated as S_1) occurred at 97° on the sail side and 115° on the bottom side of the submarine. Secondary lines of separation (indicated as S_2) were also found in some of the cases. The towed array was found to have a substantial effect on the flow especially with respect to separation.

At $Re = 6.85 \times 10^6$ and $\beta = 5°$, separation occurred at roughly $\phi' = -135°$ on the sail side and $\phi' = 150°$ on the bottom side. Figure 29 shows oil flow 7 for which $Re = 6.8 \times 10^6$ and $\beta = 10°$. The flow separated at $\phi' = -130°$ on the sail side and $\phi' = 119°$ on the bottom side of the submarine. As expected, separation occurred earlier in this 10° sideslip case than in the 5° sideslip case. In comparison, Figure 30 shows the separation line for β = 10°, but $Re = 4.5 \times 10^6$. The flow separated at $\phi' = -114°$ on the sail side and $\phi' = 109°$ on

the bottom side of the submarine. This seems to indicate some Reynolds number dependence.

Figure 31 documents oil flow 9, with $Re = 6.78 \times 10^6$ and $\beta = 15°$. All of the vortex generator runs were compared to this configuration. Separation occurred considerably earlier in this case due to the steeper sideslip angle, with $\phi' = -100°$ on the sail side and $\phi' = 109°$ on the bottom side. Also, this flow had a secondary separation line at roughly $\phi = -150°$ on the sail side and $\phi = 145°$ on the bottom side. Figure 32 shows the same configuration at $Re = 4.5$ million. This time the separation line does not seem to show any significant Reynolds number dependence, with $\phi' = -100°$ on the sail side and $\phi' = 102°$ on the bottom side of the submarine.

Also, as shown in Figures 39 to 41, the sail plays a very important role in the flow development on the submarine. At 0° sideslip (Figure 39), the flow is completely attached on the hull surface. A wake does form off the trailing edge of the diving planes. At 5°, the flow is still fully attached. At 10° sideslip (Figure 40), the flow seems to separate off the trailing edge of the sail and in fact initiates the main vortex sheet that separates off the submarine on that side of the body. The wake on the trailing edge of the sail is bigger, and the flow separates on the inboard section of the diving planes. At 15° sideslip, (Figure 41), a large vortex sheds off the sail. This is accompanied by some very complex flow patterns, which include a smaller vortex now on the sail itself, more separation on the inboard surface of the diving planes, and a stagnation point/saddle point combination on the submarine behind the sail. Because of the sail, appreciable dissimilarities between the sail side and the bottom of the submarine should be expected.

The towed-array housing also affects the flow. Figure 43 is from oil flow 1, which was run at $Re = 6.78 \times 10^6$ and $\beta = 15°$. This figure shows that a small amount of separation occurs off the semi-circular leading edge of the housing. Also, the streamlines

on the towed array housing are much steeper than those just windward of the housing. Careful inspection reveals slight separation on the leeward side of the towed array housing for its entire length. Figure 44 shows the trailing edge of the towed array housing from the same flow. In this photo, the primary separation line is seen to converge onto the trailing edge of the towed array.

Submarine With Fins

All data presented in this section involves Model 1 with the fins skew at 55° off the centerline, unless otherwise noted. Figure 28 shows the separation line for the same portion of the submarine as shown in Figure 27. The run in Figure 28, oil flow 20, was also done at 15° of sideslip and $Re = 6.43 \times 10^6$, but this run included the larger vortex generators placed along the submarine. It is quite clear that the separation line has moved toward the leeside as compared to Figure 27. In fact, separation was delayed by as much as 33° on the sail side and 37° on the bottom side.

Figures 29 through 37 show plots of the separation line for each of the cases where the separation line was recorded on the model. Examination of these separation lines shows the improvement made with the addition of the vortex generators.

Figure 31 reiterates that the flow separates at $\phi' = -100°$ on the sail side and $\phi' = 109°$ on the bottom for $\beta = 15°$ and $Re = 6.78 \times 10^6$ for the naked submarine. This contrasts with oil flow 20, Figure 37, which represents the most successful configuration tested. For this flow, the separation line is delayed even beyond 135° in some places. The only place where the separation line hasn't moved is just behind the sail on the sail side. The mean separation lines for this vortex generator configuration are $\phi' = -129°$ on the sail side and $\phi' = 147°$ on the bottom.

Several observations were made during these runs. First, it is important to introduce vorticity relatively far upstream. In the initial vortex generator configuration, the first half delta wing was placed at 27% of the length downstream of the nose. This configuration delayed separation by almost 25°. Later configurations added vortex generators all the way from 4.4% of the length from the nose, with a subsequent additional delay in separation of 12°.

Also, the behavior of each individual vortex generator is such that it seems to have a zone of influence. If, for example, a vortex generator is removed, the separation dips toward the windward side of the submarine just downstream of that location. Downstream at the next vortex generator, the separation line does not jump back up to the position achieved before the missing vortex generator, but instead slowly climbs and in fact never really reaches the original separation line.

More indications of this zone of influence can be seen by examining the surface flow pattern between the row of vortex generators and the separation line. The separation line is seen to oscillate a little in coordination with the placement of the vortex generators. Also, the dark stripe off each vortex generator (see Figure 28), which is an indication of the vortical wake produced by each vortex generator, shows where downstream the produced vorticity affects the separation line. By examining this figure, this zone of influence seems to be a band four inches wide (the distance between vortex generators) that extends downstream at about a 30° angle off horizontal from the vortex generators to the separation line.

The oil flows clearly delineate the difficulties in reducing separation on the sail side of the submarine as opposed to the bottom of the submarine. First of all, the flow separates off the towed array housing, and then reattaches to the submarine surface closely behind the towed array (see Figure 43). Also, as shown in Figures 41 and 42, at 15° sideslip, the

flow separates off the sail. Consequently, a large vortex forms off the sail, and the hull flow separation line aft of the sail is forced down to the trailing edge of the sail. This greatly limits the amount of separation reduction possible on this side of the submarine. Also, the vortex generators ahead of the sail modify these complex flow structures. While the location of these structures really is not changed, the size and rotational orientation of the main vortex off the sail is affected. It is hard to predict what effect this has on the submarine performance.

During the study, attempts were made to reduce the separation off the sail by putting small vortex generators on the sail itself. For oil flow 23, two small vortex generators were placed on the sail just behind the trip posts (about 0.5" from the sail leading edge), at 0.5" and 1.5" from the hull surface (see Figure 45). For oil flow 24, these two vortex generators were moved just ahead of the trip posts (Figure 46). Neither of these attempts proved effective. One potential reason for this is that the sail's maximum thickness is so far forward that the resultant adverse pressure gradient is extremely strong and may therefore require a very strong vortex generator system. Also, the scale of the flow structures involved in this region coupled with the relative violence of the flow around the sail makes diagnosis much more difficult.

Several runs point to the effect of local vortex generator skew, θ, on the flow separation. For oil flow 19, two vortex generators were added at x = 8" at peripheral locations $\phi = \pm 135°$ (Figure 47). They were placed at 15° to the local flow, but since the flow is only about 15° off horizontal, this means they were only 30° off horizontal. For oil flow 20 these two vortex generators were inclined a little steeper so that they were 55° off horizontal (Figure 48). By examining Figures 47 and 48, it is clear that the steeper vortex generators in oil flow 20 produced the stronger vortices and pushed the separation line slightly farther towards the leeside. So as expected, the steeper vortex generators produce

stronger vortices which are more effective at delaying separation. However, it was found that these particular vortex generators had a minimal effect on the overall flow. On the sail side, $\phi' = -129°$ for oil flow 19 and $\phi' = -128°$ for oil flow 20. On the bottom side, $\phi' = 145°$ for oil flow 19 and $\phi' = 147°$ for oil flow 20.

It was noted that these leeside vortex generators at $x = 8"$ were in an unfavorable pressure gradient. Therefore, the top two vortex generators were moved to $x = 4"$. In addition, these vortex generators were moved to $\phi = \pm 150°$. Also, two more vortex generators were added at $x = 4"$, $\phi = \pm 90°$ (Figure 49). Neither of these changes delayed separation any farther than the configuration in oil flow 20.

For oil flow 23, two of the leading vortex generators were rotated so their true skew, θ', was negative instead of positive in order to examine the effect of the sign of true skew and resulting vorticity rotation direction on the flow (see Figure 50). These two vortex generators allowed the flow to separate earlier than in the previous run and were therefore detrimental to the configuration.

For oil flows 16 and 17, smaller vortex generators (0.25" high, 0.5" long, 1/32" thick) were used on the sail side. For oil flow 16, the vortex generators were placed just ahead on the towed array. This configuration was relatively ineffective, as the separation line was delayed by only about 5°. Then for oil flow 17, the vortex generators were moved up to $\phi = 90°$, which is where the vortex generators had been placed on the bottom side of the sub. These vortex generators were more effective and delayed separation by almost 13° (see figure 51). For oil flow 18, the small vortex generators were replaced with the larger ones so that the same vortex generators were being used on both sides of the sub. The larger vortex generators delayed separation an additional 15° (see figure 52).

Submarine With Jets

The jets were tested at a Re=4.6 million in order to maximize the jet velocity ratio *VR* at 3.54. Oil flow results for ϕ=30°, θ=90°, and *VR*=3.54 (Figure 55) show the separation line at about 105°. There is little measurable improvement compared to the submarine without jets. Therefore, the oil flows seem to indicate that the jets are less effective than the fins.

It was conjectured that perhaps the jets were less effective because they weren't positioned far enough towards the bow. However, Figure 23 shows the forces and moments for the fins in the exact configuration as the jets, corresponding to *n*=24 of Series 1 on the graphs. It is evident that the fins affect the forces and moments more drastically than those produced by a comparable jet configuration, even at high jet velocity ratios.

Full Scale Design Issues

Throughout the design and construction of the wind tunnel models, several design issues came up that are applicable to full scale design. These are discussed briefly below.

Power Consumption

The main advantage of the jets over the fins is the jets do not have the huge drag penalty of the fins. The data in Figure 21 through 27 show that the jets were less effective than the fins. Basically, in any process, including delaying flow separation, the fundamental goal is to efficiently use available energy. In this case, the goal is to somehow inject energy into a boundary layer that is progressing toward separation. Since the jets were not very effective, a possible solution would be to increase the "energy" of the jets, i.e. increase jet speed or jet size or the number of jets. It is desirable to make some rough estimates of the comparative, full-scale power consumption of the jets and fins.

The full scale power consumption of the jets can be obtained from the energy equation, ignoring heat transfer and body forces, as

$$\dot{W}_{jets} = \left[\frac{\Delta p}{\rho} + \frac{V_j^{\,2}}{2}\right]\dot{m}. \quad (17)$$

According to the jet pressure-loss model, the pressure rise in the circuit is typically 1.5 times the jet dynamic pressure. The following substitutions lead to a relation for the power consumption of the jet system in terms of jet parameters and the submarine speed:

$$\Delta p = 1.5(\frac{1}{2}\rho_{H_2O}V_j^{\,2}),\ \dot{m} = \rho_{H_2O}V_jA_j,\ V_j = VRU_\infty \quad (18)$$

$$then\ \dot{W}_{jets} = \frac{5}{4}\rho_{H_2O}A_jVR^3U_\infty^{\,3} \quad (19)$$

An important issue here is scaling. It would be easiest to scale jet speed by the free-stream velocity and the jet diameter by the submarine length. If so, VR = 3.5 and A_j = 4" at full scale. However, it is possible that A_j could be scaled with some boundary layer parameter, such as δ, δ^*, or θ. Also, the jet speed may scale with VR, C_μ, or even some other parameter. Some scaling studies probably need to be done. For the purpose of this analysis, this original, simpler scaling scheme is used.

The fins, in comparison, consume energy in the form of lost momentum. The power loss can be estimated as the product of the increase in axial force and the submarine velocity:

$$\dot{W}_{fins} = |\Delta X| U_\infty = \frac{1}{2} |\Delta C_x| c^2 \rho_{H_2O} U_\infty^3 \qquad (20)$$

For the worst case, $|\Delta C_x|$ = 0.002. For the full size submarine, c = 360 feet.

In order to get a grasp on the relative order of magnitude for these values, they can be compared to the submarine cruise power. The cruise power is similar to the fin power, namely

$$\dot{W}_{cruise} = |X_0| U_\infty = \frac{1}{2} |C_{x0}| c^2 \rho_{H_2O} U_\infty^3 \quad (21)$$

Unfortunately, no good estimate for $|C_{x0}|$ is available because of the removal of the tail on the wind tunnel model. Nevertheless, wind tunnel data will be used as it is the only data available. Therefore, $|C_{x0}|$ is approximately 0.001. The ratios of the jet and fin power to cruise power can be calculated:

$$\frac{\dot{W}_{jets}}{\dot{W}_{cruise}} = \frac{5}{2} \frac{A_j VR^3}{|C_{x0}| c^2} \quad (22)$$

$$\frac{\dot{W}_{fins}}{\dot{W}_{cruise}} = \frac{|\Delta C_x|}{|C_{x0}|} \quad (23)$$

$$\text{so } \frac{\dot{W}_{jets}}{\dot{W}_{cruise}} = 1.7, \text{ and } \frac{\dot{W}_{fins}}{\dot{W}_{cruise}} = 2.0 \qquad (24)$$

Thus, the power consumption of each of these concepts is more than that required in cruise. This means that the pumps required for the jets may get very large, and the fins may overcome the propulsive ability of the submarine. However,such large burst of energy may be justifiable over a relatively short time for an emergency maneuver. Also, the high drag of the fins may actually improve turning performance.

Typically, when vortex generators are used to delay separation, the resultant drag penalty is small compared to the benefits of separation reduction. It is unclear whether the benefits outway the costs when applying the vortex generators to a submarine. The general explanation for the large power consumption of the vortex generators in this case is that the adverse pressure gradient of the leeward side of a submarine-like body is large. In contrast, these kind of flow control devices are typically applied to airfoils, where the adverse pressure gradients are much less severe.

Other Design Considerations

There were other design difficulties. It was difficult to fit the servos in the wind tunnel model, especially in the tail. It may be even more difficult to find the space on an existing full-scale platform for a retrofitted vortex generator system. In particular, the jets need a finite straight length in order to guarantee uniform flow. At any given inclination angle, that results in a finite penetration distance into the submarine. While the premise was made that perhaps any flow control devices may fit in between hulls on a double hulled submarine, this is increasingly unlikely. The fins would probably need to fold down flush with the submarine surface, as opposed to retracting into the submarine, due to their size.

Whether the fins are scaled on the submarine length or boundary layer thickness, they would be about 2 feet high in full scale.

Data Interpretation - Turning Performance

In classical analysis, the equations of motion for submarines and other vehicles has been linearized in order to facilitate analytical solutions. However, the linearization assumptions do not account for the non-linearity in the dynamic response and neglect the memory effects making a detailed analysis impossible. It has been emphasized that new methods must be developed that not only model the non-linearities of the equations of motion and flow-field dynamics, but also model the time-varying transients in the flowfield (Fein, 1992). So far, attempts have been made at full NS equations solvers and semi-empirical flow solvers, but a complete, reliable capability is years away. Still, the most reliable trajectory simulation is with remote controlled models or full-scale sea trials.

Despite this computational limitation, it is desired to examine the potential effects of vortex generators on the turning performance of a submarine. On top of the above limitations is the fact that all of the data presented is *static* data. Dynamic data is required for even the limiting linear analysis. Therefore, few quantitative results will be presented. Instead, a qualitative analysis is provided.

Linear Stability Analysis

A few assumptions must be made. The first is that submarines of contemporary configurations and capabilities can be approximately modeled in a steady, gentle turn with linearized equations of motion. The attempt then is to analyze the linear turning performance results, and account for predictable, qualitative trends due to the addition of vortex generators.

The linear solution depends on linearized forces and moments, which results in the definitions of stability derivatives. Only the sway (y direction) and yaw equations will be examined. As a result, six stability derivatives are required for the solution: C_{yv}, C_{nv}, C_{yr}, C_{nr}, $C_{y\delta}$, and $C_{n\delta}$. The v terms are the sideslip derivatives are related to the β derivatives presented by

$$C_{yv} = C_{y\beta}/cos\beta. \qquad (25)$$

Linearized equations are valid only for small β, so $cos\beta \approx 1$. The r terms are the yaw rate derivatives. None of the presented data can yield a numerical value for these terms. Finally, the δ terms are the control derivatives, which in a turning maneuver represents the effect of the rudder. Each of these derivatives has a probable sign or magnitude for most submarines:

$$C_{yv<0} \quad (26)$$

$$C_{nv<0} \text{ (usually)} \quad (27)$$

$$C_{yr} \text{ is either, but usually small} \quad (28)$$

$$C_{nr<0} \quad (29)$$

$$C_{y\delta>0} \quad (30)$$

$$C_{n\delta<0} \quad (31) \qquad \text{(Crane et. al., 1989)}$$

Now the problem is to examine the effect that the vortex generators has on each of these terms. It would make sense to start with the v terms, since data are available for them. For both the side force and yaw moment versus sideslip, the relative magnitude of each is decreased by adding vortex generators. However, these data are for the wind tunnel model, which had no tail or appendages. Straight line fits for the side force and yaw moment data, re-referenced at midships, at $\beta<5°$ are presented below. For the submarine with fins, it is assumed that the fins are deployable. Therefore, while the plots in Figure 21 indicate very small slope changes and curve translation, the curve for the submarine with

fins considered here does go through the origin. These linear fits result in the following stability derivatives:

Without Vortex Generators	With Vortex Generators
$(C_{yv})_{body} = -0.0298$	$(C_{yv})_{body}^{*} = -0.0155$
$(C_{nv})_{body} = -0.0281$	$(C_{nv})_{body}^{*} = -0.0206$

For all quantities examined, starred notation (*) represents the submarine with vortex generators.

The contributions due to the tail are computed as follows. First, since the tail and appendages are not modeled, the combination of the two are modeled simply as the entire projected planform area of the rudders. Real rudder dimensions are not available, so the estimated dimensions given in Figure 54 are used (Scale Shipyard). The incompressible lift and drag acting on a rudder of aspect ratio AR and quarter chord sweep Λ due to an angle of attack is (Shevell, 1989):

$$C_L = C_{L\alpha}\alpha, \quad C_{L\alpha} = \frac{2\pi\ AR}{2+\sqrt{AR^2(1+\tan^2\Lambda)+4}} \qquad (32)$$

$$C_D = C_{D0} + \frac{C_L^{\ 2}}{\pi\ AR} \qquad (33)$$

These values are referenced in terms of C_y and C_n by the following relations:

$$\alpha = \beta - \delta + \varepsilon \qquad (34)$$

$$C_{y_{tail}} = (-C_{L_{tail}}\cos\beta - C_{D_{tail}}\sin\beta)\frac{S_{tail}}{c^2} \qquad (35)$$

$$C_{n_{tail}} = -C_{y_{tail}}\frac{h}{c} \qquad (36)$$

where ε is the local sidewash angle, and δ is the rudder deflection angle. These equations were applied to both the upper and lower rudders and summed. Substituting in the estimated values results in the following relations:

$$C_{y_{tail}} = -\ 0.0129(\beta - \delta + \varepsilon)\cos\beta \qquad (37)$$

$$C_{n_{tail}} = 0.00817(\beta - \delta + \varepsilon)\cos\beta \qquad (38)$$

Now the total sideslip stability derivatives are:

$$C_{y_v} = (C_{y_v})_{body} + (C_{y_v})_{tail} \qquad (39)$$

$$C_{n_v} = (C_{n_v})_{body} + (C_{n_v})_{tail} \qquad (40)$$

The numerical results, assuming small β, are:

Without Vortex Generators	With Vortex Generators
C_{yv}=-0.0427	C_{yv}*=-0.0198
C_{nv}=-0.0199	C_{nv}*=-0.0028

This leaves the task of estimating the dynamic (yaw rate) term. From the data, there is *no way to numerically estimate the yaw rate derivatives.* Instead, the effect the vortex generators may have on the yaw rate derivatives can be hypothesized. Since the vortex generators reduce the region with separated flow, that means the flowfield is less affected by boundary layer phenomena and is tending towards potential flow. This is consistent with the side force and yaw moment trends. The *magnitudes* of the side force and yaw moments decreased; in potential flow, there are no forces and moments. For a body in a potential uniform-velocity flowfield with a yaw rate imposed on the body, the forces should still be zero. Therefore, it can be hypothesized that the yaw rate derivatives will *decrease* in magnitude.

In fact, before analyzing any equations, this analogy can be extended. On a submarine with no hull separation, the flowfield can be modeled as potential flow on the body (i.e., no forces and moments); and potential flow on the rudder surfaces with bound circulation (i.e. lift). This idealized submarine would have a completely effective rudder with no turning resistance whatsoever. It would simply spin about its c.g. as fast as its inertia would allow until the rudder was returned to neutral.

These trends can be examined mathematically. The linearized equations of motion for a submarine in a steady turn must meet the following criteria in order to guarantee stability (Crane et. al., 1989):

$$C > 0, \text{ where}$$

$$C = C_{y_v}\left(C_{nr} - \frac{mux_{cg}}{\frac{1}{2}\rho\ U_\infty c^4}\right) - C_{nv}\left(C_{y_r} - \frac{mu}{\frac{1}{2}\rho\ U_\infty c^3}\right) \qquad (41)$$

C_{yv}, C_{nv}, C_{yr}, and C_{nr} are non-dimensional stability derivatives. If it is assumed that the c.g. is at midships (where the forces and moments are referenced), β is small, and if the signs for each term are as listed in equations 26 through 31, then C can be represented as

$$C = \left|C_{y_v}\right|\left|C_{nr}\right| + \left|C_{nv}\right|\left(C_{y_r} - \frac{m}{\frac{1}{2}\rho\ c^3}\right) \qquad (42)$$

One way to improve turning performance is to tend to make the vehicle less stable or in fact unstable, which is done by decreasing C. For the first term in C, we have seen that the magnitudes of each of these terms decreases, which tends to destabilize the submarine. C_{nv} decreases, so its term decreases if $C_{y_r} > m/\frac{1}{2}\rho\ c^3$. Often C_{yr} is neglected, which means it may be less than the mass term. If $C_{y_r} < m/\frac{1}{2}\rho\ c^3$, then the vortex generators have a *stabilizing* effect on the submarine according to the second term. In such a case, the relative benefits of the destabilization of the first term must be weighed against the stabilizing effects on the second term in order to determine the overall effect of vortex generators on the turning performance.

The mass term can be estimated as follows. Mass divided by density is volume, which for a submarine-like body can be written in terms of a block coefficient η as

$$V = \eta\pi\ \frac{d^2}{4}c, \qquad (43)$$

so the non-dimensional mass term can be written as

$$\frac{m}{\frac{1}{2}\rho\, c^3} = \frac{V}{\frac{1}{2}c^3} = \eta\pi\ \frac{d^2}{2c^2} = \tilde{m}. \quad (44)$$

For this submarine, d = 33 ft, c = 360 ft, and η = 0.72, so the non-dimensional mass is $\tilde{m}$ = 0.00945.

The results thus far are as follows. The sideslip derivatives are estimated. The magnitudes of both go down, but the yaw moment decreases more than the side force derivative. The mass term has been estimated. C_{yr} is neglected, but C_{nr} is not and can't be estimated. Therefore, it is important to determine C_{nr}'s effect on the stability of the ship.

We can start by examining the ship without vortex generators. We assume that the ship is stable, but not too stable, so C is a small, positive number. The only unknown term is C_{nr}, which leads us to

$$|C_{nr}| > \frac{|C_{nv}|}{|C_{y_v}|}\tilde{m},\ so\ |C_{nr}| = \zeta\frac{|C_{nv}|}{|C_{y_v}|}\tilde{m},\ \zeta > 1, \quad (45)$$

so C for the baseline submarine is

$$C = \tilde{m}|C_{nv}|(\zeta - 1) \qquad (46)$$

When vortex generators are added to the submarine, the magnitude of C_{nr} decreases, so

$$|C_{nr}^*| = \sigma|C_{nr}|,\ \sigma < 1 \quad (47)$$

Then C^* can be written as

$$C^* = \frac{|C_{y_v}^*|}{|C_{y_v}|}|C_{nv}|\tilde{m}\zeta\sigma\ - |C_{nv}^*|\tilde{m}. \qquad (48)$$

Now, we want at least $C^*<C$, and it would be good if $C^*<0$. Examining the first condition leads to the following inequality:

$$\frac{|C_{y_v}^*|}{|C_{y_v}|}\zeta\sigma\ - \frac{|C_{nv}^*|}{|C_{nv}|} < \zeta - 1,\ or\ \sigma < \frac{\zeta - 1 + |C_{nv}^*|/|C_{nv}|}{\zeta|C_{y_v}^*|/|C_{y_v}|}. \quad (49)$$

For $C^*<0$ (unstable), the relation is much simpler:

$$\frac{|C_{y_v}{}^*|}{|C_{y_v}|}\zeta\sigma - \frac{|C_{nv}{}^*|}{|C_{nv}|} < 0, \; or \; \sigma < \frac{|C_{nv}{}^*|/|C_{nv}|}{\zeta|C_{y_v}{}^*|/|C_{y_v}|} \quad (50)$$

Remember, ζ is a factor that describes how stable the naked submarine is, and ε describes how much the vortex generators affect the C_{nr} term. If the numerical estimates from above are substituted into equation 50, the following relationships for each of the two conditions are obtained:

$$\sigma < \frac{\zeta - 0.859}{0.464\zeta} \; for \; C^* < C, \; or \; \sigma < \frac{0.303}{\zeta} \; for \; C^* < 0 \quad (51)$$

Therefore, to guarantee that the fins work and meet the first criteria ($C^*<C$), either $\zeta>1.6$ or $\sigma<0.3$. Most likely, however, neither of these criteria is met. Therefore, the determining factor is the effect the fins have on C_{nr}. This points out the necessity of performing dynamic tests on this configuration.

Non-linearities

Of course, the original premise was that linear analyses are inadequate. The above analysis pointed out some trends, but the non-linear effects are very important, especially considering that any drastic improvement in turning performance will result in a non-linear vessel response. Some qualitative non-linear observations were made.

In the relations for the side force and yaw moment contribution of the tail is a "sidewash" term ε. For an airplane, such a term might be due to the downwash of a wing. But for this body of revolution, it is clear by studying the oil flows that the effect of the body is to increase the effective angle of attack of the rudder. On an airplane, this effect is usually small due to the relative size and aspect ratio of the wing to the body. The vortex

generators tend to increase this sidewash effectiveness, which should increase rudder effectiveness and further improve turning performance.

Finally, there is one other major effect on turning performance that can not be considered by standard linear results. As has been seen, the vortex generators add a huge amount of drag to the submarine. One underlying assumption in the linear development is that the propulsive and axial forces cancel out, so that u is assumed constant. The drastic increase in drag due to vortex generators challenges this assumption. One of two cases may exist. The first is that a conventional submarine never negotiates a turn under full power. Therefore, there may be sufficient excess power available to overcome this drag increase and permit constant velocity throughout the turning maneuver. The other possibility is that the drag does drastically deccelerate the submarine. This will result in less translation, or "drift", of the submarine in the maneuver, but it will also result in a lower turn exit velocity. It is almost analogous to a race car sliding through a turn. While large drag is typically regarded as a "penalty", in this case it may actually play a positive role in improving turning performance. The real issue becomes defining the actual ideal turning maneuver trajectory.

Recommendations for Future Work

Without a doubt, the fins provide the designer the ability to significantly control flow separation, and this is indeed a potentially powerful capability. There are issues that must be dealt with before a complete, design-ready capability is realistic. The first basic question that must be answered is do the fins in fact improve turning performance at all?

The evidence so far seems to indicate that the answer is yes, but firm proof will require further study. The next step in this program should involve dynamic tests of a submarine configuration with the fins. This need falls in line with the recent development of the DyPPiR at Virginia Tech. The DyPPiR, which stands for Dynamic Plunge-Pitch-Roll apparatus, can dynamically maneuver a sting mounted wind tunnel model in any prescribed combination of plunge, pitch, and/or roll. Force and moment measurements, as well as surface pressure measurements, can be obtained. With dynamic tests, enough data could be obtained to accurately model a steady, non-linear turning maneuver. In fact, it is possible that a three-dimensional turning maneuver could be studied in order to examine the out-of-plane motions developed by the fins.

Any new tests need to include tail control surfaces on the model in order to study the effects of the fin configuration on the control effectiveness. This is hard to accomplish with a sting-mounted model, but it is crucial for any further study.

Without any other study, the data would have to be analyzed using standard, stability derivative techniques. By using a high order model, this should be adequate initially to prove comparativley whether or not turning performance is improved and if so, by how much. However, further research should be performed on modeling real submarine performance in general in order to aid conventional design, as well as any unconventional design using vortex generators.

Once this next stage is complete, the whole turning maneuver process will be much better understood. This knowledge will provide qualitative guidance for all further studies. Then, the fin configuration can be refined. Fin spacing, fin size, and fin skew could be studied in even more detail and refined. With the development of separation location sensors, a study could be performed that aims to optimize each individual fin skew angle and compare the flow control to systems where all the fins are at some uniform skew angle. This has serious implications on final control system design in a real application. Eventually, as the phenomenon is better understood, a control system could be developed that links the skew setting to the separation location sensors, so that the fins always set themselves to minimize separation. A final goal could be to install a model with such a system on the DyPPiR, perform dynamic maneuvers, and have the separation sensor/vortex generator control system respond dynamically with the maneuver.

Conclusions

The turning performance of a submarine is limited by the crossflow separation off the leeward side. Vortex generators offer a possible means of lessening that crossflow separation and improving turning performance.

It has been shown that fins placed along the submarine centerline from bow to stern do indeed significantly reduce crossflow separation on a submarine in a turning maneuver. Oil flow visualization was used to locate flow separation. With the addition of fins, the peripheral angular location of separation was delayed by as much as 35°. Comparable jet configurations were found to be less effective.

The fins tremendously alter the force and moment distribution. Due to the vortex generators, the normal force was reduced by up to 50%, the axial force was increased by up to 300%, and the yaw moment was decreased up to 35%. In addition, the vertical force and pitching moments were increased by up to 300%, and the roll moment was unaffected. It was also found that skew angles of 30° to 45° are most effective.

During tests in which the number of fins on the submarine was varied, it was found that the sail plays a critical role in the effectiveness of a vortex generator configuration. Because the flow separates off the sail leading edge at 15° sideslip, the separation line immediately aft of the sail is pinned to the sail trailing edge regardless of the vortex generator syste,. Therefore, the vortex generators delay separation by different amounts on the top and bottom of the submarine, which induces the severe out of plane forces and moments. The same series of tests revealed that the rear fins are responsible for reductions in side force, while forward fins are responsible for reductions in yaw moment.

The jets, in comparison, were found to be less effective and did not delay separation appreciably. No strong trends were noted for the force and moments versus skew angle, and the velocity ratio had only a very small affect.

Not enough data was collected in order to examine the specific affects the vortex generators might have on submarine turning performance. Dynamic test are a necessary next step.

As a concept, the fins are definitely a viable means for flow control. Further reductions in separation could most likely be achieved by more carefully optimizing size, shape, distribution, and orientation of the vortex generator system. In order to make definite conclusions about turning performance, unsteady dynamic tests with transient flow effects must be performed.

References

Ahn, S. and Simpson, R.L., 1992: *Cross-Flow Separation on a Prolate Spheroid at Angles of Attack*, AIAA-92-0428.

Akemi #7 Polyester Repair Material, Akemi Plastics Inc., 5265 S. Clinton Trail, Eaton Rapids, Michigan, 48827.

Bertin, John J. and Smith, Michael L, 1989: *Aerodynamics for Engineers*, Prentice Hall, Inc., Englewood Cliffs, New Jersey, pp.282-289.

Bragg, M.B. and Gregorek, G.M. 1987: "Experimental Study of Airfoil Performance with Vortex Generators," *Journal of Aircraft*, Vol 24., pp. 305-309.

Bushnell, D.M., and Donaldson, C.D., 1990: *Control of Submersible Vortex Flows*, NASA Technical Memorandum no. 102693.

Compton, D.A., and Johnston, J.P.,1992: "Streamwise Vortex Production by Pitched and Skewed Jets in a Turbulent Boundary Layer", AIAA-91-0038, *AIAA J.*, vol. 30, n0. 3, pp. 640-647, presented as AIAA-91-0038 at AIAA 29th Aerospace Sciences Meeting, Reno, NV, Jan. 7-10, 1991..

Crane, C. Lincoln, Haruzo, Eda, and Landsburg, Alexander C., 1989: "Controllability", *Principles of Naval Architecture,* Volume 3, Society of Naval Architects and Marine Engineers, Jersey City, NJ, pp. 191-424.

Fein, James, 1992: *Undersea Maneuverability Workshop,* unpublished comments, David Taylor Model Basin.

Goodman, Alex, 1960: "Experimental Techniques and Methods of Analysis used in Submerged Body Research", *Third Symposium on Naval Hydrodynamics; High Performance Ships*, Report No. ACR-65, Office of Naval Research, Department of the Navy, David Taylor Model Basin.

Ha, S., 1993: *An Experimental Study of Coherent Structure in a Turbulent 3-D Boundary Layer*, Ph.D. Dissertation, Aerospace and Ocean Engineering Department, Virginia Polytechnic Institute and State University.

Hansen, Arthur G., 1967: *Fluid Mechanics*, John Wiley and Sons, Inc., New York, N.Y, pp. 418-445.

Huffman, J.K. and Fox, C.J., 1978: *Subsonic Lateral/Directional Static Aerodynamic Characteristics of a General Research Fighter Configuration Employing a Jet Sheet Vortex Generator*, NASA-TM-74049.

Johnston, J.P. and Nishi, Michihiro, 1990: "Vortex Jets - A Means for Flow Separation Control", *AIAA J*, Vol. 28, No. 6, pp. 989-994.

Lee, K.T., Wood, N.J., and Roberts, L., 1989: *Controlled Vortical Flow on Delta Wings through Unsteady Leading Edge Blowing*, Stanford University.

Lin, J.C., Howard, F.G., Bushnell, D.M., and Selby, G.V., 1990: *Investigation of Several Passive and Active Methods for Turbulent Flow Separation Control*, AIAA-84-1276, presented at AIAA 21st Fluid Dynamics, Plasma Dynamics, and Lasers Conference, Seattle, WA, June 18-20, 1990.

Malcolm, G.N. and Skow, A.M., 1986: *Enhanced Controllability Through Vortex Manipulation of a Fighter Aircraft at High Angle of Attack*, AIAA-CP-86-2777.

Morin, Bruce L., Patrick, William P., and Schlinker, Robert H., 1992: *A Parametric Study of Vortex Generator Jets for Three-Dimensional Separation Alleviation*, United Technologies Research Center, Report No. R92-970141.

Ng, T.T. and Malcolm, G.N., 1991: *Aerodynamic Control Using Forebody Blowing and Suction*, AIAA-91-0619.

Pearcey, H.H., 1961: "Shock-Induced Separation and its Prevention by Design and Boundary Layer Control," *Boundary Layer and Flow Control, Its Principal and Applications*, Vol. 2, edited by G.V. Lachman, Pergamon Press, Oxford, England, pp. 1166-1344.

Poll, D.I.A., 1985: "On the Effect of Boundary Layer Transition on a Cylindrical Afterbody at Incidence in Low-speed Flow", *Aero J.*, pp. 315-327.

The Scale Shipyard, 5866 Orange Ave. #3, Long Beach, CA 90805-4146.

Shevell, Richard S., 1989: *Fundamentals of Flight*, Prentice Hall, Englewood Cliffs, NJ.

Simpson, R. L., Walker, D.A., and Shinpaugh, K.A., 1992: *Description of a 1000 Sensor Constant Current Anemometer System for Locating Three-Dimensional Turbulent Boundary Layer Separations*, Report VPI-AOE-185, distributed by DTIC for Defense Advanced Research Projects Agency.

Smith, D. G.,1989: *Private Communication*, Aerodynamics Laboratory, Boeing Commercial Airplanes.

Wetzel, T.G. and Simpson, R.L., 1992(a): *The Effect of Vortex Generators on Crossflow Separation on a Submarine in a Turning Maneuver,* Report VPI-AOE-186, distributed by DTIC for Defense Advanced Research Projects Agency.

Wetzel, T.G. and Simpson, R.L., 1992(b): "The Effect of Vortex Generators on Crossflow Separation on a Submarine in a Turning Maneuver", *Proceedings of the Fifth Submarine Technology Symposium,* Applied Physics Laboratory, Johns Hopkins University, Laurel, Maryland, pp. 185-198.

Wetzel, T.G. and Simpson, R.L., 1993: *The Effect of Vortex Generating Fins and Jets on Crossflow Separation on a Submarine in a Turning Maneuver,* 31st Aerospace Sciences Meeting and Exhibit, Reno, Nevada, AIAA 93-0862.

Ziegler, H. and Wooler, P.T., 1978: *Aerodynamic Characteristics of a Jet Sheet Vortex Generator*, NASA-CR-158904.

Table 1. Boundary layer data at x/c=0.43. ϕ=90° for different *Re* and β.

Flow Parameter	S11	S12	S13	S14	S24	S34
Re (mill)	4.92	4.92	4.91	5.07	7.36	9.70
ß, °	0	5	10	15	15	15
δ (in)	0.498	0.526	0.417	0.356	0.275	0.216
δ*(in)	0.101	0.0858	0.0598	0.0508	0.0343	0.0299
θ(in)	0.0748	0.0610	0.0429	0.0382	0.0252	0.0217
Re_θ	3961	3523	2566	2657	2316	2363

Table 2. Mean separation location for select cases.

Side	ß,°	ϕ' Re=6.77 million	ϕ' Re=4.60 million
Sail Side	15	99.8	99.5
Bottom	15	108.8	101.6
Sail Side	10	130.1	113.5
Bottom	10	119.5	108.9

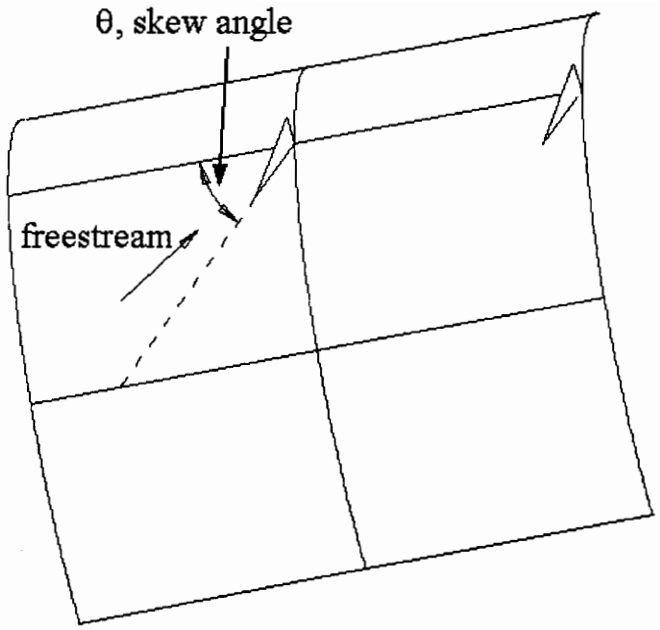

Figure 1. Fin configuration.

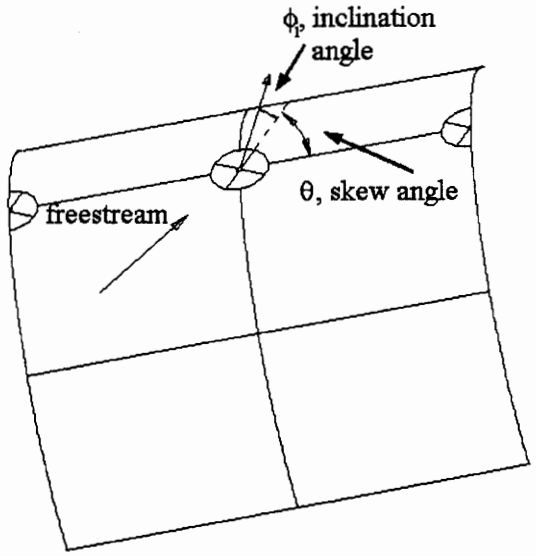

Figure 2. Jet configuration.

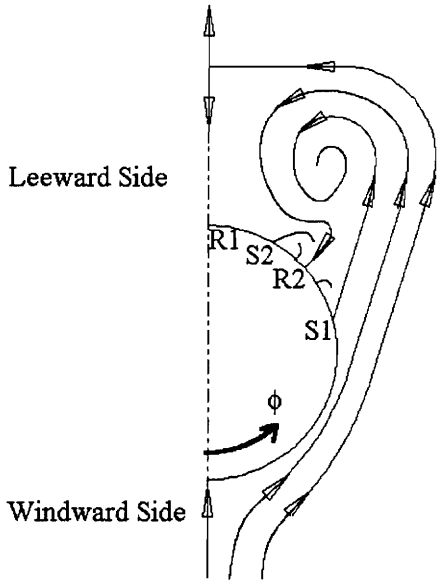

Figure 3. Crossflow separation (Ahn, 1992). This half-cross-section of the submarine shows the important flow phenomena. The addition of vortex generators delays separation (S1 and S2) farther around the leeward side of the submarine. Primary separation (S1) is the flow phenomenon discussed in this report.

Figure 4. Submarine Model 1.

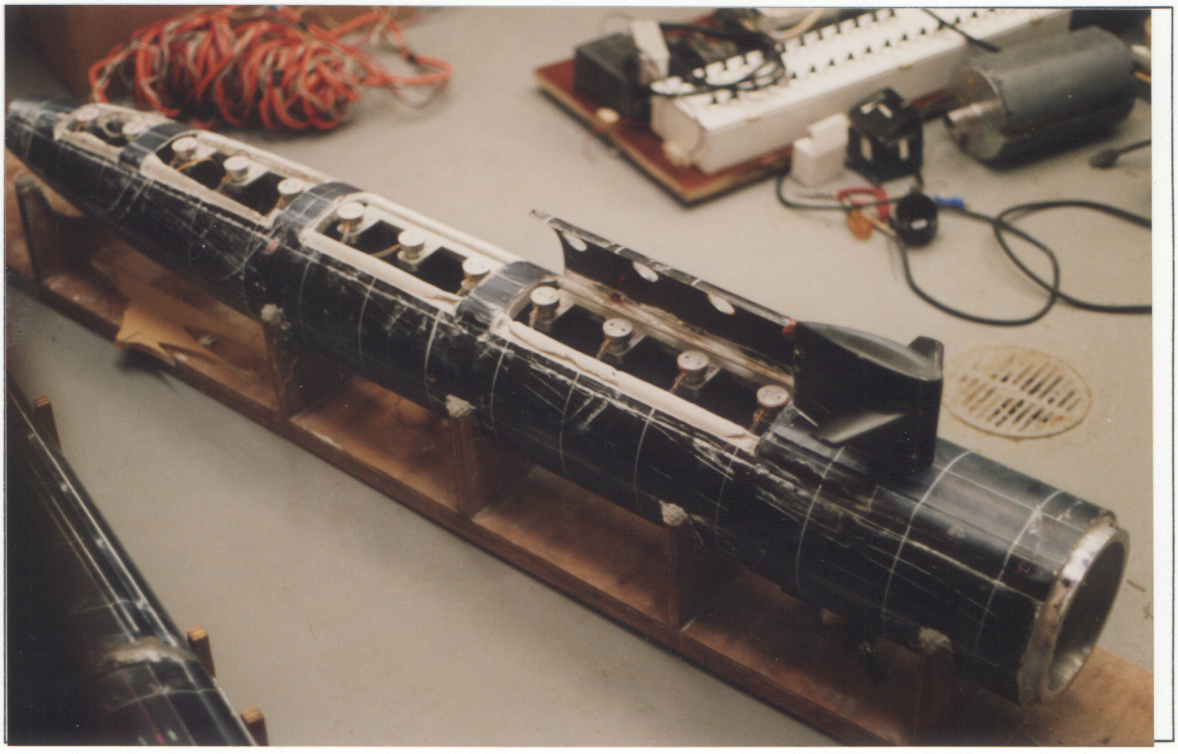

Figure 5. Submarine Model 2.

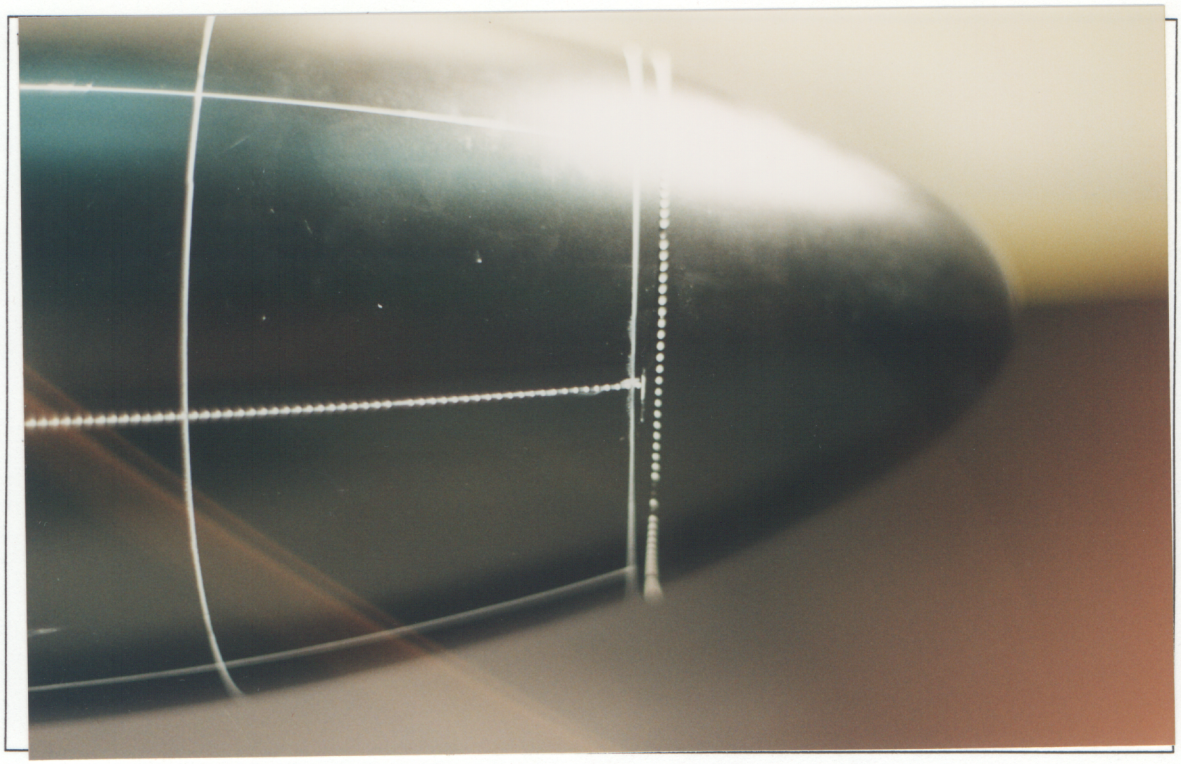

Figure 6. Trip strips.

Figure 7. Model in the wind tunnel.

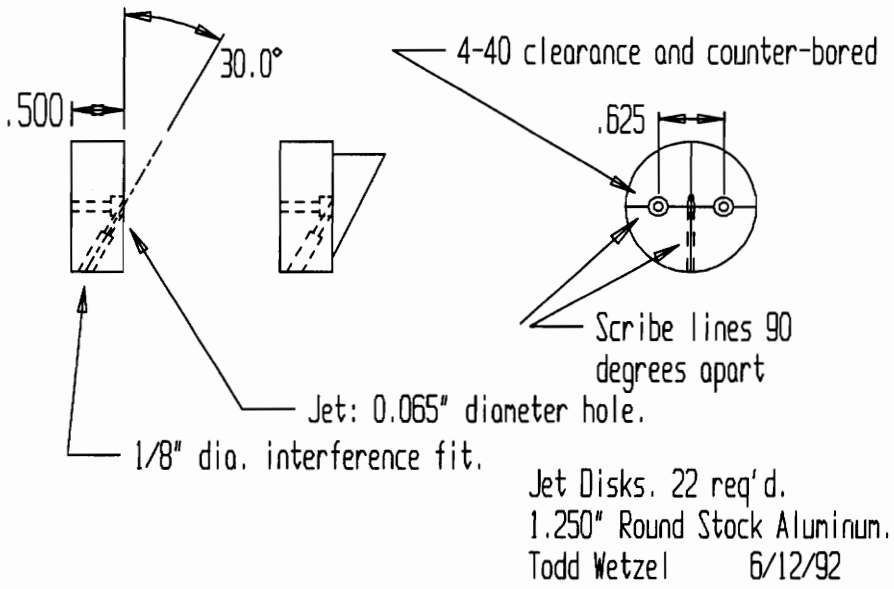

Figure 8. Typical jet disk construction, Model 2. Also shown is fin mounted to such a disk.

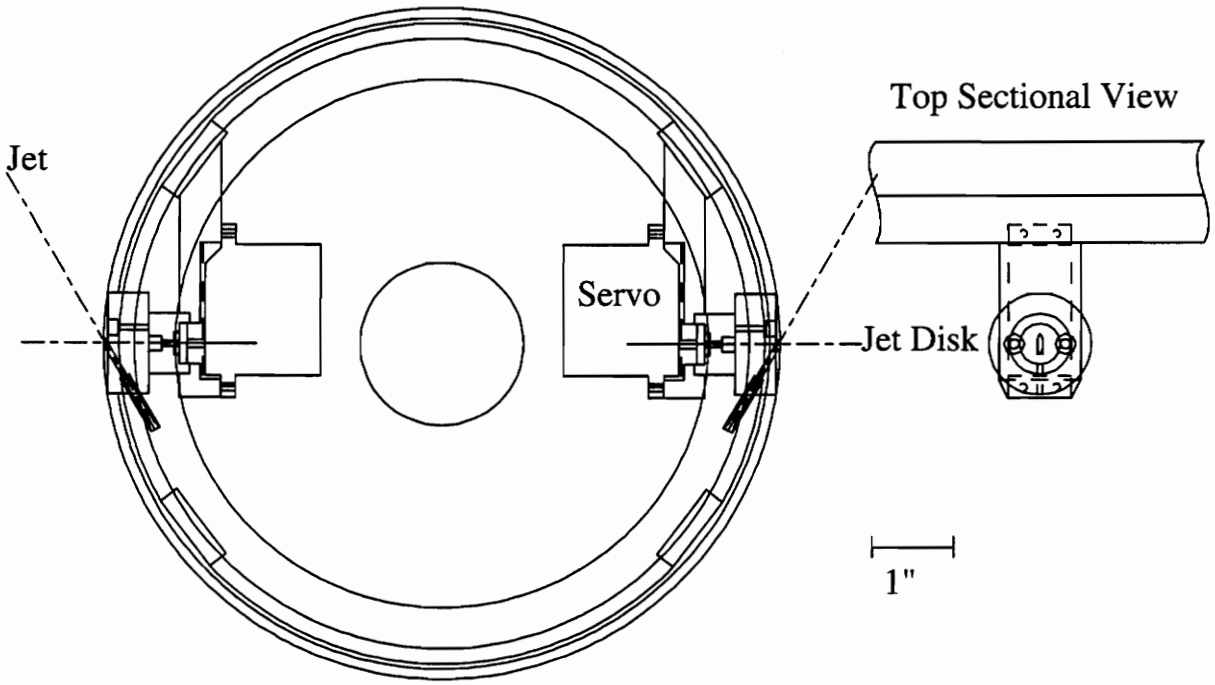

Figure 9. Model 2 cross section configuration.

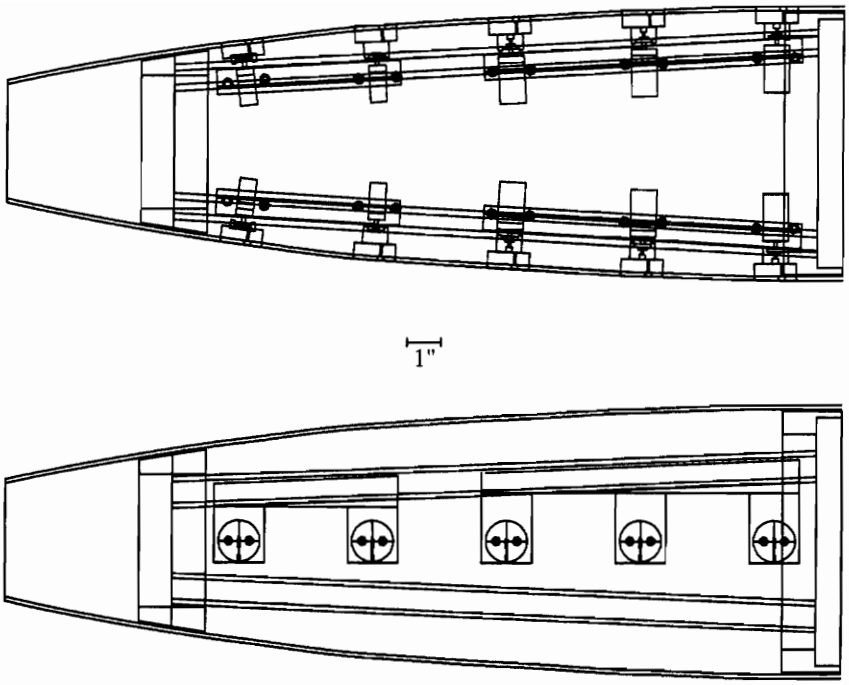

Figure 10. Model 2 tail configuration top and side views.

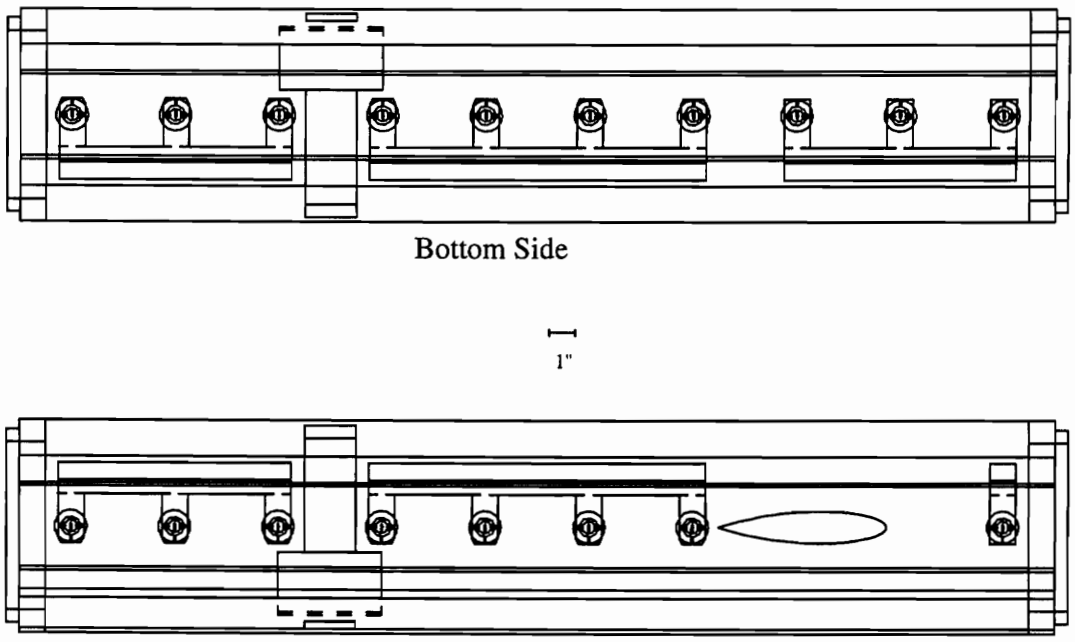

Figure 11. Model 2 midbody side views (sail side and bottom side).

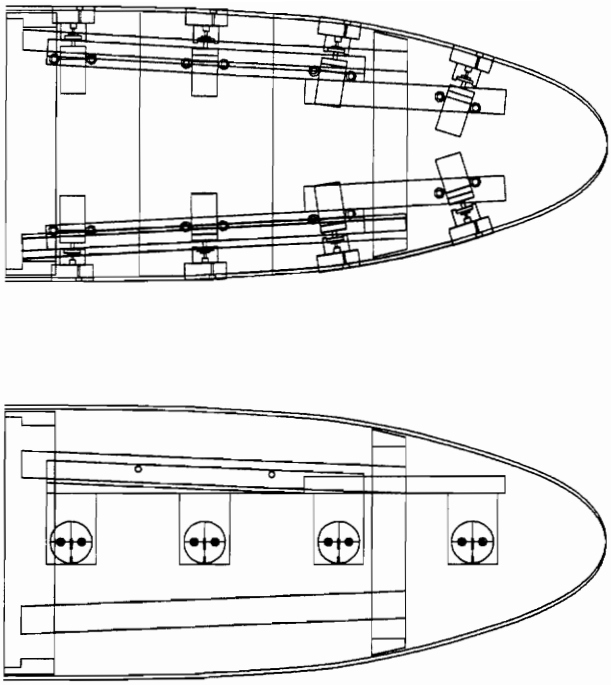

Figure 12. Model 2 nose configuration top and side views.

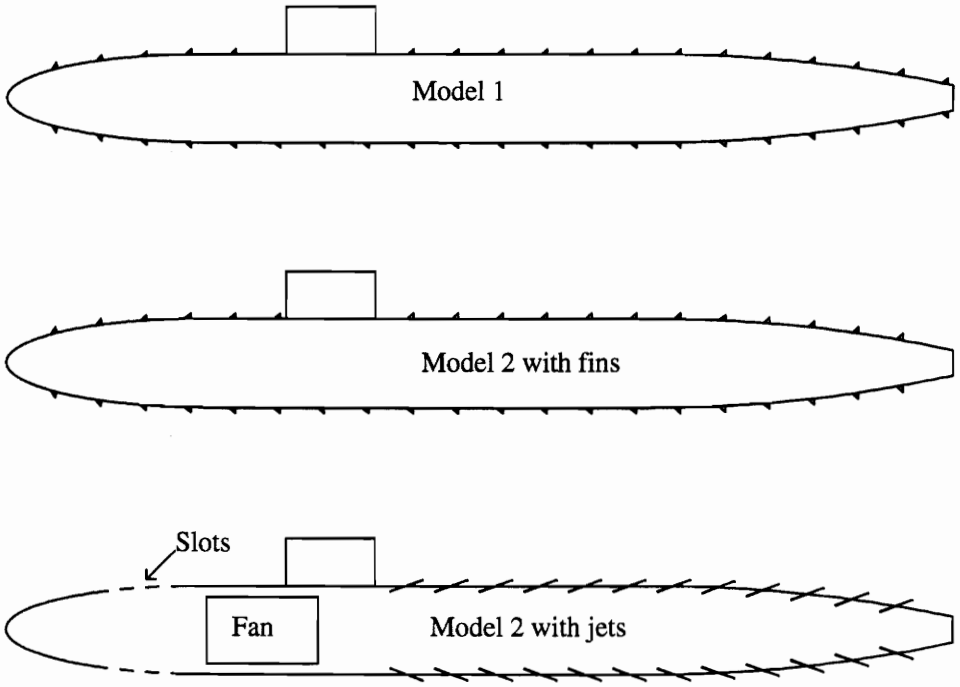

Figure 13.Model fin and jet configurations.

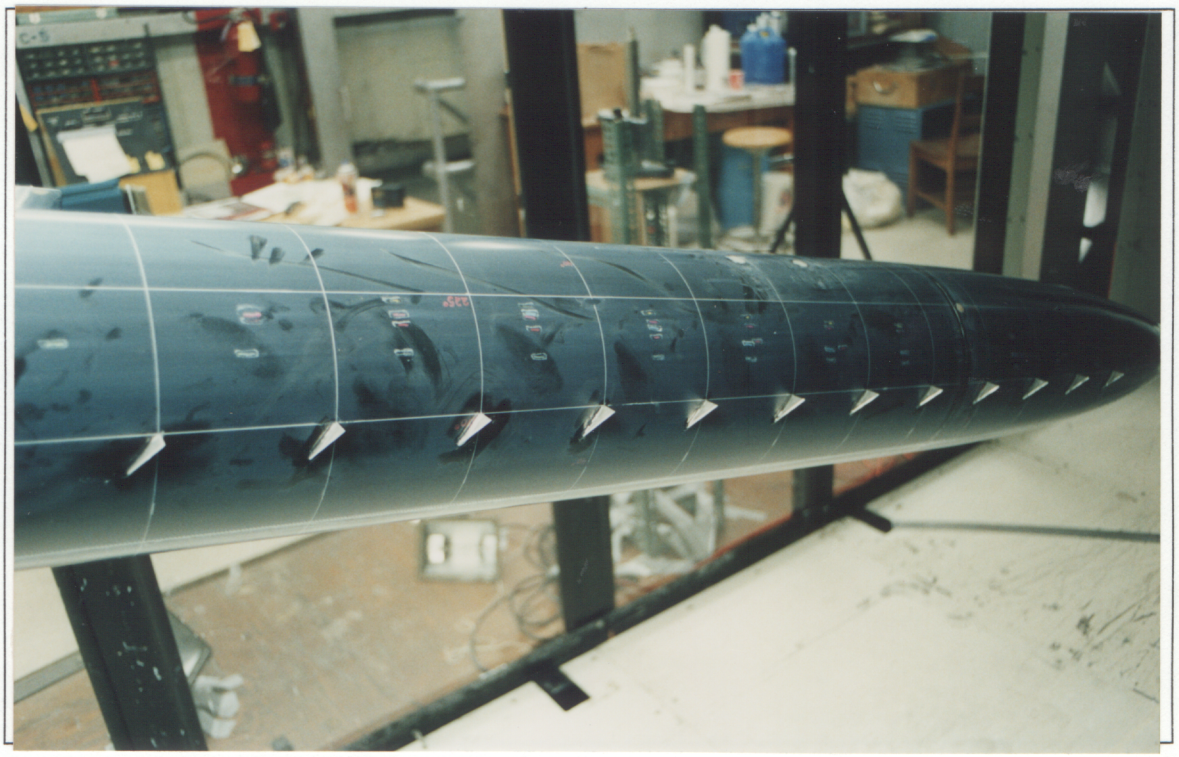

Figure 14. Fins glued on Model 1.

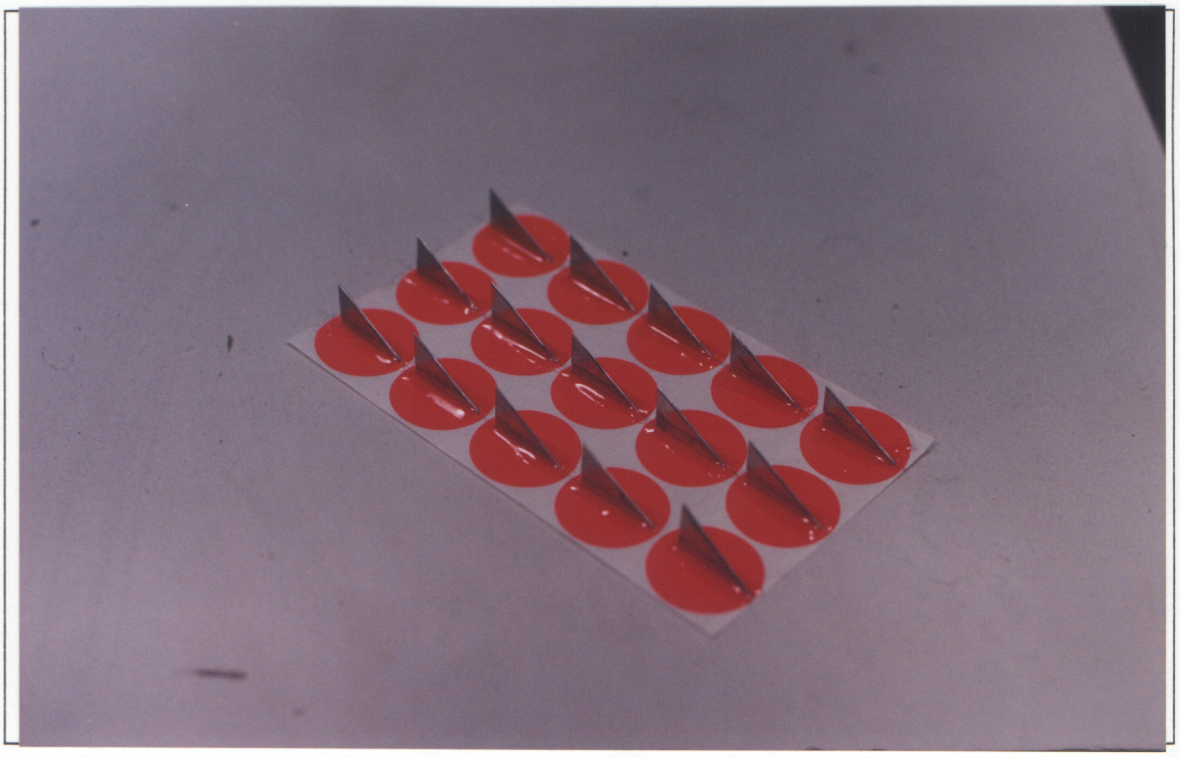

Figure 15. Fins glued to stickers.

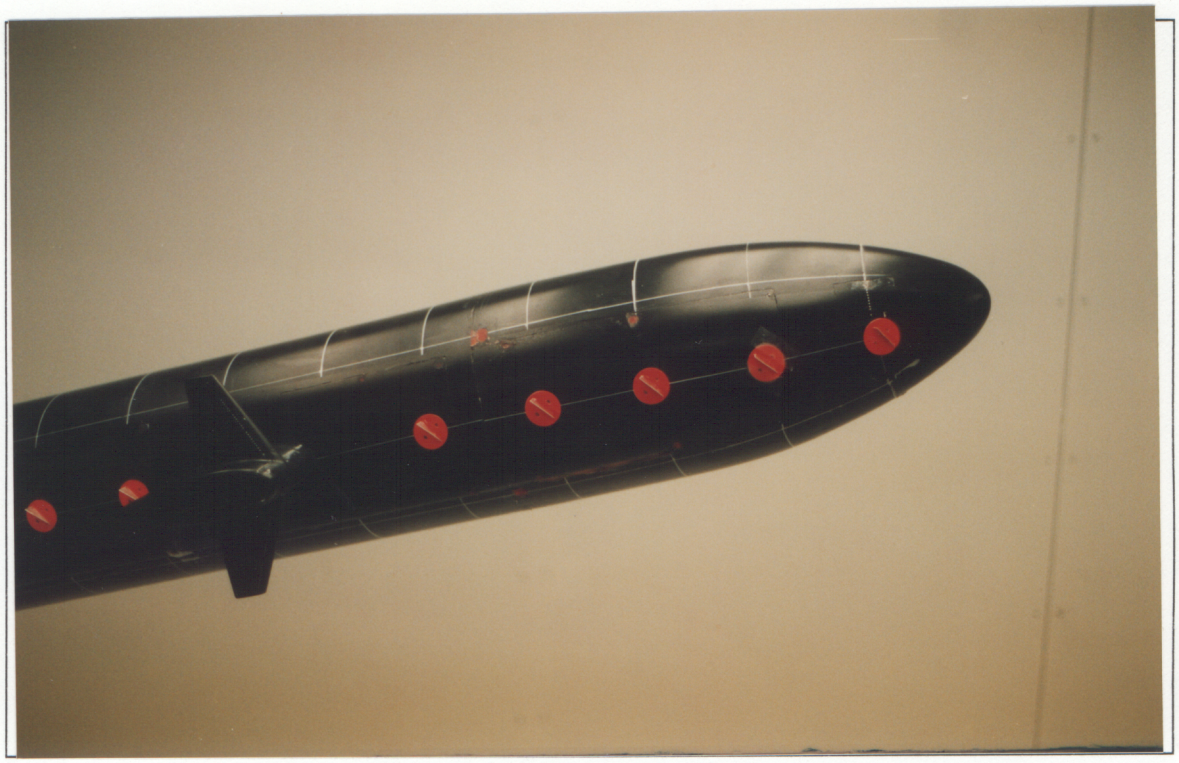

Figure 16. Fins on stickers stuck to Model 2.

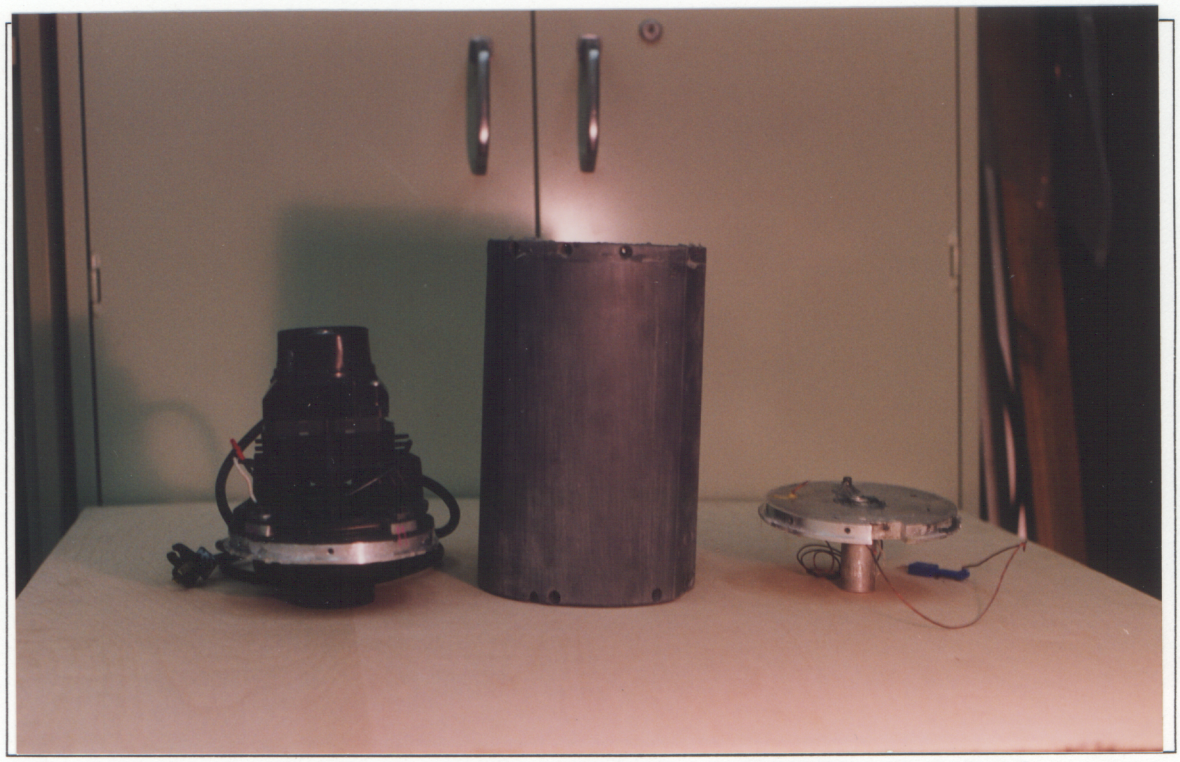

Figure 17. Fan motor (left), housing (middle), and end plate(right). End plate has pressure transducer and thermocouple embedded in it.

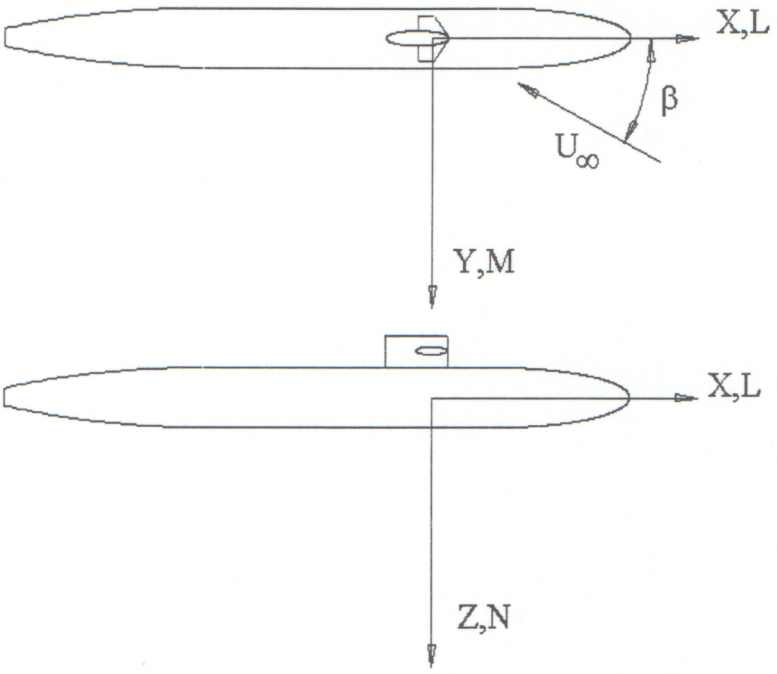

Figure 18. Body axes notation.

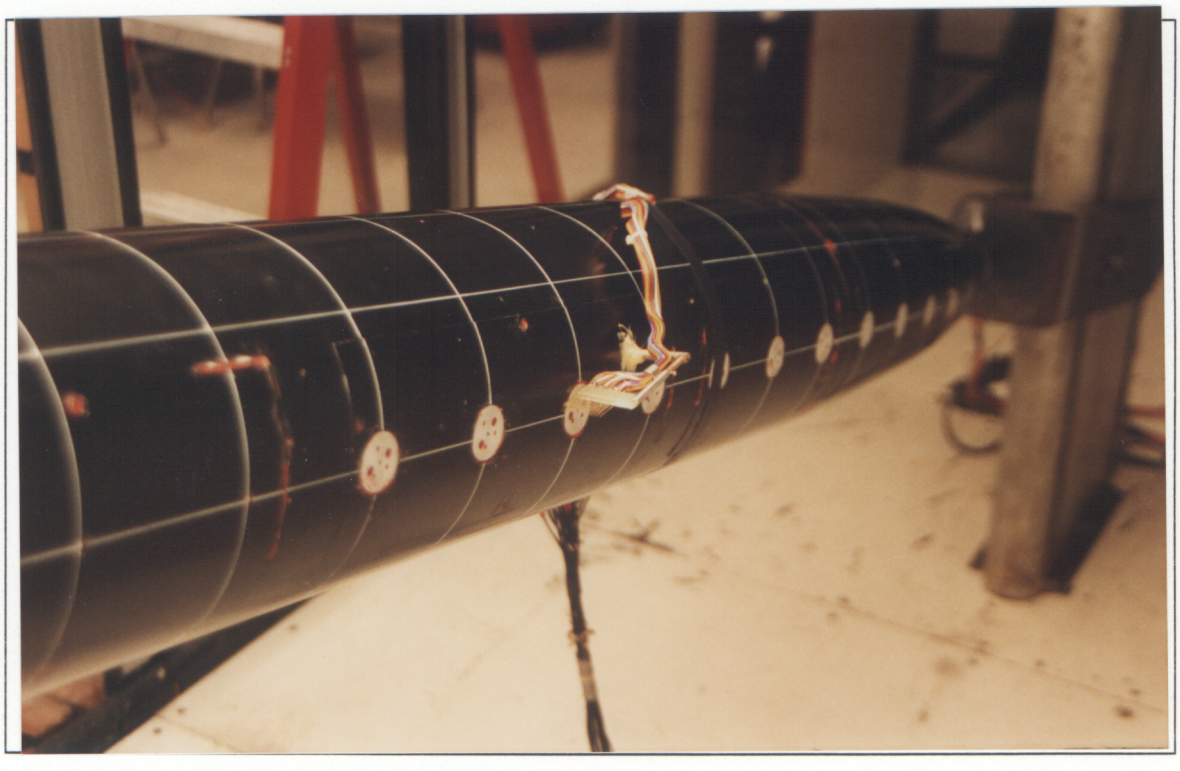

Figure 19. Hot wire rake mounted on Model 2.

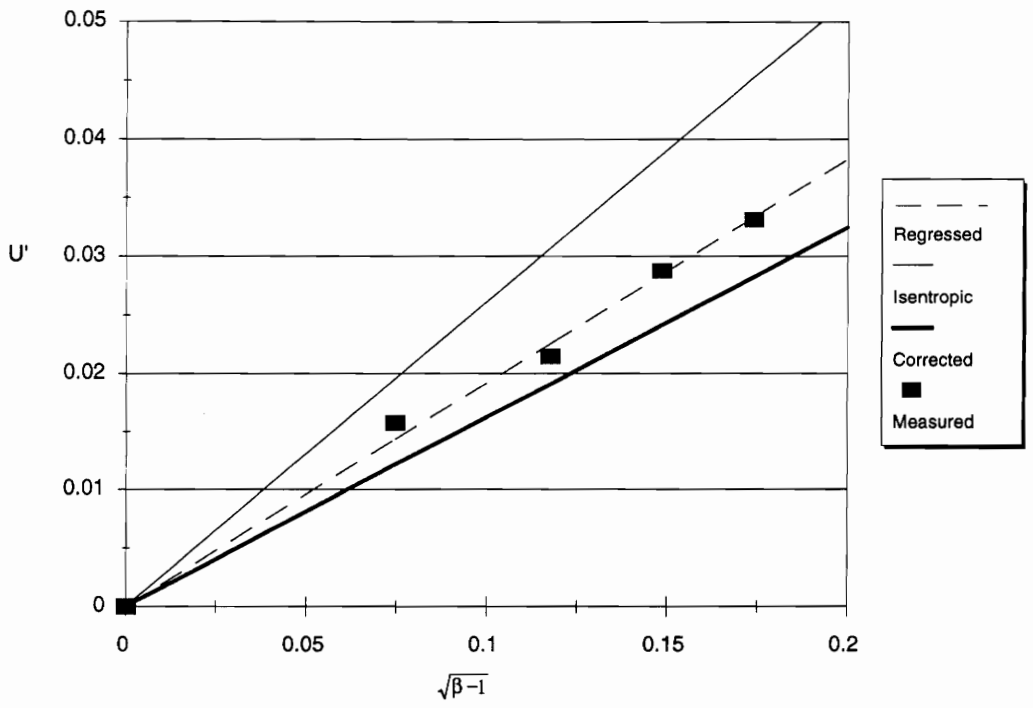

Figure 20. Jet speed calibration. Isentropic predictions (solid line) tend to be high, while the results corrected for losses (heavy line) are too low. The jet speed was finally calibrated with a rotameter (squares). The dashed line is the linear regression of the measured data.

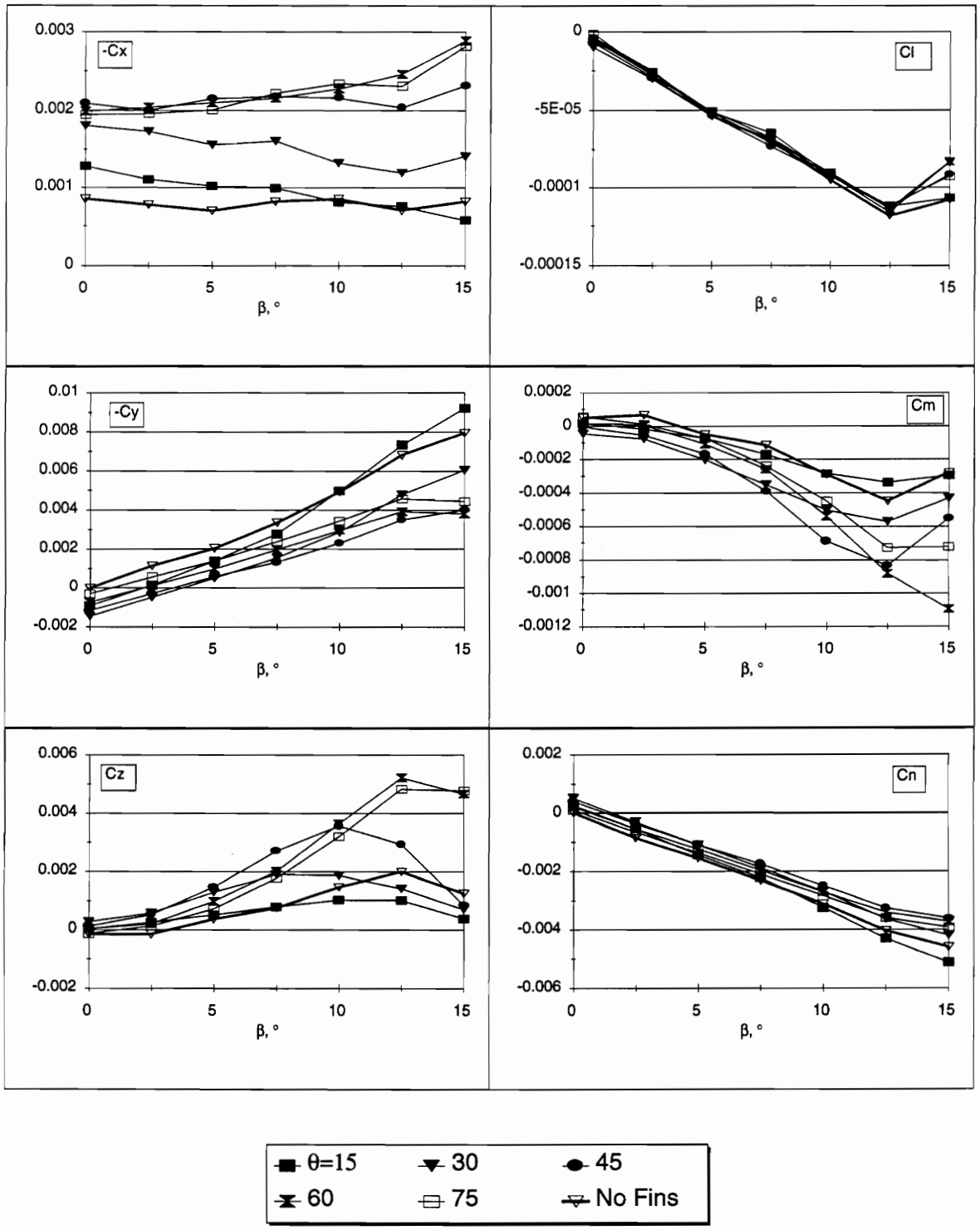

Figure 21. Forces and moments versus sideslip for different θ for Model 2 with fins. Re = 6.8 million.

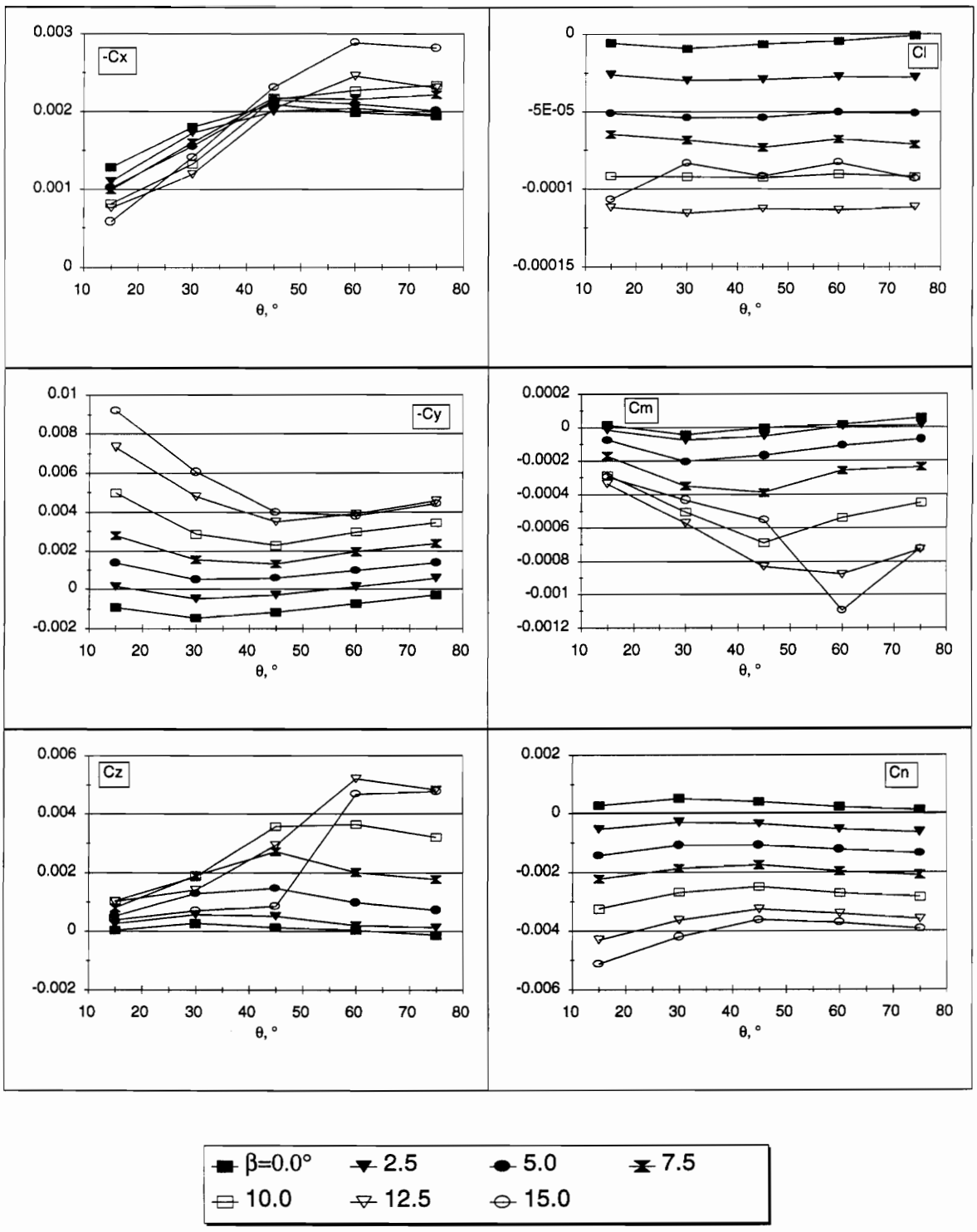

Figure 22. Forces and moments versus θ (skew referenced from model centerline) for the Model 2 with fins. Re=6.8 million.

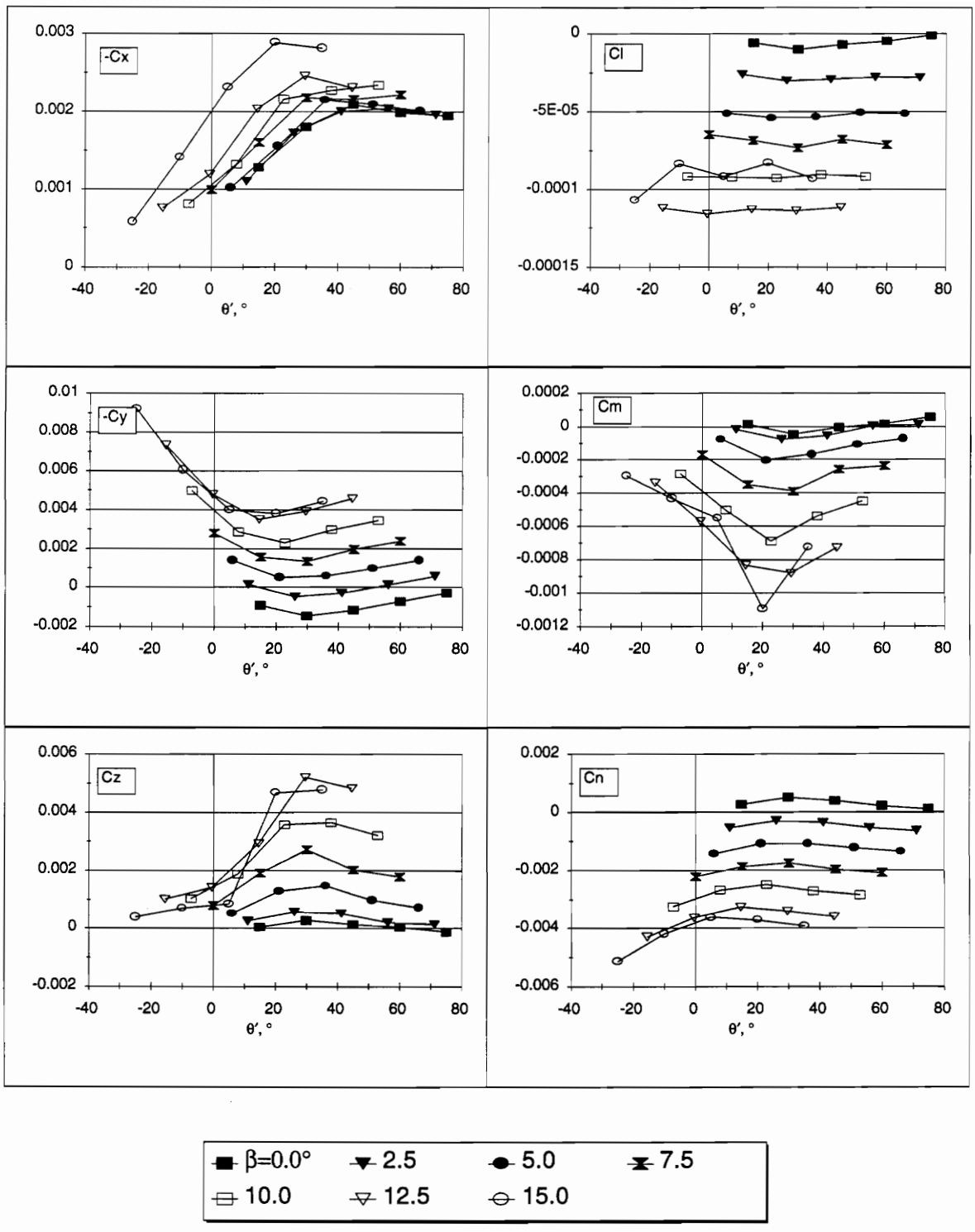

Figure 23. Forces and moments versus θ' (skew referenced from average local flow direction) for Model 2 with fins. Re=6.8 million.

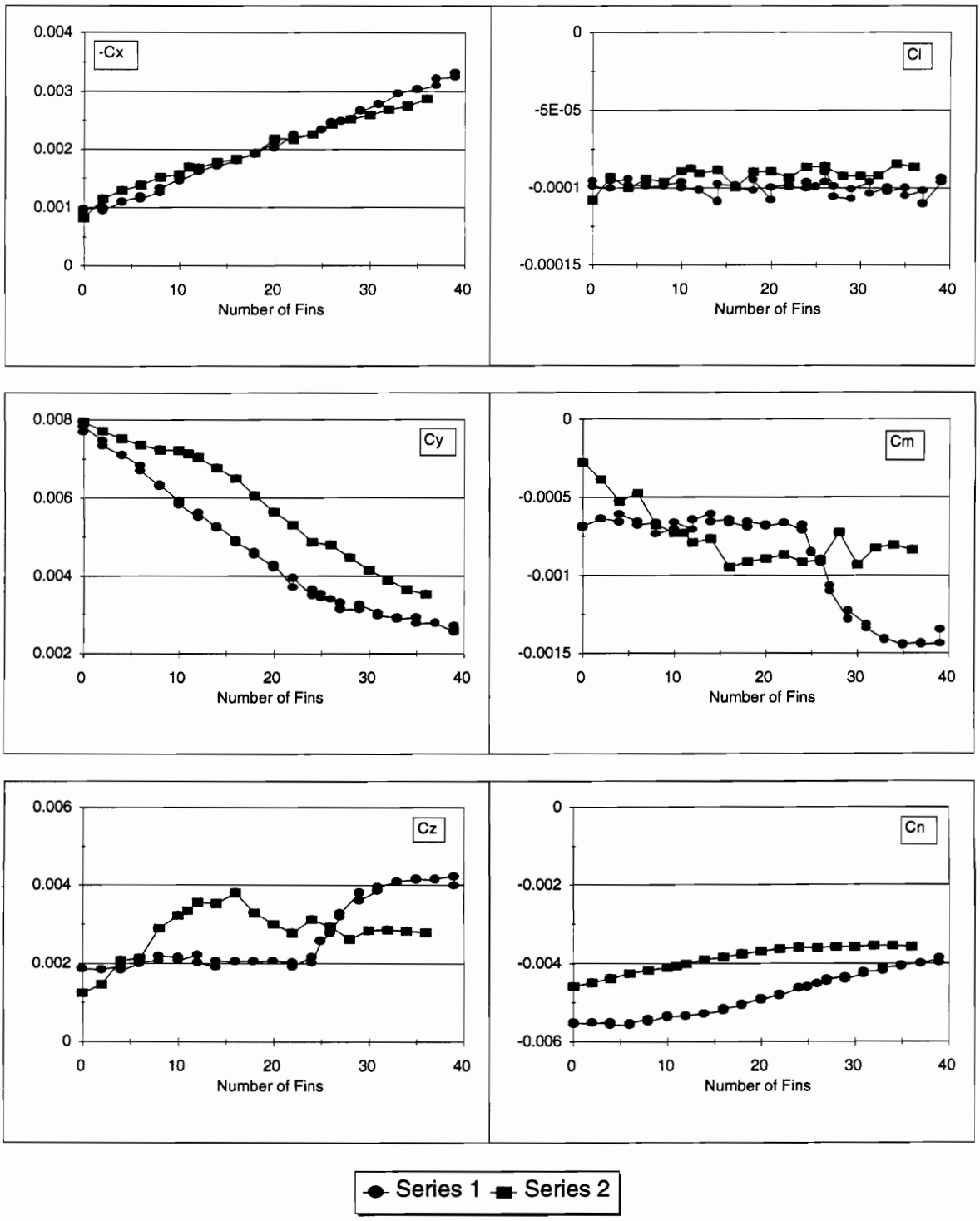

Figure 24. Forces and moments versus number of vortex fins. ß=15°, θ=55°, Re=6.8 million. Series 1 involved removing fins from the nose rearward, while Series 2 involved removing fins from the tail forward. Series 1 utilized Model 1 while Series 2 utilized Model 2.

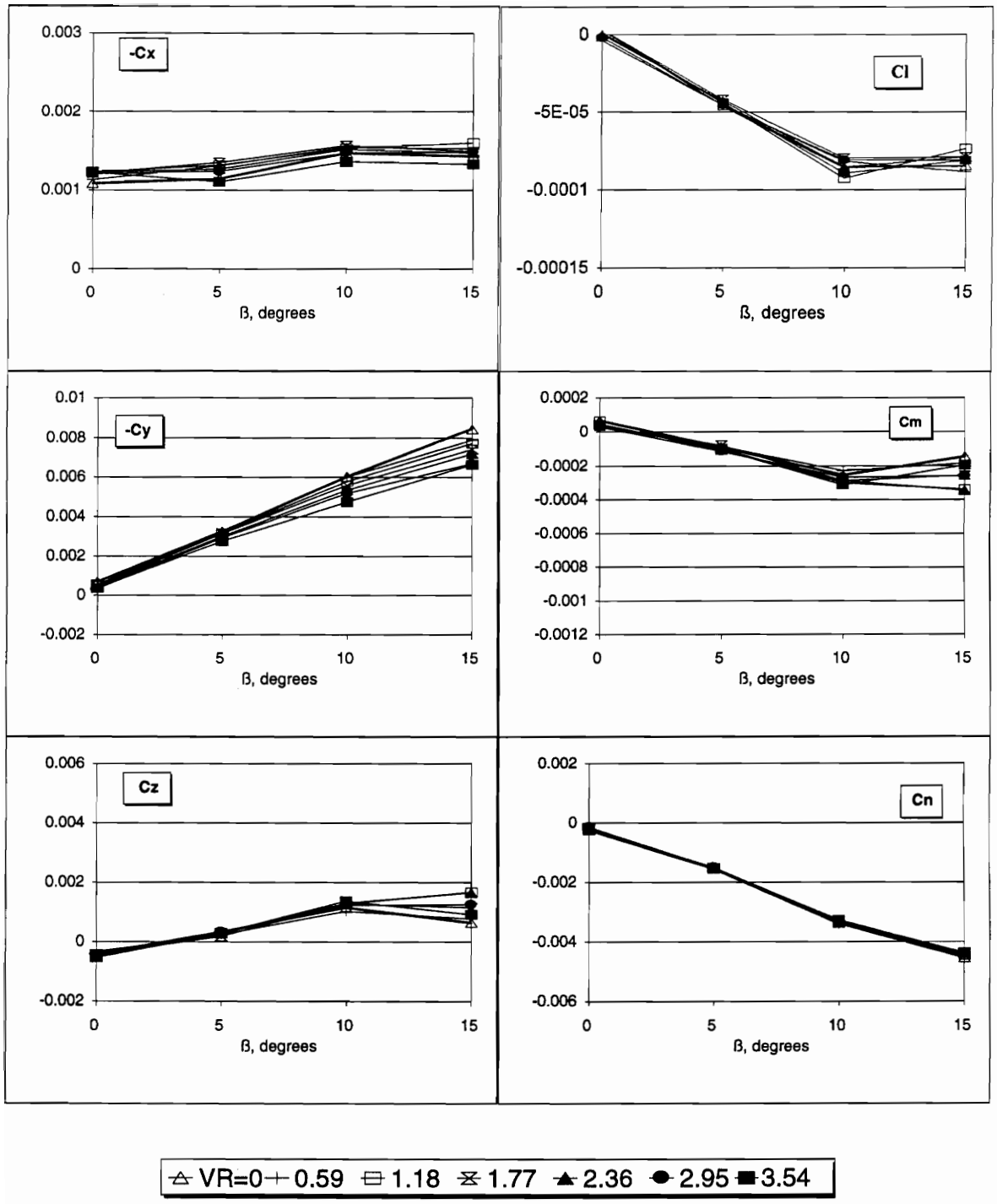

Figure 25. Forces and moments versus sideslip for different VR for Model 2 with jets. θ = 90°, Re=4.6 million.

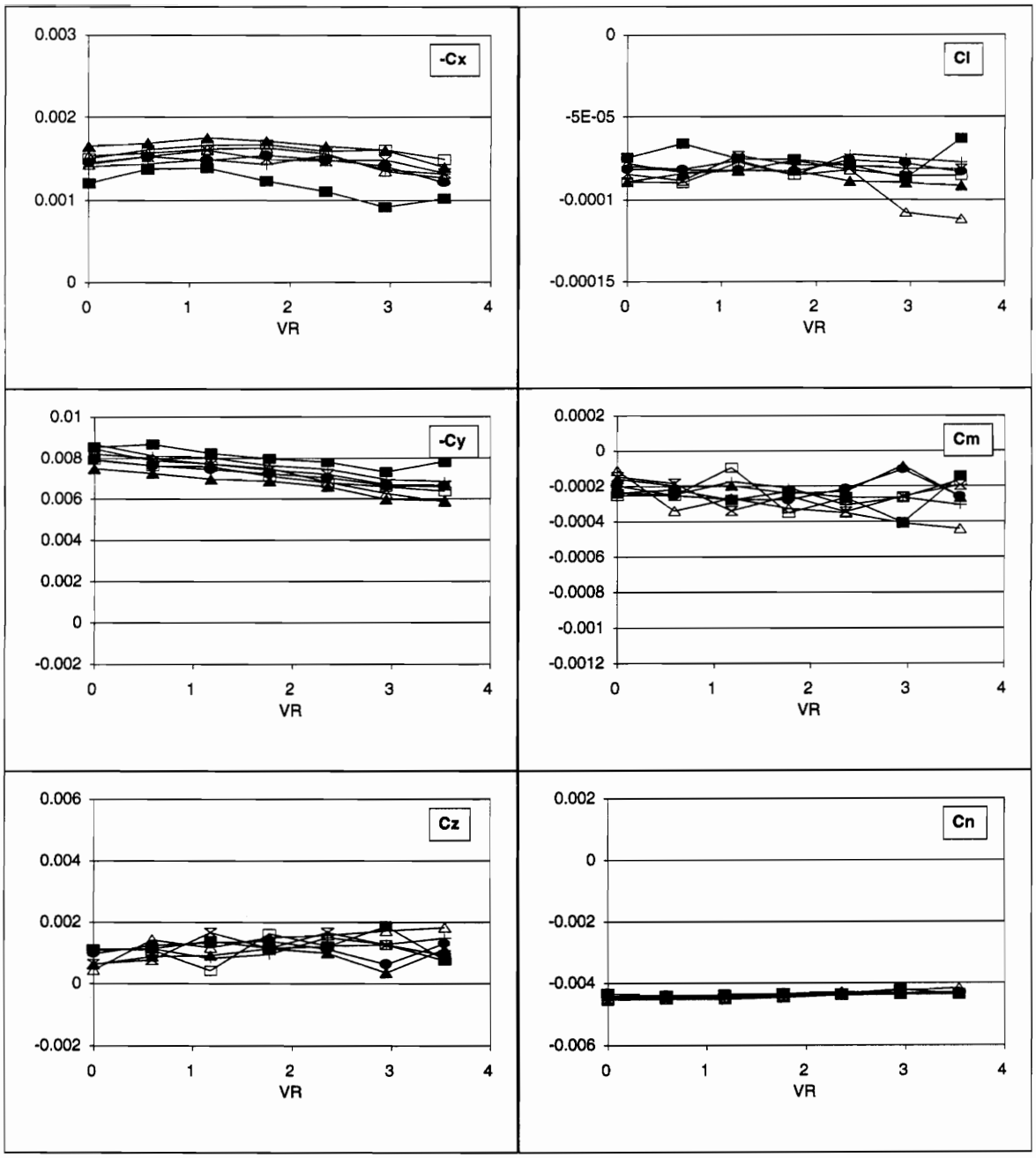

Figure 26. Forces and moments versus VR for different skew angles for Model 2 with jets. ß=15°, Re=4.6 million.

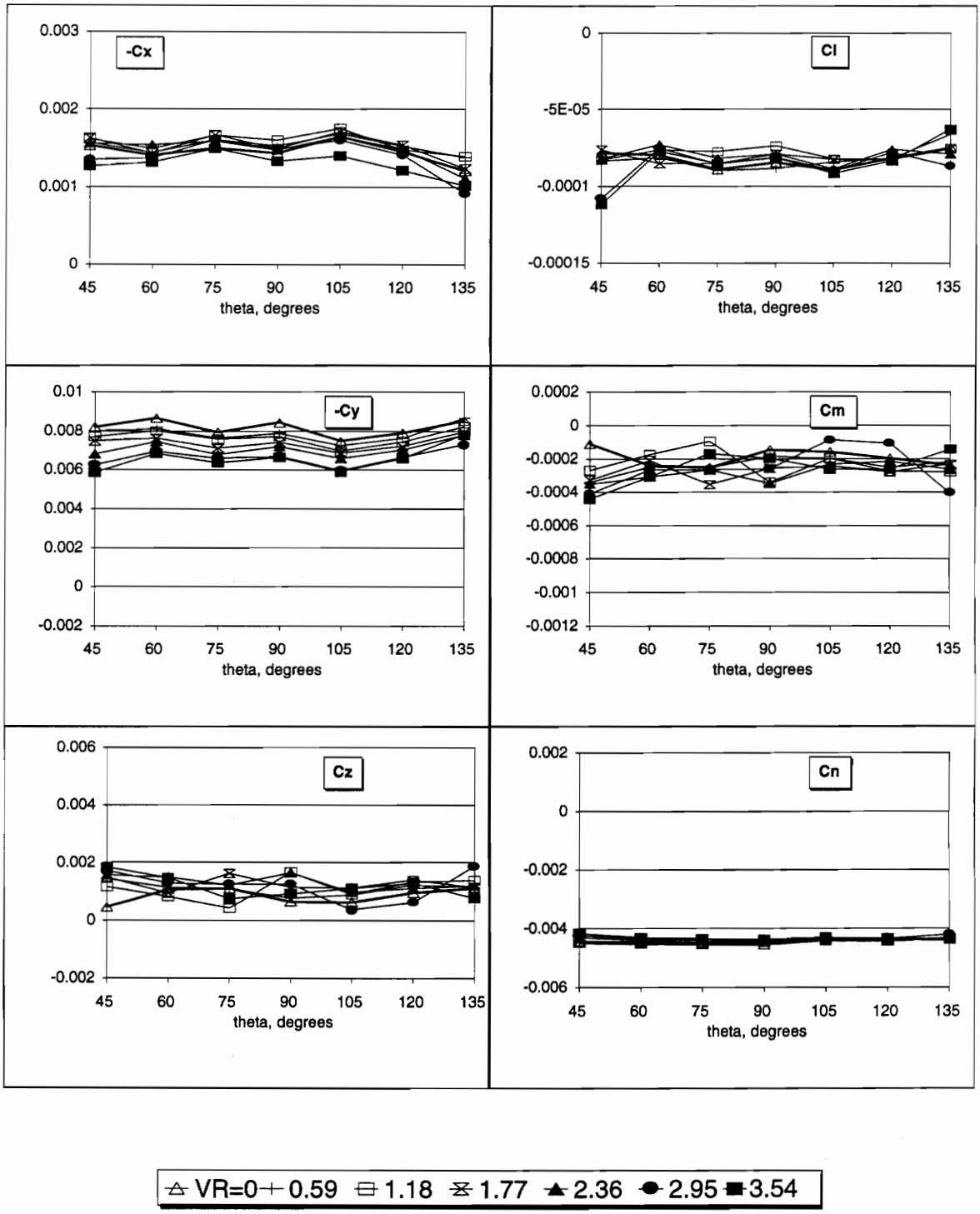

Figure 27. Forces and moments versus skew angle theta for different VR's for Model 2 with jets. Re=4.6 million, ß=15°.

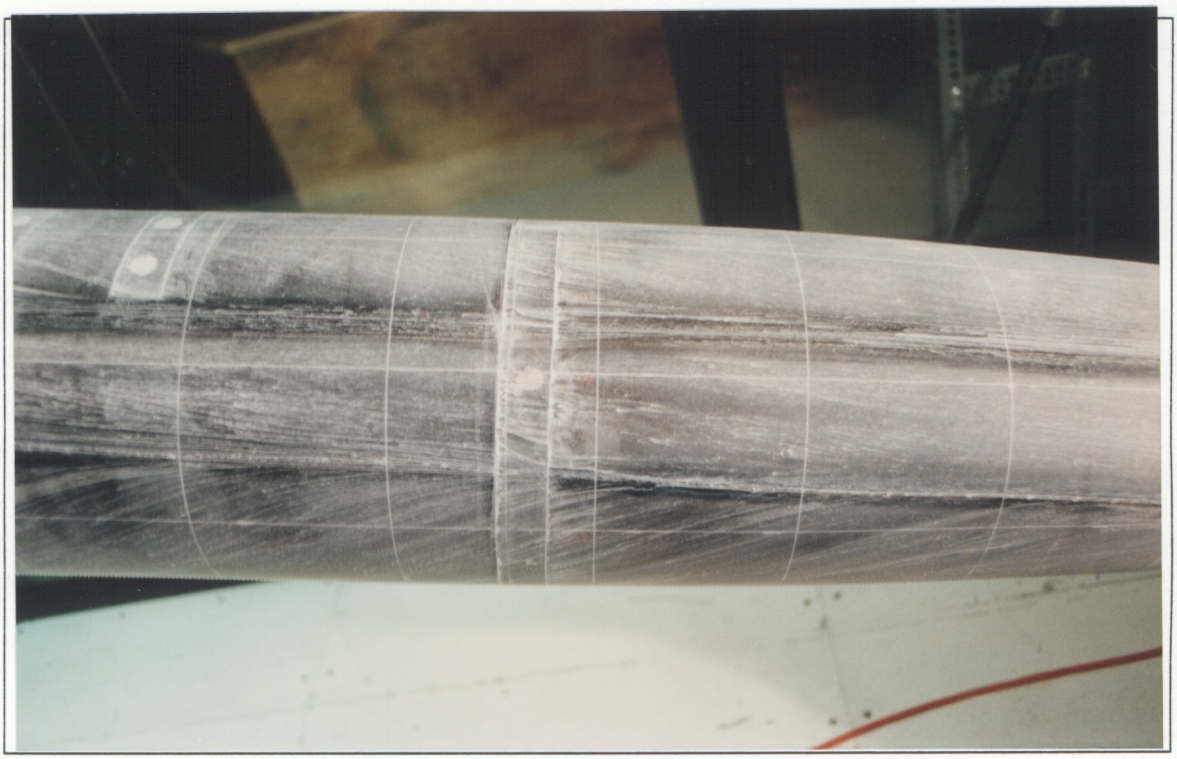

Figure 28. Oil flow 3, Model 1, naked submarine, β=15°, Re = 6.8 million.

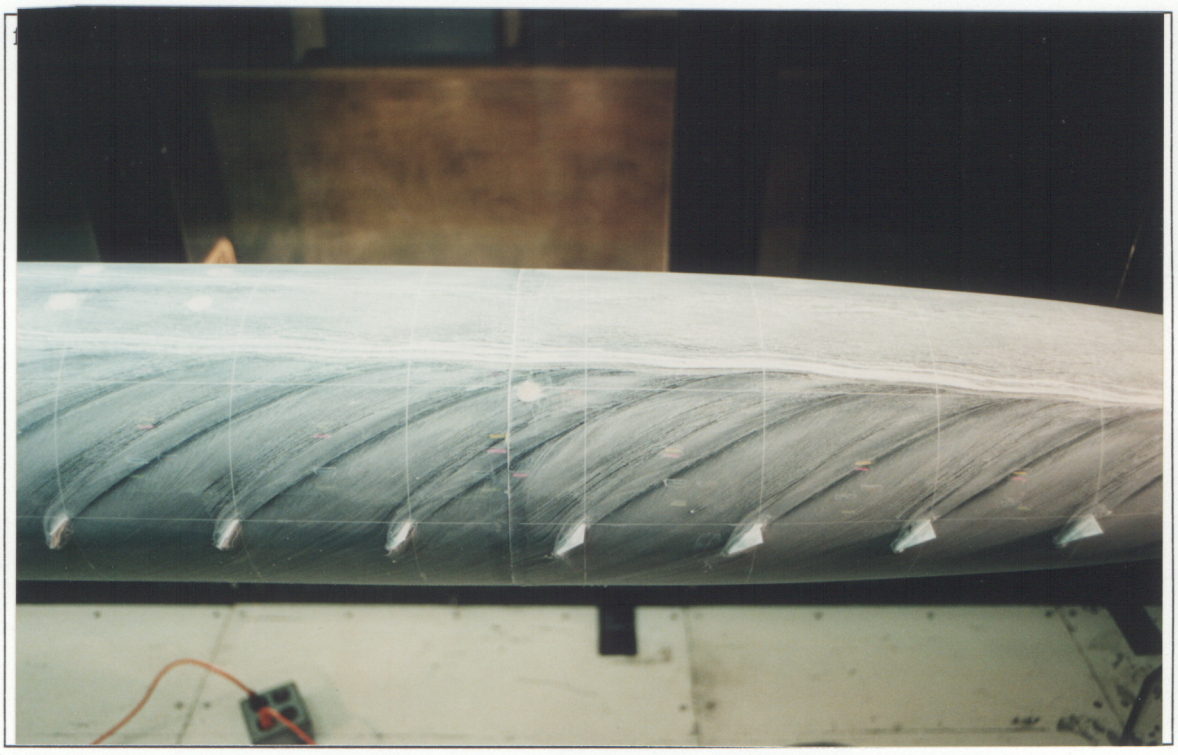

Figure 29. Oil flow 20, Model 1, submarine with fins, β=15°, Re = 6.4 million.

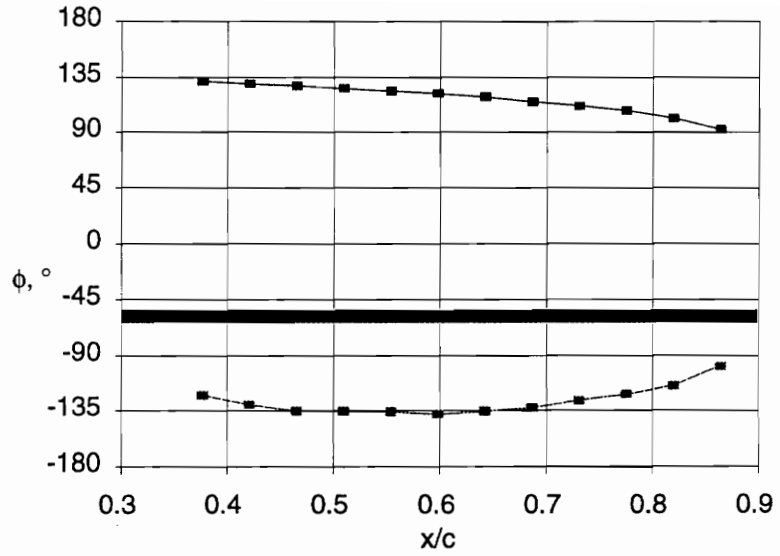

Figure 30. Separation line for oil flow 7. Naked submarine, Re = 6.8 million, β=10°. Shaded bar represents towed array housing.

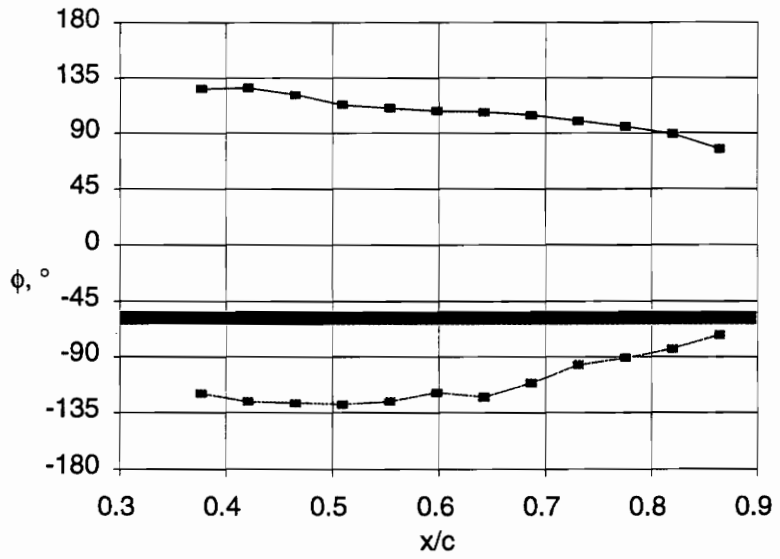

Figure 31. Separation line for oil flow 8. Naked submarine, Re = 4.5 million, β=10°. Shaded bar represents towed array housing.

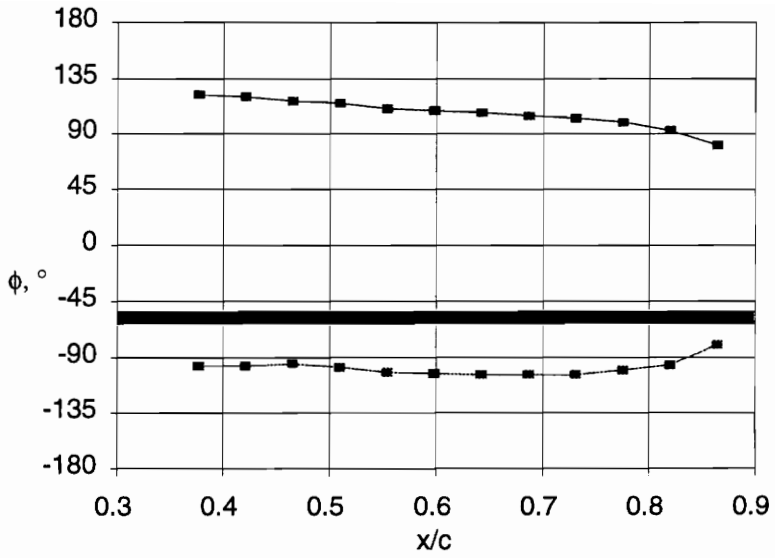

Figure 32. Separation line for oil flow 9. Naked submarine, Re =6.8 million, β=15°. Shaded bar represents towed array housing.

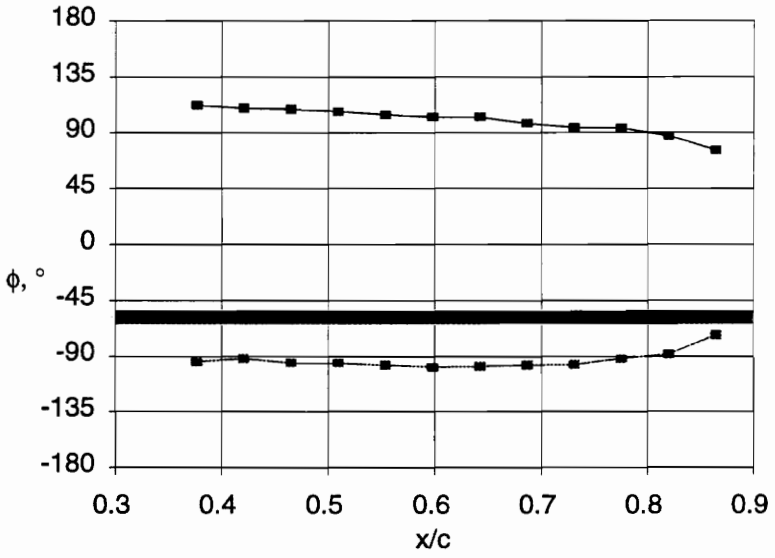

Figure 33. Separation line for oil flow 10. Naked submarine, Re = 4.5 million, β=15°. Shaded bar represents towed array housing.

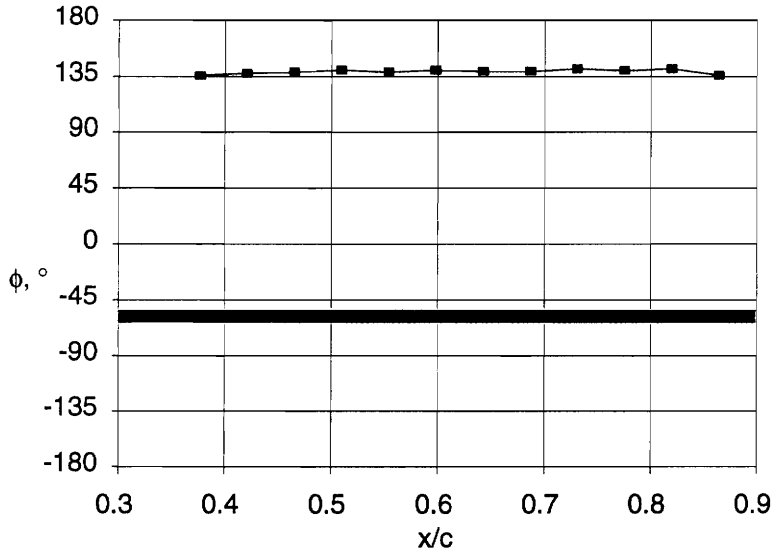

Figure 34. Separation line for oil flow 15. Bottom side, with fins on bottom only from x = 24" to x = 72", Re =6.8 million, β=15°. Shaded bar represents towed array housing.

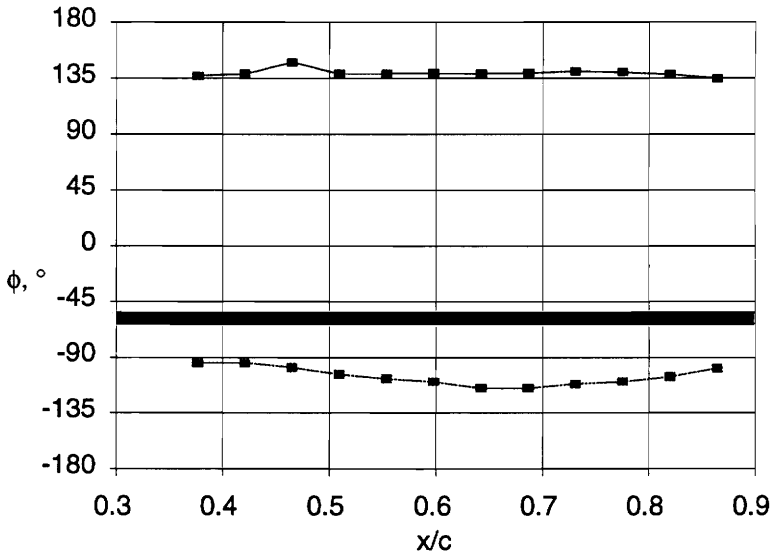

Figure 35. Separation line for oil flow 16. On the sail side, small vortex generators at ϕ = -60° extend from x = 12" to x = 76". On the bottom side, large vortex generators extend from x = 24" to x = 72". Re =6.8 million, β=15°. Shaded bar represents towed array housing.

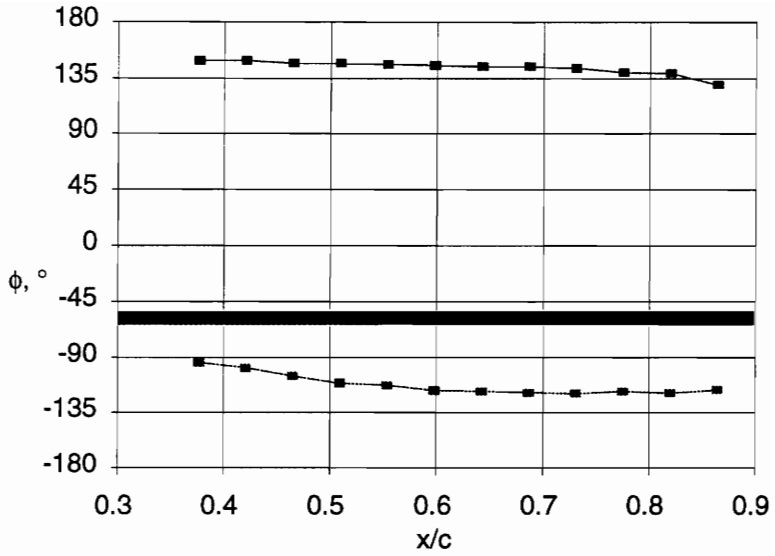

Figure 36. Separation line for oil flow 17. On the sail side, small vortex generators relocated to ϕ = -90° extend from x = 12" to x = 76". On the bottom side, large vortex generators extend from x = 12" to x = 76". Re =6.8 million, β=15°. Shaded bar represents towed array housing.

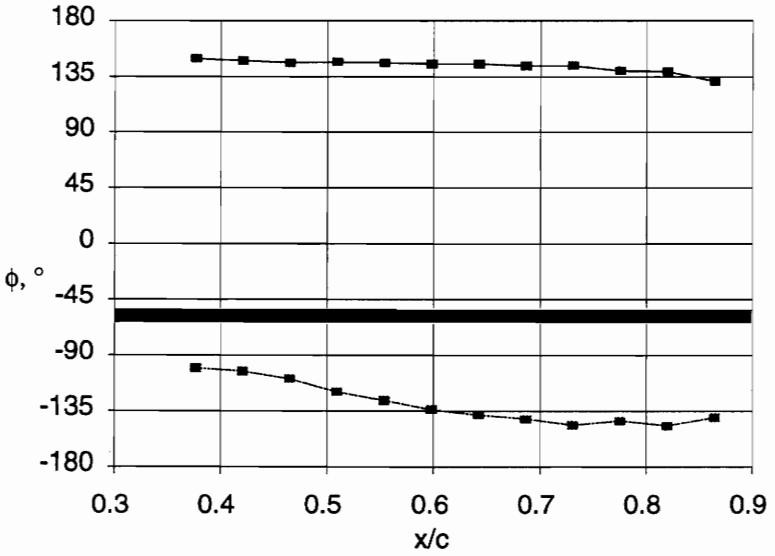

Figure 37. Separation line for oil flow 19. On both sides, large vortex generators extend from x = 8" to x = 80", with two additional vortex generators at x = 8", ϕ = +/-135°, and inclined 30° off centerline. Re =6.5 million, β=15°. Shaded bar represents towed array housing.

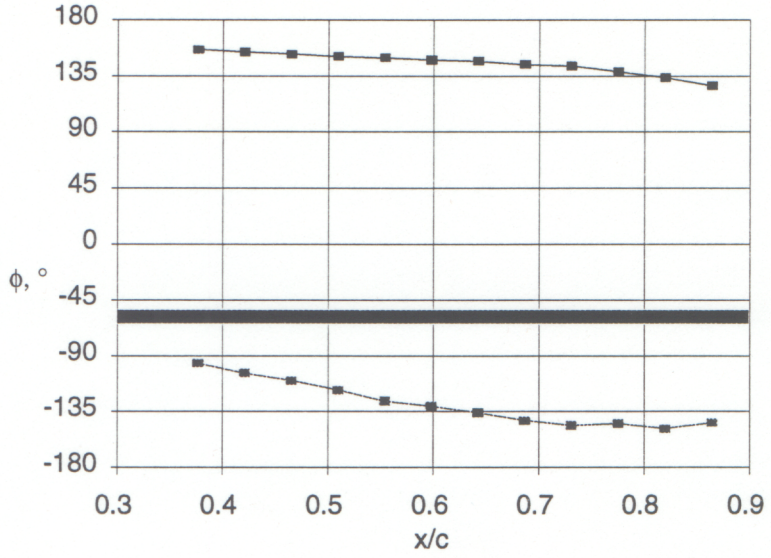

Figure 38. Separation line for oil flow 20. On both sides, large vortex generators extend from x = 8" to x = 80", with two additional vortex generators at x = 8", ϕ = +/-135°, and inclined 55° off centerline. Re =6.8 million, β=10°. Shaded bar represents towed array housing.

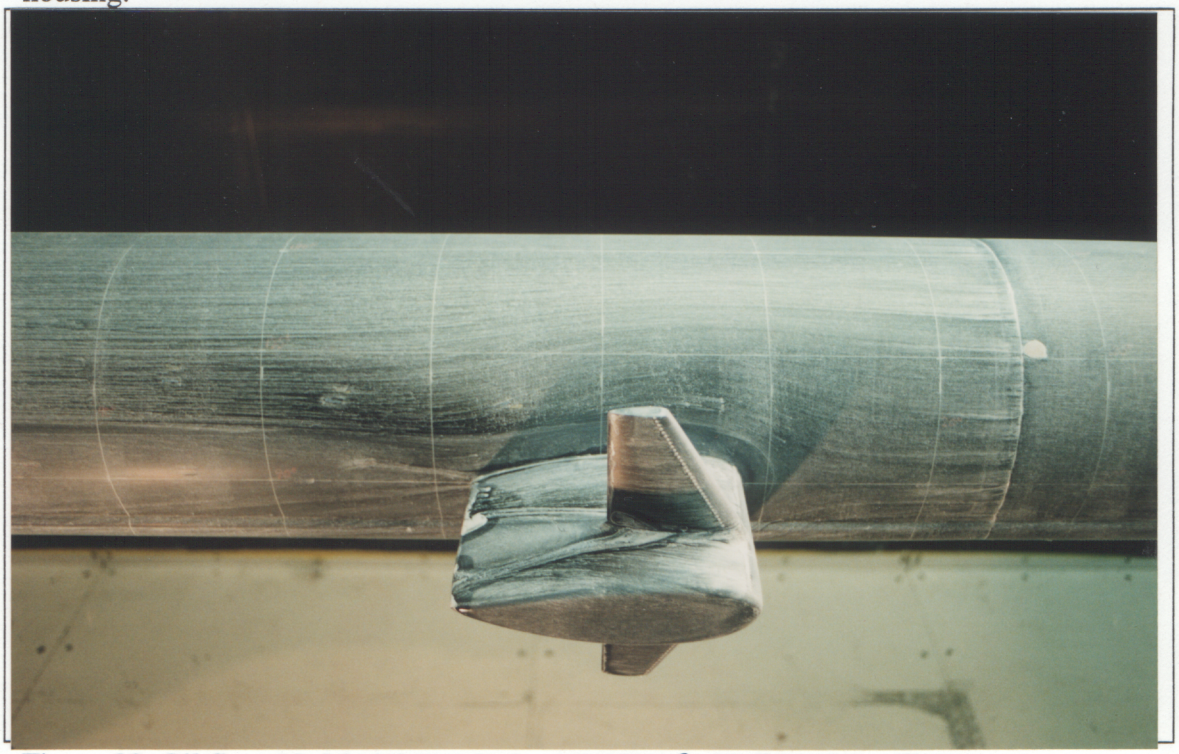

Figure 39. Oil flow 13, Model 1, naked submarine, β=0°, Re = 6.9 million.

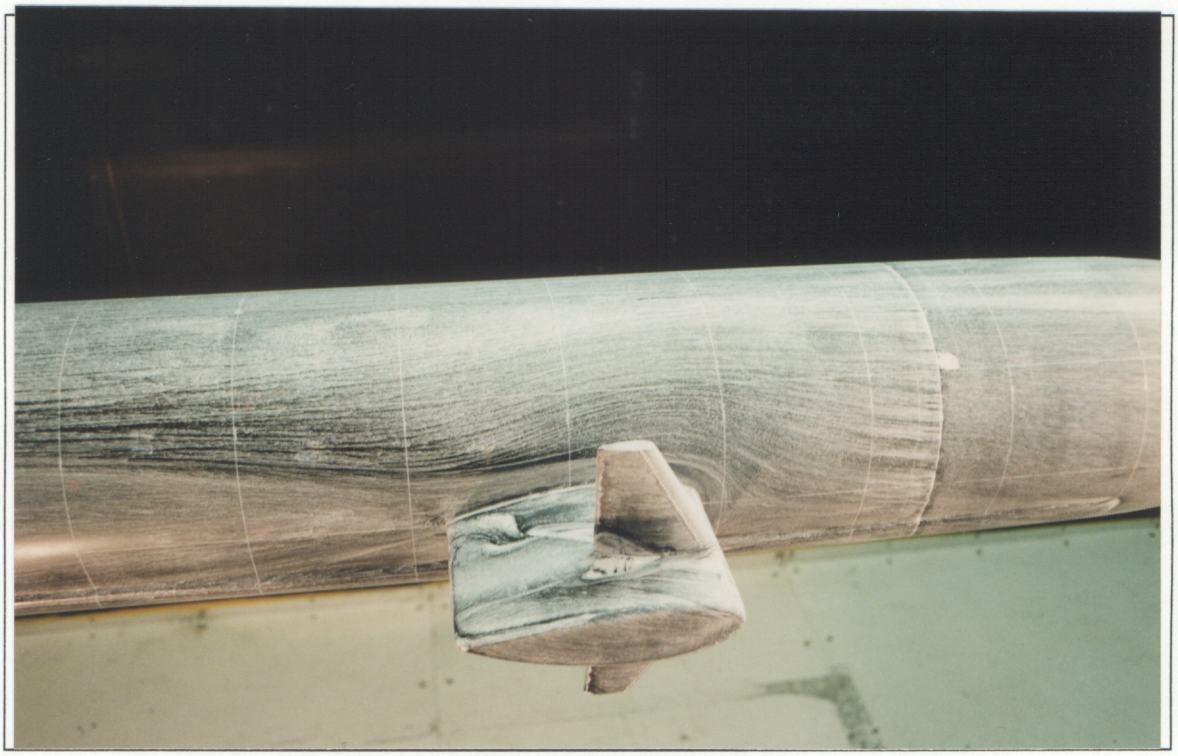

Figure 40. Oil flow 13, Model 1, naked submarine, β=5°, Re = 6.9 million.

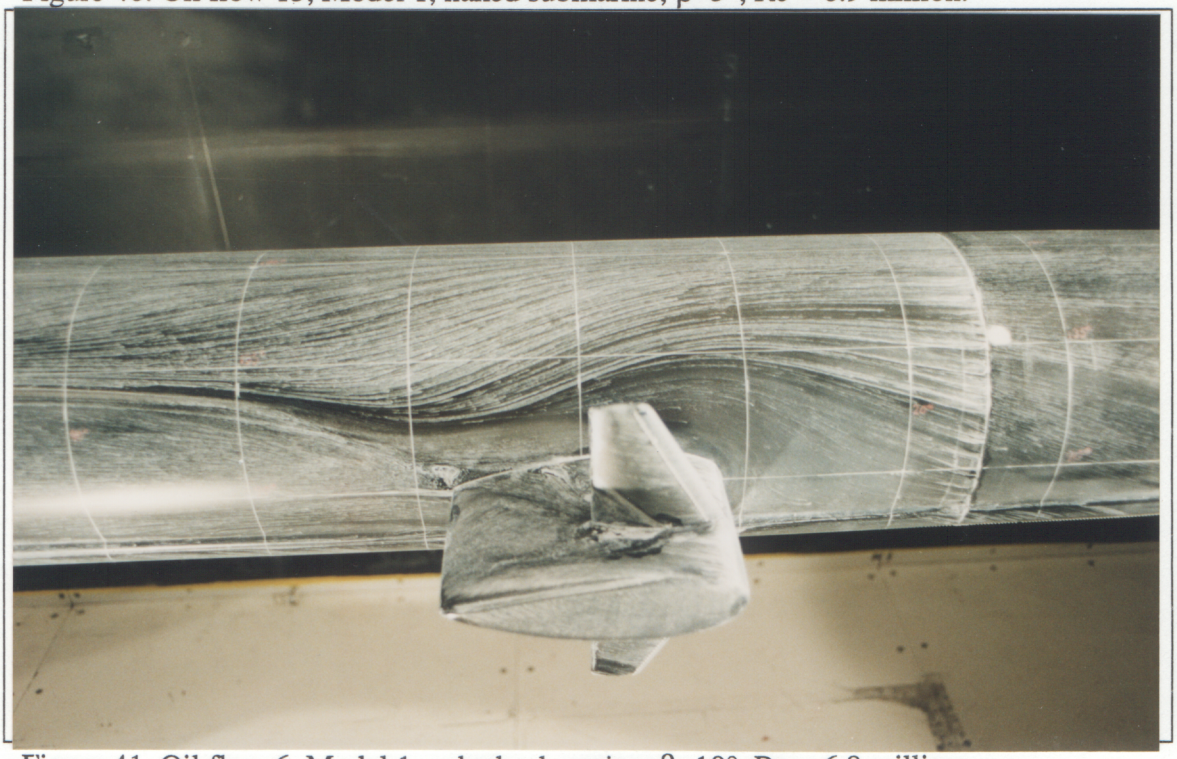

Figure 41. Oil flow 6, Model 1, naked submarine, β=10°, Re = 6.8 million.

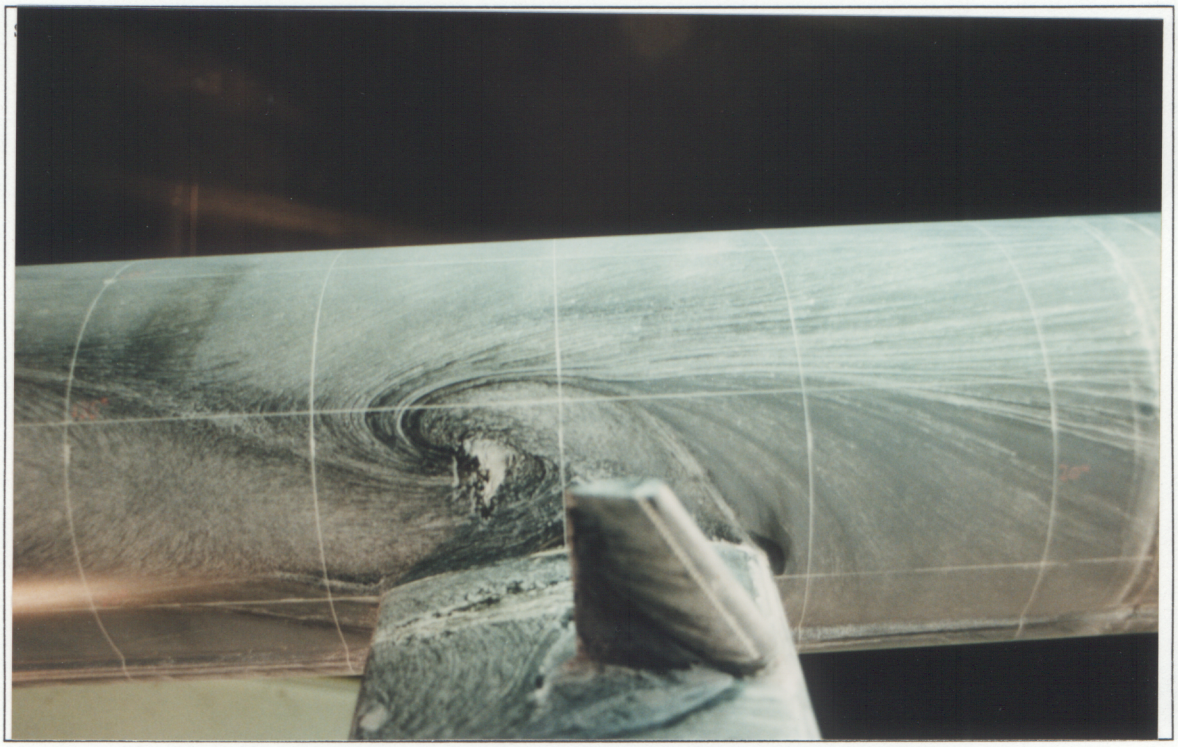

Figure 42. Oil flow 1, Model 1, naked submarine, ß=15°, Re = 6.8 million.

Figure 43. Oil flow 20, Model 1, submarine with fins, β=15°, Re = 6.4 million.

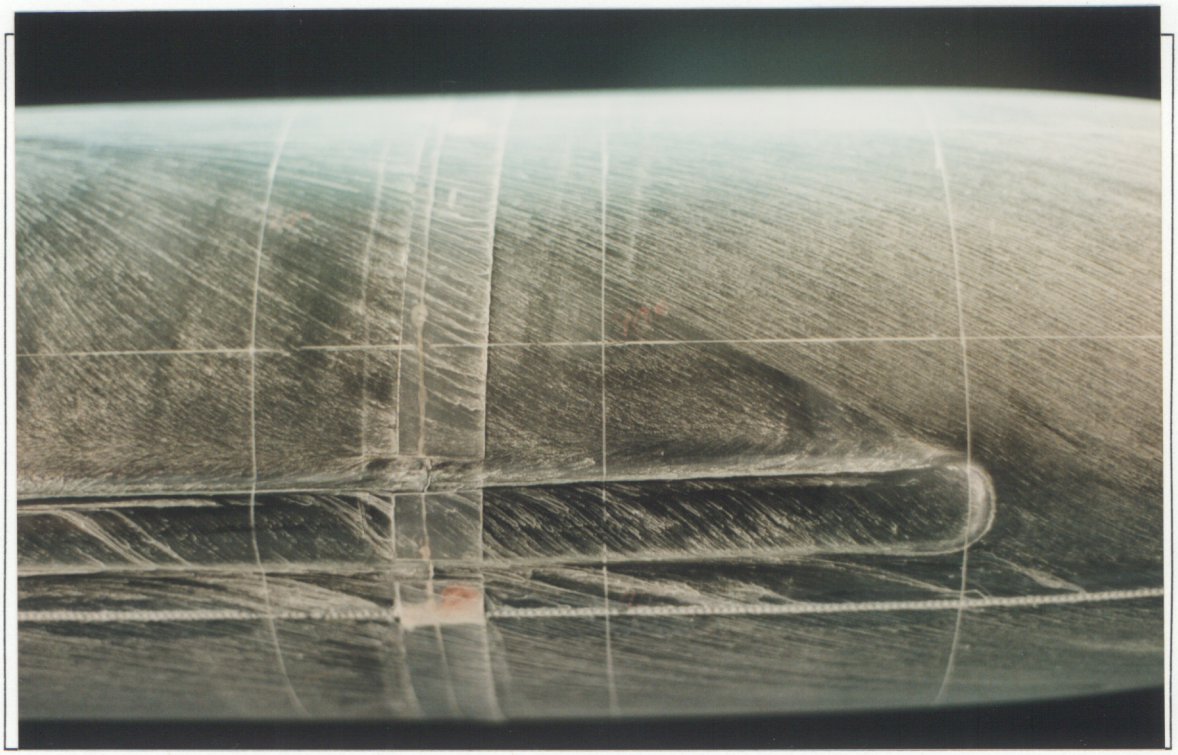

Figure 44. Flow patterns near leading edge of towed array housing. Oil flow 1, Model 1, naked submarine, β=15°, Re = 6.8 million.

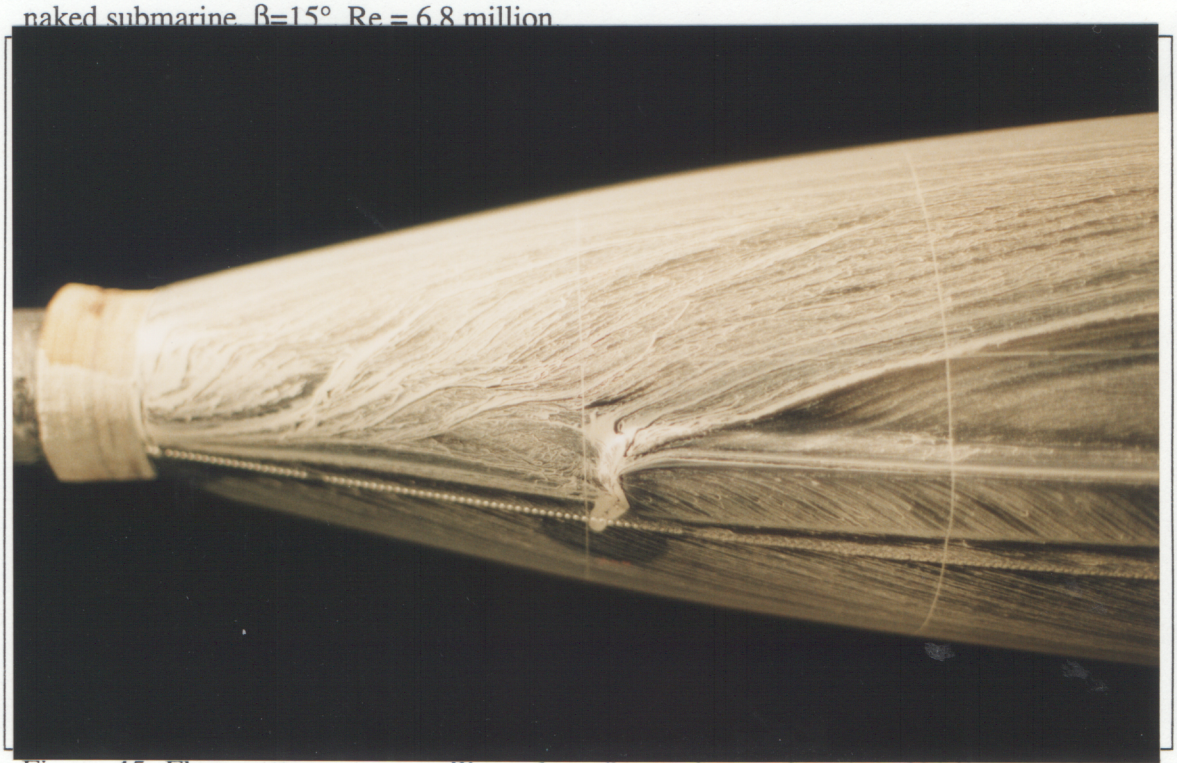

Figure 45. Flow patterns near trailing edge of towed array housing. Oil flow 1, Model 1, naked submarine, β=15°, Re = 6.8 million.

Figure 46. Fins on sail. Oil flow 23, Model 1, submarine with fins, β=15°, Re = 6.7 million.

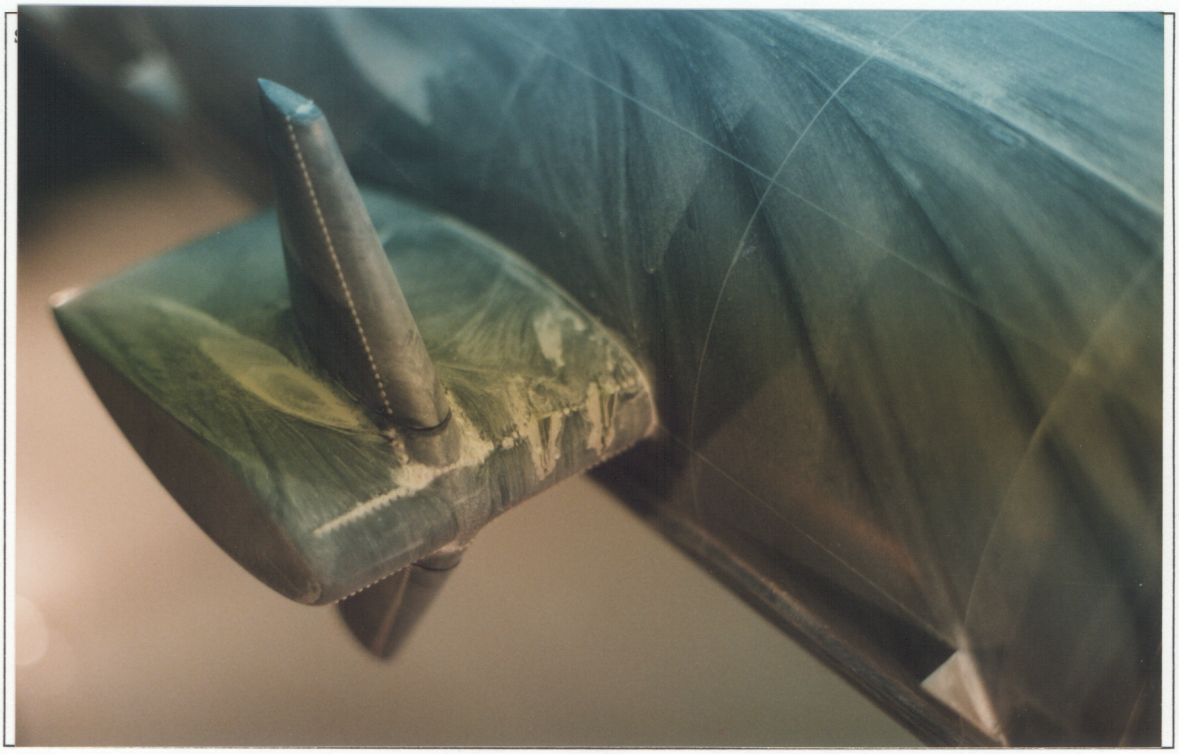

Figure 47. Fins on sail. Oil flow 24, Model 1, submarine with fins, β=15°, Re = 6.8 million.

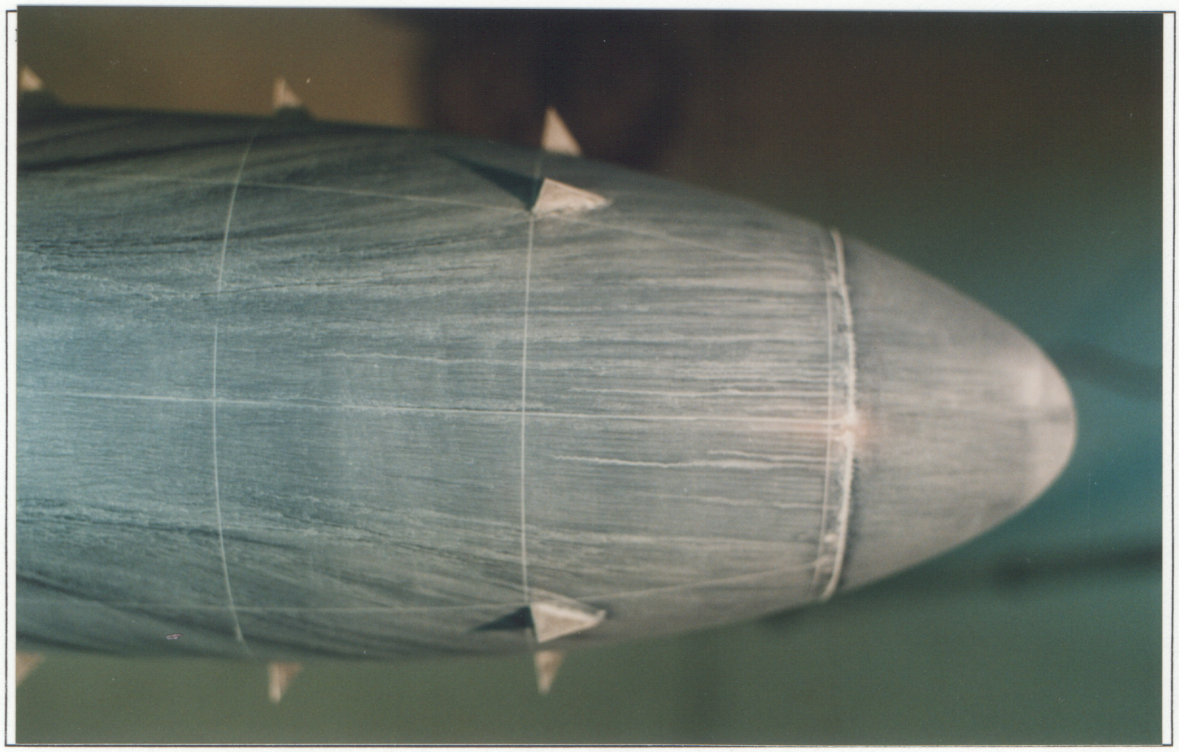

Figure 48. Oil flow 19, top view., Model 1, submarine with fins, β=15°, Re = 6.5 million.

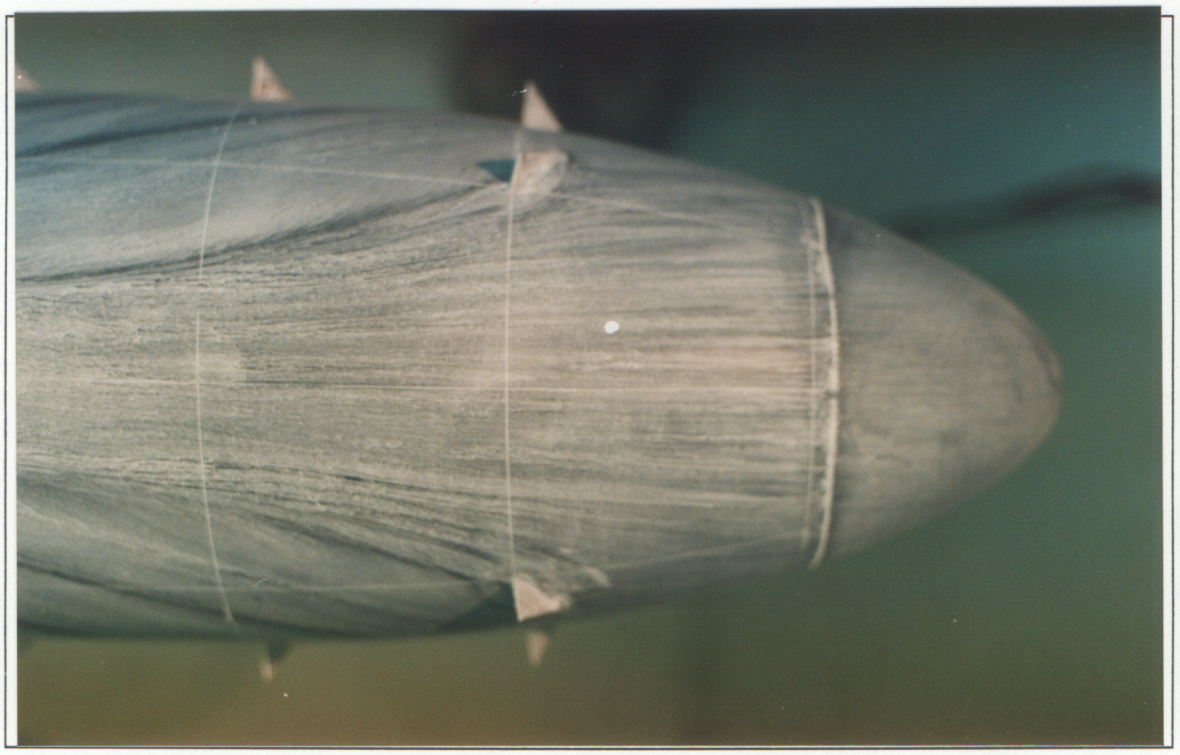

Figure 49. Oil flow 20, top view, Model 1, submarine with fins, β=15°, Re = 6.4 million.

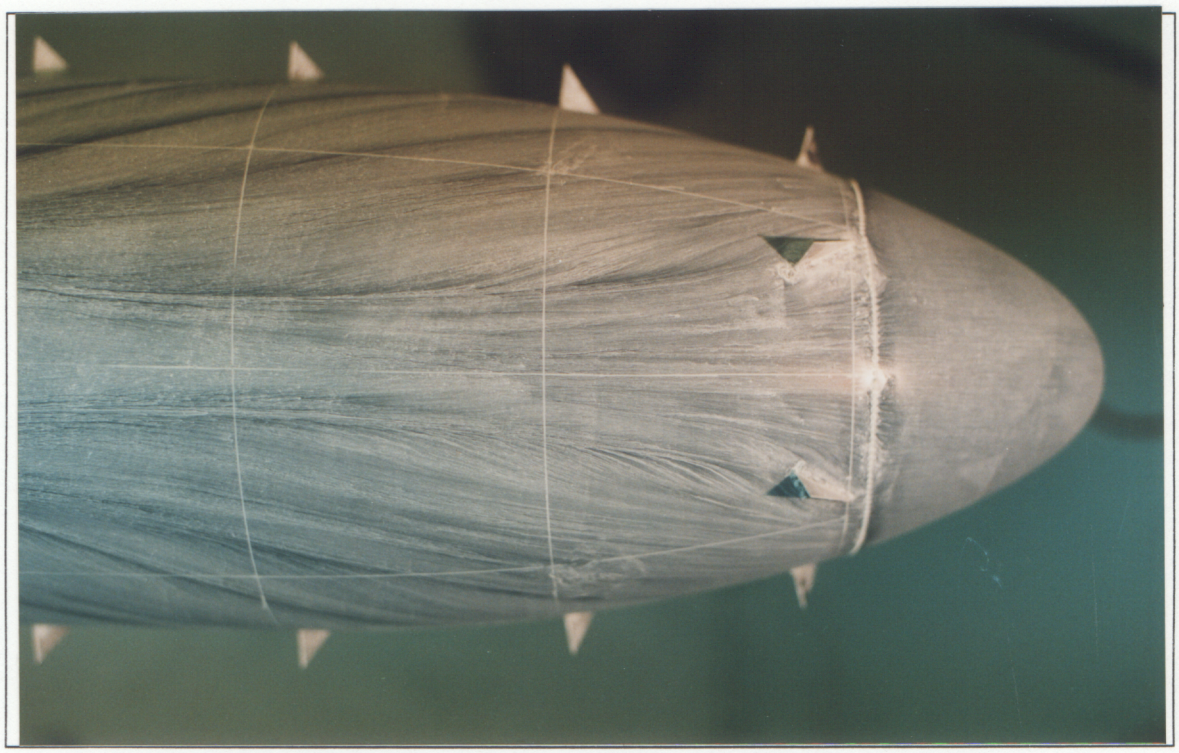

Figure 50. Oil flow 22, Model 1, submarine with fins, β=15°, Re = 6.4 million.

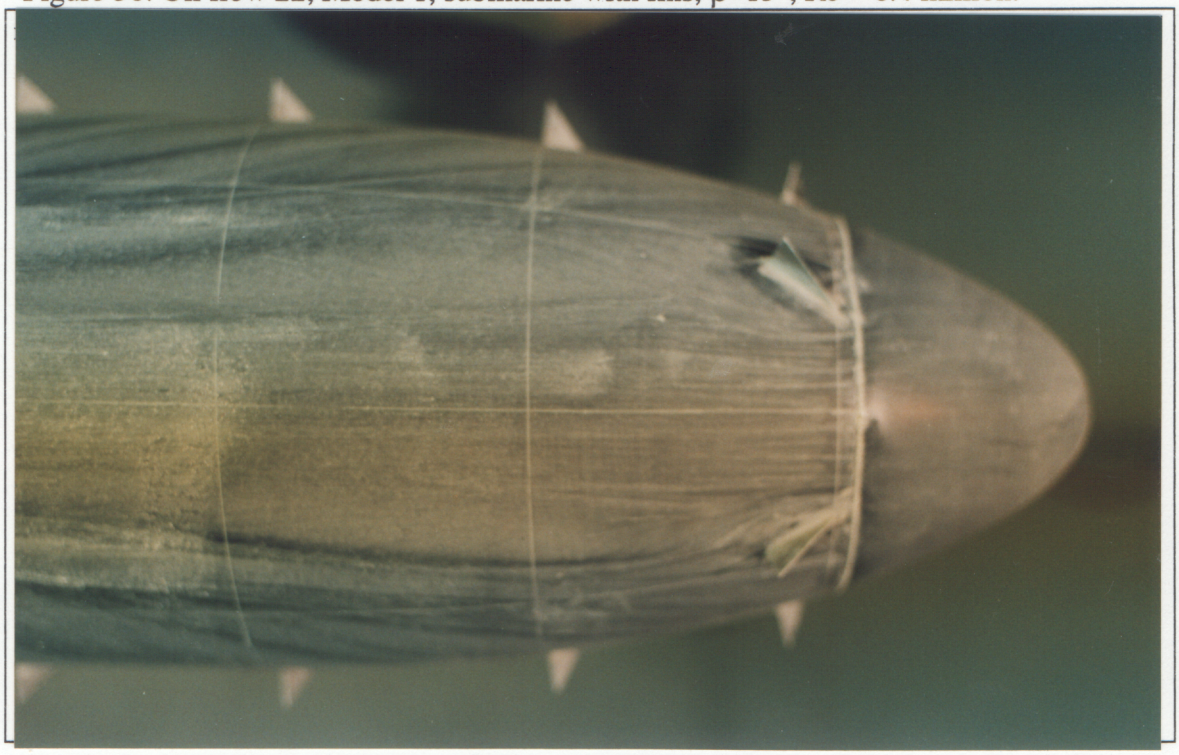

Figure 51. Oil flow 23, top view, Model 1, submarine with fins, β=15°, Re = 6.5 million.

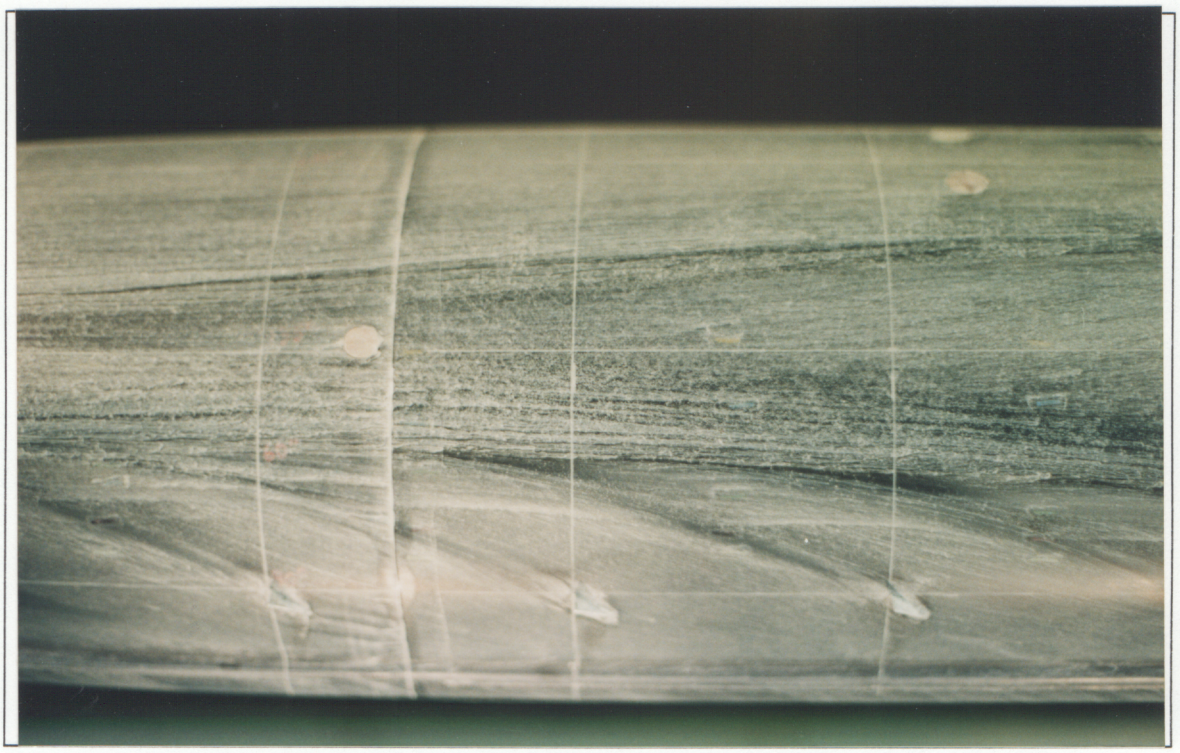

Figure 52. Oil flow 17, Model 1, submarine with small fins, β=15°, Re = 6.8 million.

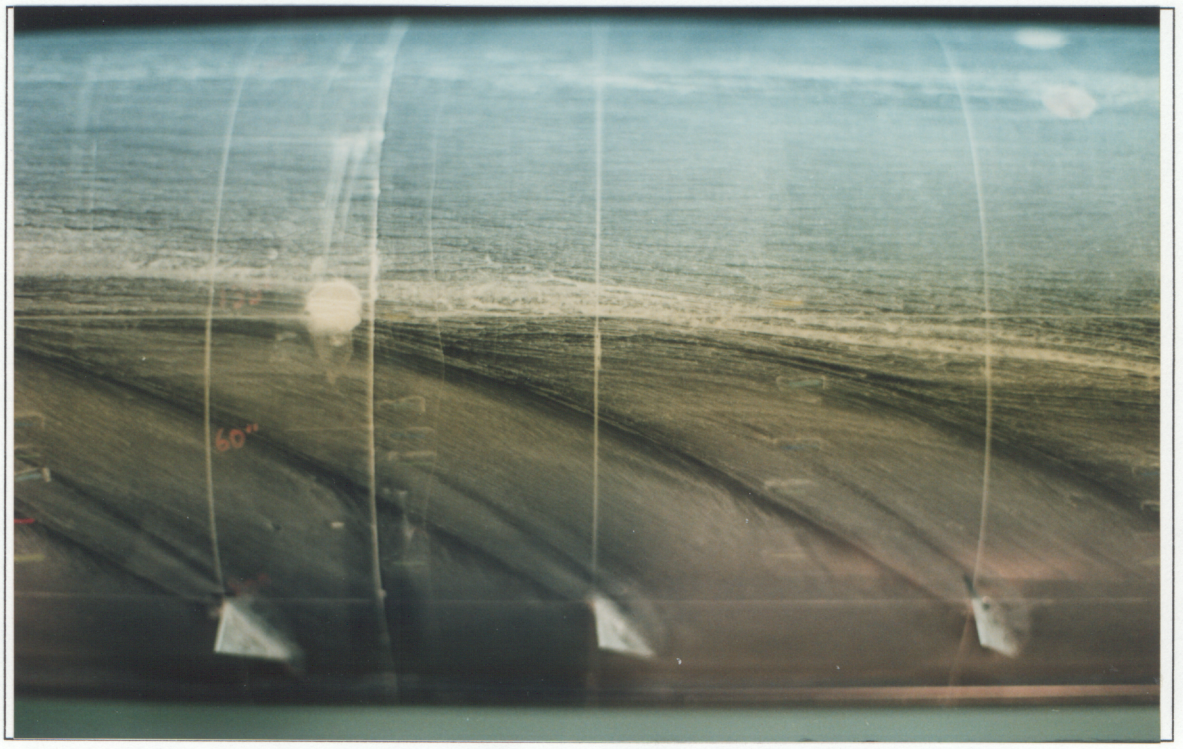

Figure 53. Oil flow 18, Model 1, submarine with fins, β=15°, Re = 6.4 million.

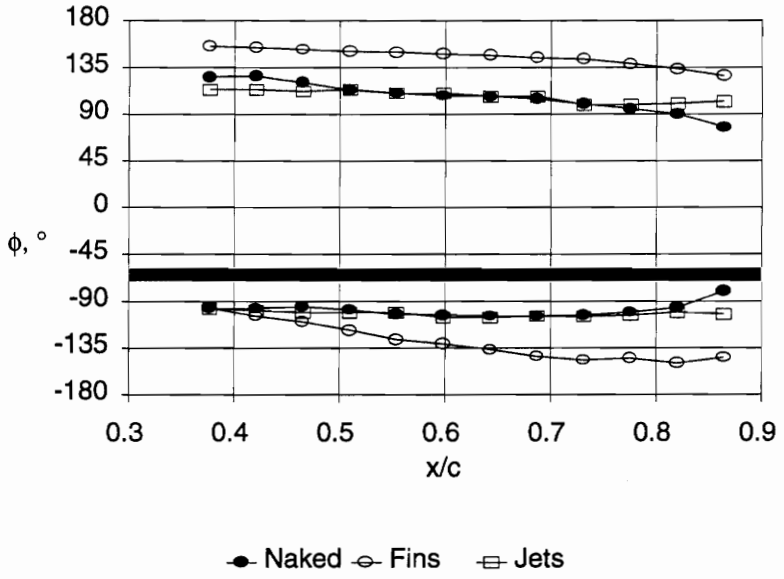

Figure 54. Separation lines for the naked submarine and the submarine with fins and jets at 15° sideslip. Notice the drastic change due to the fins. The shaded bar represents the location of the towed array housing.

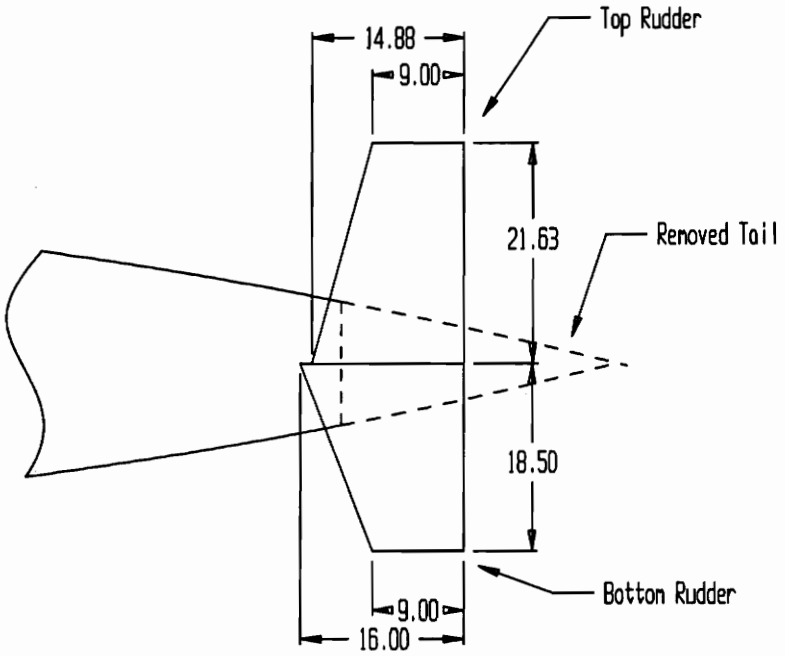

Figure 55. Rudder Dimensions. The rudder and removed tail were modeled by the entire rudder planform. Dimensions taken from plans from Scale Shipyard, and are not from actual 688 submarine. All dimensions in feet.

Appendix I - Model 1 Offsets

The following table presents the actual shape data of the Model 1. The model diameters are given for the model at stations every four inches.

Body Dimensions: Los Angeles Class 688 Submarine Model

x, in.	x/L	Dh, in.	Dv, in.	Dh/L	Dv/L
4.00	0.0443	5.675	5.605	0.06288	0.06211
8.00	0.0886	7.485	7.475	0.08294	0.08283
12.00	0.1330	8.120	8.105	0.08997	0.08981
16.00	0.1773	8.215	8.225	0.09102	0.09114
20.00	0.2216	8.220	8.215	0.09108	0.09102
24.00	0.2659	8.225	8.220	0.09114	0.09108
28.00	0.3102	8.265	-	0.09158	-
32.00	0.3546	8.250	8.225	0.09141	0.09114
36.00	0.3989	8.230	8.210	0.09119	0.09097
40.00	0.4432	8.215	8.215	0.09102	0.09102
44.00	0.4875	8.210	8.210	0.09097	0.09097
48.00	0.5319	8.220	8.240	0.09108	0.09130
52.00	0.5762	8.220	8.235	0.09108	0.09125
56.00	0.6205	8.325	8.235	0.09224	0.09125
60.00	0.6648	8.200	8.200	0.09086	0.09086
64.00	0.7091	8.000	8.025	0.08864	0.08892
68.00	0.7535	7.570	7.570	0.08388	0.08388
72.00	0.7978	7.065	7.090	0.07828	0.07856
76.00	0.8421	6.145	6.130	0.06809	0.06792
80.00	0.8864	4.870	4.900	0.05396	0.05429

Subamarine Model: Nominally 90.25" long
Nominally 8.25" wide and high

Towed Array Housing: Nominally 1.25" Wide
Start at x = 11.815"
End at x = 79.975"
Each end is semicircular in top view, and blended into body

Sail: 1.665" wide
4.285" high
Leading edge at x = 24.635"
Trailing edge at x = 33.135"

Manufacturer: The Scale Shipyard
5866 Orange Ave. #3
Long Beach, CA 90805-4146
(213)-428-5027

Appendix II - Data Acquisition Codes for Model 2

Data acquisition was performed in National Instruments' Lab Windows™ v1.2 C programming environment. The following codes were developed. First, hp3455a.h and hp3455a.c are the basic GPIB interface subroutines for the HP3455A Scanner. Second, hp3495a.h and hp3495a.c are the basic GPIB interface subroutines for the HP3459A voltmeter. The codes tunnel.h and tunnel.c utilize the previous files and provide basic wind tunnel data acquisition, such as static and dynamic pressure, flow temperature, flow speed, Reynolds number, etc. The codes sub.h and sub.c use all of the previous files and contain routines specifically for Model 2, including jet flow parameters. Finally, the rest of the codes use sub.* and tunnel.* and are the actual data acquisition codes used for various series of tests.

hp3455a.h

```
/*= Hewlett Packard Model 3455a Scanner Include File ========================*/

/*= GLOBAL FUNCTION DECLARATIONS
============================================*/

void hp3455a_init();
void hp3455a_close();
double hp3455a_getvolt();
```

hp3455a.c

```
/*= Hewlett Packard Model 3455a Digital Voltmeter Instrument Module ====================*/

#include "\lw\include\lwsystem.h"
#include "\lw\include\gpib.h"
#include "\lw\include\formatio.h"
#include "\lw\instr\hp3455a.h"

/*= UTILITY ROUTINES ====================================================*/
```

```
int hp3455a_write_data();
int hp3455a_device_closed();
int hp3455a_invalid_integer_range();

extern int hp3455a_err;

/*= STATIC VARIABLES ==========================================================*/

/* bd contains the descriptor returned by OpenDev */

static int bd;

/* cmd is a buffer for GPIB I/O strings */

static char cmd[26];

/*============================================================================*/
/* This function opens the instrument, queries for ID, and initializes the
*/
/* instrument to a known state.                                               */
/*============================================================================*/

void hp3455a_init(addr)

int addr;

{

/* Check for valid address */

   if (hp3455a_invalid_integer_range (addr, 0, 30, -1) != 0)
      return ;

/*  If device has not been opened (bd = 0), open it. */

   if (bd <= 0)   {
      CloseInstrDevs("dvm");
      bd = OpenDev ("dvm","");
      if (bd <= 0)   {
         hp3455a_err = 220;
         return;
      }
   }

/*  Change the primary address of the device    */

   if (ibpad (bd, addr) < 0)   {
      hp3455a_err = 233;
      return;
   }
```

```
   if (hp3455a_write_data ("A1H0T3", 6) != 0)
         return;

   ibrd(bd,cmd,20);

   hp3455a_err = 0;
}

/*=========================================================================*/
/* This function removes the instrument from the GPIB device table and
*/
/* sets bd = 0.                                                            */
/*=========================================================================*/

void hp3455a_close ()

{

/*  Check for device closed */

   if (hp3455a_device_closed())
      return;

/*  Close the device    */

   if (CloseDev (bd) < 0)
      hp3455a_err = 221;
   else
      hp3455a_err = 0;

   bd = 0;
}

double hp3455a_getvolt()
/* Returns voltage in milivolts. */
{
 char voltstr[16];
 double volt;

 ibtrg(bd);

 if (ibrd(bd, voltstr, 16) <= 0)
    {
    hp3455a_err = 231;
    }
 else
    {
    hp3455a_err = 0;
    }
```

```
 Fmt(&volt,"%f<%s",voltstr);

 return volt;
}


/*= UTILITY ROUTINES ================================================*/

/*====================================================================*/
/* This function checks to see if the module has been initialized.  If the
*/
/* device has not been opened, a 1 is returned, 0 otherwise.                */
/*====================================================================*/

int hp3455a_device_closed ()

{
   if (bd <= 0)  {
      hp3455a_err = 232;
      return 1;
   }
   return 0;
}

/*====================================================================*/
/* This fuction checks an integer to see if it lies between a minimum
*/
/* and maximum value.  If the value is out of range, set the global error
*/
/* variable to the value err_code.  If the value is OK, error = 0.  The    */
/* return value is equal to the global error value.
*/
/*====================================================================*/

int hp3455a_invalid_integer_range (val,min,max,err_code)

int val,min,max,err_code;

{
 if ((val < min) || (val > max)) {
   hp3455a_err = err_code;
   return 1;
 }
 return 0;
}

/*====================================================================*/
/* This function writes a buffer of data to the GPIB interface.
*/
/*====================================================================*/
```

```
int hp3455a_write_data (cmd,cnt)

char *cmd;
int cnt;

{
   if (ibwrt(bd, cmd, cnt) <= 0)
      hp3455a_err = 230;
   else
      hp3455a_err = 0;
   return hp3455a_err;
}

/*= THE END ============================================================*/
•
```

hp3495a.h

```
/*= Hewlett Packard Model 3455a Scanner Include File ==========================*/

/*= GLOBAL FUNCTION DECLARATIONS ==============================================*/

void hp3495a_init();
void hp3495a_close();
void hp3495a_setch();

/*= GLOBAL VARIABLE DECLARATIONS ==============================================*/

/* Global error variable for the instrument module */

/*int hp3495a_err;*/
```

hp3495a.c

```
/*= Hewlett Packard Model 3495a Scanner Instrument Module ======================*/

#include "\lw\include\lwsystem.h"
#include "\lw\include\gpib.h"
#include "\lw\include\formatio.h"
#include "\lw\instr\hp3495a.h"

/*= UTILITY ROUTINES ==========================================================*/

int hp3495a_device_closed();
int hp3495a_invalid_integer_range();

int hp3495a_err;
```

```
/*= STATIC VARIABLES ================================================*/

/* bd contains the descriptor returned by OpenDev */

static int bd;

/* cmd is a buffer for GPIB I/O strings */

static char cmd[26];

/*====================================================================*/
/* This function opens the instrument, queries for ID, and initializes the
*/
/* instrument to a known state.                                       */
/*====================================================================*/

void hp3495a_init(addr)

int addr;

{

/* Check for valid address */

   if (hp3495a_invalid_integer_range (addr, 0, 30, -1) != 0)
      return ;

/*  If device has not been opened (bd = 0), open it. */

   if (bd <= 0)   {
      CloseInstrDevs("scanner");
      bd = OpenDev ("scanner", "");
      if (bd <= 0)   {
         hp3495a_err = 220;
         return;
      }
   }

/*  Change the primary address of the device   */

   if (ibpad (bd, addr) < 0)  {
      hp3495a_err = 233;
      return;
   }

   hp3495a_err = 0;
}

/*====================================================================*/
/* This function removes the instrument from the GPIB device table and
*/
```

```
/* sets bd = 0.                                                                    */
/*=================================================================================*/

void hp3495a_close ()

{

/*  Check for device closed */

   if (hp3495a_device_closed())
      return;

/*  Close the device    */

   if (CloseDev (bd) < 0)
      hp3495a_err = 221;
   else
      hp3495a_err = 0;

   bd = 0;
}

/*=================================================================================*/
/* This function sets the scanner channel.
*/
/*=================================================================================*/

void hp3495a_setch(channel)

int channel;


{
  char chstr1[2],chstr2[3];

  hp3495a_err=0;
  ibclr (bd);
  if ((channel<=0)||(channel>80))
     {
      hp3495a_err = 290;
      return;
     }

  Fmt(chstr2,"%d[w2p0]",channel);
  chstr1[0]=chstr2[0];
  chstr1[1]=chstr2[1];


  ibwrt(bd,chstr2,2);
  ibtrg (bd);
```

```
  return;

}


/*= UTILITY ROUTINES ========================================================*/

/*===========================================================================*/
/* This function checks to see if the module has been initialized.  If the
*/
/* device has not been opened, a 1 is returned, 0 otherwise.                 */
/*===========================================================================*/

int hp3495a_device_closed ()

{
   if (bd <= 0)  {
      hp3495a_err = 232;
      return 1;
   }
   return 0;
}

/*===========================================================================*/
/* This fuction checks an integer to see if it lies between a minimum
*/
/* and maximum value.  If the value is out of range, set the global error
*/
/* variable to the value err_code.  If the value is OK, error = 0.  The     */
/* return value is equal to the global error value.
*/
/*===========================================================================*/

int hp3495a_invalid_integer_range (val,min,max,err_code)

int val,min,max,err_code;

{
 if ((val < min) || (val > max)) {
   hp3495a_err = err_code;
   return 1;
 }
 return 0;
}

/*= THE END =================================================================*/
```

tunnel.h

```
/*= Stability Wind Tunnel Include File ======================================*/
```

```
/* Functions */

void tunnel_balance();
double tunnel_alpha();
double tunnel_p();
double tunnel_q();
double tunnel_temp();
double tunnel_uinf();
double tunnel_dens();
double tunnel_mu();
void tunnel_tare();
void tunnel_FandM();

/* Global Variables */

int tunnel_err,tunnel_balid,tunnel_sweeps;
double tunnel_T[6],tunnel_F[6],tunnel_CF[6];
double tunnel_calvolt[8],tunnel_calalpha[8];
```

tunnel.c

```
/*--------- LabWindows Generated Code:   Tue Jan 01 00:43:28 1980 ---------*/

/*#include      "C:\lw\include\lwsystem.h"
#include      "C:\lw\include\formatio.h"*/
/*= Stability Wind Tunnel Driver Software ==================================*/
#include      "c:\lw\instr\tunnel.h"
#include      "c:\lw\instr\hp3495a.h"
#include      "c:\lw\instr\hp3455a.h"

int tunnel_err,tunnel_balid,tunnel_sweeps;
double tunnel_T[6],tunnel_F[6],tunnel_CF[6];
double tunnel_calvolt[8],tunnel_calalpha[8];

/* lbs/V (not lbs./mV), in-lbs/V */
void tunnel_balance (balid, sweeps)
int balid;
int sweeps;
{

      tunnel_balid = balid;
      tunnel_sweeps = sweeps;
      if (balid == 1)  {
            /* Sting (ST01) */
            tunnel_CF[0] = 15610.0;
            tunnel_CF[1] = 8030.0;
            tunnel_CF[2] = 6770.0;
            tunnel_CF[3] = 5940.0;
            tunnel_CF[4] = 7010.0;
```

```
        tunnel_CF[5] = 18170.0;
    }
    else {
        /* Strut (STO3M with SR-1) */
        tunnel_CF[0] = 22400.0;
        tunnel_CF[1] = 24700.0;
        tunnel_CF[2] = 21600.0;
        tunnel_CF[3] = 28800.0;
        tunnel_CF[4] = 21200.0;
        tunnel_CF[5] = 24800.0;
    }
    tunnel_calvolt[0] = 0.916;
    tunnel_calvolt[1] = -0.023;
    tunnel_calvolt[2] = -0.896;
    tunnel_calvolt[3] = -1.729;
    tunnel_calvolt[4] = -2.742;
    tunnel_calvolt[5] = -3.544;
    tunnel_calvolt[6] = -4.36;
    tunnel_calvolt[7] = -4.986;
    tunnel_calalpha[0] = -5.2;
    tunnel_calalpha[1] = 0.30;
    tunnel_calalpha[2] = 5.4;
    tunnel_calalpha[3] = 9.85;
    tunnel_calalpha[4] = 15.7;
    tunnel_calalpha[5] = 20.5;
    tunnel_calalpha[6] = 25.30;
    tunnel_calalpha[7] = 29.8;
    hp3495a_init (9);
    hp3455a_init (22);
}

/* This function reads in the inclinometer angle of attack. */
double tunnel_alpha ()
{
    double volt;
    double alpha;
    int i;
    int flag;

    hp3495a_setch (11);
    volt = 0.0;
    for (i = 0; i < tunnel_sweeps; i++)
        volt += hp3455a_getvolt ();
    volt /= (double)tunnel_sweeps;
    flag = 0;
    for (i = 0; i < 7 && !flag; i++)
        if (volt >= tunnel_calvolt[i + 1]) {
            alpha = tunnel_calalpha[i] + (volt - tunnel_calvolt[i]) * (tunnel_calalpha[i + 1] -
            tunnel_calalpha[i]) / (tunnel_calvolt[i + 1] - tunnel_calvolt[i]);
            flag = 1;
        }
```

```
    if (!flag)
        return -1000.0;
    else
        return alpha;
}

/* This function returns the pressure in psi. */
double tunnel_p ()
{

    hp3495a_setch (1);
    return hp3455a_getvolt () * 10.0 * 0.50308;

}

/* This function returns the dynamic pressure in psi. */
double tunnel_q ()
{
    double r;

    hp3495a_setch (9);
    r = 10.0 * hp3455a_getvolt () / 27.6;
    if (r >= 0.0)
        return r;
    else
        return 0.0;

}

/* This function returns the temperature in Rankine */
double tunnel_temp ()
{
    double volt;

    hp3495a_setch (2);
    volt = hp3455a_getvolt ();
    return 459.0 + volt * 1798.0;

}

/* This function returns the flow velocity in ft/s */
double tunnel_uinf ()
{

    return 12.0 * sqrt (2.0 * tunnel_q () / tunnel_dens ());
}

/* This function returns the flow density in slugs/ft^3 */
double tunnel_dens ()
{
```

```
	return tunnel_p () * 144.0 / 1716.0 / tunnel_temp ();
}

/* This function returns the flow viscosity in lb-s/ft^2 */
double tunnel_mu ()
{
	double t;

	t = tunnel_temp ();
	return 2.27 * pow (t, 1.5) / (t + 198.6) / 100000000.0;
}

/* This function reads in the tares */
void tunnel_tare ()
{

	tunnel_FandM ();
	tunnel_T[0] = tunnel_F[0];
	tunnel_T[1] = tunnel_F[1];
	tunnel_T[2] = tunnel_F[2];
	tunnel_T[3] = tunnel_F[3];
	tunnel_T[4] = tunnel_F[4];
	tunnel_T[5] = tunnel_F[5];
	return;
}

/* This function reads in the actual forces and moments from the balance. */
void tunnel_FandM ()
{
	int i;
	int j;
	double v;

	for (j = 0; j < 6; j++)
		tunnel_F[j] = 0.0;
	for (i = 1; i <= tunnel_sweeps; i++)
		for (j = 0; j < 6; j++)  {
			hp3495a_setch (j + 3);
			v = hp3455a_getvolt ();
			tunnel_F[j] += tunnel_CF[j] * v;
		}
	for (j = 0; j < 6; j++)
		tunnel_F[j] /= (double)tunnel_sweeps;
}

double tunnel_Re(l)

double l;

{
return tunnel_dens()*tunnel_uinf()*l/tunnel_mu();
```

```
}
```

sub.h

```
/*   Sub Include File */

#define jet 1
#define fin 0
#define L 7.5
#define Ajet 5.539E-4  /* sq. ft */
#define Sref 0.371     /* sq. ft */
#define bref 0.6875    /* ft */
#define cref 7.5       /* ft */
#define RePort   6
#define VePort   7
#define BetaPort  8
#define ServoPort 9
#define JetPort   12

/* Global Variables */

char string[80];
int sub_ch[39],sub_numservo,sub_config;
double sub_servoslope,sub_servooffset;
int hand[18];

/* Functions */

double sub_jettemp();
double sub_jetpres();
double sub_jetspeed();
double sub_jetVR();
double sub_jetCmu();
double sub_gettheta();
void sub_vidinput();
void updateflow();
void sub_setupgraphics();
void sub_setupmodel();
void sub_settheta();
void sub_setbeta();
void sub_setRe();
void sub_setVR();
void sub_setCmu();
```

sub.c

```
/*#include      "C:\LW\INSTR\hp3455a.h" */      /* hp3455a */
/*#include      "C:\LW\INSTR\hp3495a.h"  */     /* hp3495a */
```

```
#include      "C:\LW\INSTR\tunnel.h"       /* Tunnel Instruments */
#include      "C:\LW\INSTR\sub.h"          /* Sub Instruments */

/*extern char string[80];
extern int sub_ch[39],sub_numservo,sub_config;
extern double sub_servoslope,sub_servooffset;
extern int hand[18];*/

 char string[80];
 int sub_ch[39],sub_numservo,sub_config;
 double sub_servoslope,sub_servooffset;
 int hand[18];

double sub_jettemp()
{
 double volt;

 hp3495a_setch (11);
 volt=-hp3455a_getvolt();
 return volt*1000+459.69;
}

double sub_jetpres() /* inches of water */
{
 double volt;
 int i;

 hp3495a_setch (10);
 volt=0;
 for (i=0;i<1;i++)
   {
    volt+=hp3455a_getvolt();
   }
 return 26.23*volt/1.0+238.3;
}

double sub_jetspeed() /* ft/s */
{
 double p,t,q;

 q=sub_jettemp()*(sub_jetpres()/(tunnel_p()*27.68)-1.0);
 if (q>=0.0)
   {
    return 36.2*sqrt(q);
   }
 else
   {
    return 0.0;
   }
}
```

```
double sub_jetVR()
{
 return sub_jetspeed()/tunnel_uinf();
}

double sub_jetCmu()
{
 return 2.0*pow(sub_jetVR(),2.0)*Ajet/Sref;
}

double sub_gettheta(servo)

int servo;
{
 double servovolt, theta;

 hp3495a_setch(sub_ch[servo]);
 servovolt=hp3455a_getvolt();
 theta=servovolt*sub_servoslope+sub_servooffset;

 return theta;
}

void sub_vidinput(inmsg,res)

 char *inmsg,*res;
{
 char buff[80];
 int q,i,flag,len;

 for (i=0;i<80;i++)
   {
    buff[i]=0;
   }

 Fmt(buff,"%s",inmsg);

 for(i=0;i<80;i++)
   {
    if (buff[i]==0)
      {
       len=i+1;
       i=81;
      }
   }

 GrfMsg (buff, 4);

 q=getkey();
 while (q!=13)
   {
```

```
  if ((q==27)||(q==8))
    {
     flag=1;
     for(i=79;(i>=0)&&flag;i--)
       {
        if (buff[i]!=0)
          {
           flag=0;
          }
       }
     buff[i+1]=0;
     }
   else
     {
     Fmt(buff,"%s%c",buff,q);
     }

   GrfMsg(buff,4);
   q=getkey();
   }

 Fmt(res,"%s[i*]",len-1,buff);

}

void updateflow()

{
 GrfNumeric(hand[RePort],tunnel_Re(L));
 GrfNumeric(hand[VePort],tunnel_uinf());

 if (sub_config==jet)
   {
    GrfNumeric(hand[JetPort],sub_jetspeed());
    GrfNumeric(hand[JetPort+1],sub_jettemp()-459.69);
    GrfNumeric(hand[JetPort+2],sub_jetpres());
    GrfNumeric(hand[JetPort+3],sub_jetVR());
    GrfNumeric(hand[JetPort+4],sub_jetCmu());
   }
}

void sub_setupgraphics()

{
 int t__00000,i,numports;
 char *title[7];

 /* Set up graphics display */
 SetAdapter (0, 20, &t__00000);
 GrfLReset (0, 0, 1, 1);
 SetDisplayMode (1);
```

```
hand[0]= CreatePort (0, 66, 33, 33);     title[0]="Cx";
hand[1]= CreatePort (33, 66, 33, 33);    title[1]="Cy";
hand[2]= CreatePort (66, 66, 33, 33);    title[2]="Cz";
hand[3]= CreatePort (0, 33, 33, 33);     title[3]="Cl";
hand[4]= CreatePort (33, 33, 33, 33);    title[4]="Cm";
hand[5]= CreatePort (66, 33, 33, 33);    title[5]="Cn";
hand[RePort]=     CreateNumericPort (0,22,2,9,3,"",   " Reynolds # ");
hand[VePort]=     CreateNumericPort (0,11,1,6,2,"ft/s","  Velocity  ");
hand[BetaPort]=      CreateNumericPort (0,0,1,5,2,"deg","    Beta    ");
hand[ServoPort]=  CreateNumericPort (18,22,0,6,3,"",    "  Servo    ");
hand[ServoPort+1]= CreateNumericPort (18,11,1,6,3,"deg","Desired Skew");
hand[ServoPort+2]= CreateNumericPort (18,0,1,6,3,"deg", "Actual Skew ");

if (sub_config==jet)
  {
   hand[JetPort]=    CreateNumericPort (36,22,1,6,2,"ft/s","  Jet Speed  ");
   hand[JetPort+1]=  CreateNumericPort (36,11,1,6,2,"F",   "  Jet Temp   ");
   hand[JetPort+2]=  CreateNumericPort (36,0,1,6,2,"in Hg","Jet Pressure ");
   hand[JetPort+3]=  CreateNumericPort (56,22,1,6,2,"","Jet V/Vr");
   hand[JetPort+4]=  CreateNumericPort (56,11,1,6,2,"","Jet Cmu ");
  }

for (i=0;i<6;i++)
  {
   SetActivePort (hand[i]);
   SetFrmColor (1);
   SetTtlColor (0);
   SetGrdColor (1);
   SetLblColor (8);
   SetBckColor (15);
   SetAxAuto(-1,21);
   SetCurv2D(1);
   SetAxName (0, "theta (skew)");
   SetAxName (1, title[i]);
   SetCrvColor(4);
  }

if (sub_config!=jet)
  {
   numports=ServoPort+2;
  }
else
  {
   numports=JetPort+4;
  }

for (i=6;i<=numports;i++)
  {
   SetActivePort(hand[i]);
   SetFrmColor (1);
```

```
   SetTtlColor (15);
   SetBckColor (8);
   SetTxColor (4);
   DisplayPort(hand[i]);
  }

 updateflow();
}

void sub_setupmodel(config)

 int config;

{
 int i;

 sub_config=config;

/* setup gpib and tunnel stuff */
 tunnel_balance (1, 50);

 sub_ch[1]=20; sub_ch[2]=21; sub_ch[3]=22; sub_ch[4]=23; sub_ch[5]=24;
 sub_ch[6]=25; sub_ch[7]=26; sub_ch[8]=27; sub_ch[9]=28; sub_ch[10]=29;
 sub_ch[11]=30; sub_ch[12]=31; sub_ch[13]=32; sub_ch[14]=33; sub_ch[15]=34;
 sub_ch[16]=35; sub_ch[17]=36; sub_ch[18]=37; sub_ch[19]=38; sub_ch[20]=39;
 sub_ch[21]=40; sub_ch[22]=41; sub_ch[23]=42; sub_ch[24]=43; sub_ch[25]=-1;
 sub_ch[26]=44; sub_ch[27]=-1; sub_ch[28]=45; sub_ch[29]=46; sub_ch[30]=47;
 sub_ch[31]=48; sub_ch[32]=49; sub_ch[33]=50; sub_ch[34]=51; sub_ch[35]=52;
 sub_ch[36]=53; sub_ch[37]=54; sub_ch[38]=55;

 sub_servoslope=90.0;
 sub_servooffset=0;

 if (config==jet)
   {
   sub_numservo=24;
   for (i=26;i<39;i++)
     {
     sub_ch[i]=-1;
     }
   }
 else sub_numservo=38;

}

void sub_settheta(servo,thetareq)

double thetareq;
int servo;

{
```

```
double servovolt,theta;
int q,flag;

if (sub_ch[servo]>=0)
  {
  GrfNumeric(hand[ServoPort],1.0*servo);
  GrfNumeric(hand[ServoPort+1],thetareq);
  GrfMsg("Hit any key to accept reading.",14);
  flag=1;
  while (flag)
    {
    while (!(keyhit()))
      {
      GrfNumeric(hand[ServoPort+2],sub_gettheta(servo));

    }
    GrfMsg("VERIFY: Accept theta?",12);
    q=getkey();
    q=getkey();
    if ((q==89)||(q==121))
      {
      flag=0;
      }
    else
      {
      GrfMsg("Hit any key to accept reading.",14);
      }
    }
  }
 GrfMsg("",2);
}

void sub_setbeta(betareq)

double betareq;

{
 double beta;
 int q,flag;
 char s[80];

 GrfNumeric(hand[BetaPort],/*tunnel_alpha ()*/ betareq);
 Fmt(s,"Target Beta: %f deg. Hit any key to accept reading.",betareq);
 GrfMsg(s,14);
 flag=1;
 while (flag)
   {
   while (!(keyhit()))
     {
     beta=/*tunnel_alpha()*/ betareq;
     GrfNumeric(hand[BetaPort],beta);
```

```
      }
    Fmt(s,"Target Beta: %f deg. VERIFY: Accept beta?",betareq);
    GrfMsg(s,12);
    q=getkey();
    q=getkey();
    if ((q==89)||(q==121))
      {
       flag=0;
      }
    else
      {
      GrfMsg("Hit any key to accept reading.",14);
      }
    }
  GrfMsg("",2);
}

void sub_setRe(Rereq)

double Rereq;

{
 double Re;
 int q,flag;
 char s[80];

 GrfNumeric(hand[RePort],tunnel_Re (L));
 Fmt(s,"Target Re: %f . VERIFY: Accept Re?",Rereq);
 GrfMsg(s,14);
 flag=1;
 while (flag)
   {
   while (!(keyhit()))
      {
      GrfNumeric(hand[RePort],tunnel_Re (L));
      }
    GrfMsg(s,12);
    q=getkey();
    q=getkey();
    if ((q==89)||(q==121))
      {
       flag=0;
      }
    else
      {
      GrfMsg(s,14);
      }
    }
  GrfMsg("",2);
}
```

```
void sub_setVR(VRreq)

double VRreq;

{
 double VR;
 int q,flag;
 char s[80];

 GrfNumeric(hand[JetPort+3],sub_jetVR());
 Fmt(s,"Target VR: %f . VERIFY: Accept VR?",VRreq);
 GrfMsg(s,14);
 flag=1;
 while (flag)
  {
   while (!(keyhit()))
     {
     GrfNumeric(hand[JetPort+3],sub_jetVR());
     }
   GrfMsg(s,12);
   q=getkey();
   q=getkey();
   if ((q==89)||(q==121))
     {
     flag=0;
     }
   else
     {
     GrfMsg(s,14);
     }
   }
  GrfMsg("",2);
}
void sub_setCmu(Cmureq)

double Cmureq;

{
 double Cmu;
 int q,flag;

 GrfNumeric(hand[JetPort+4],sub_jetCmu());
 GrfMsg("Hit any key to accept reading.",14);
 flag=1;
 while (flag)
  {
   while (!(keyhit()))
     {
     GrfNumeric(hand[JetPort+4],sub_jetCmu());
     }
   GrfMsg("VERIFY: Accept Cmu?",12);
```

```
    q=getkey();
    q=getkey();
    if ((q==89)||(q==121))
      {
       flag=0;
      }
    else
      {
      GrfMsg("Hit any key to accept reading.",14);
      }
   }
  GrfMsg("",2);
}
```

jetvrswp.c

This program was used to take the jet force and moment data for different θ, β and VR.

```
#include      "C:\lw\include\lwsystem.h"
#include      "C:\lw\include\gpib.h"
#include      "C:\lw\include\formatio.h"
#include      "C:\lw\include\graphics.h"
#include      "C:\LW\INSTR\tunnel.h"       /* Tunnel Instruments */
#include      "C:\LW\INSTR\sub.h"          /* sub */

/* This program sweeps through beta and theta. VG Fins. */
/* it uses VRreq as the constant jet parameter.        */

double F[6][4][7][7],CF[6][4][7][7],theta[7],beta[4],VRreq[7];

char string[80],des[80];
int sub_ch[39],sub_numservo,sub_config;
double sub_servoslope,sub_servooffset;
int hand[18];
int tunnel_err,tunnel_balid,tunnel_sweeps;
double tunnel_T[6],tunnel_F[6],tunnel_CF[6];
double tunnel_calvolt[8],tunnel_calalpha[8];
int hp3455a_err,hp3495a_err;

main()
{
 int i,j,k,l,numtheta,numbeta,numVR,raw,red,tare;
 double q,T,p,Re,Uinf,Vj,Tj,VR,Cmu,Pj;
 char *msg,*res;
 char *Fname[6];

 msg="                                                    ";
 res="                                          ";
 Fname[0]="Axial    (X)";
 Fname[1]="Normal   (Y)";
 Fname[2]="Vertical (Z)";
```

```
Fname[3]="Roll    (L)";
Fname[4]="Pitch   (M)";
Fname[5]="Yaw     (N)";

theta[0]=45.0;        beta[0]=0.0;
theta[1]=60.0;        beta[1]=5.0;
theta[2]=75.0;        beta[2]=10.0;
theta[3]=90.0;        beta[3]=15.0;
theta[4]=105.0;
theta[5]=120.0;
theta[6]=135.0;
numtheta=7;           numbeta=4;

VRreq[0]=0.0;
VRreq[1]=0.5;
VRreq[2]=1.0;
VRreq[3]=1.5;
VRreq[4]=2.0;
VRreq[5]=2.5;
VRreq[6]=3.0;
numVR=7;

sub_setupmodel (jet);
sub_setupgraphics ();

raw=0;
while (raw<=0)
  {
   sub_vidinput("Enter data filename prefix: ",msg);
   Fmt(res,"c:\\lw\\data\\%s.raw",msg);
   raw=OpenFile(res,2,1,1);
   Fmt(res,"c:\\lw\\data\\%s.red",msg);
   red=OpenFile(res,2,1,1);
   Fmt(res,"c:\\lw\\data\\%s.tar",msg);
   tare=OpenFile(res,2,1,1);
   }
sub_vidinput("Enter a description: ",des);
FmtFile(raw,"%s : %s\n\n",datestr(),des);
FmtFile(red,"%s : %s\n\n",datestr(),des);
FmtFile(tare,"%s : %s\n\n",datestr(),des);

/* File Header. */
FmtFile(raw,"UNITS:\n");
FmtFile(raw,"All pressures are in psi.\n");
FmtFile(raw,"All velocities are in ft/s.\n");
FmtFile(raw,"All temperatures are in ϕR.\n");
FmtFile(raw,"All forces are in lbs. \n");
FmtFile(raw,"All angles are in degrees. \n\n");

FmtFile(raw,
```

```
"\n%s[w11] %s[w11] %s[w11] %s[w11] %s[w11] %s[w11] %s[w11] %s[w11] %s[w11]
%s[w11] %s[w11] %s[w11] %s[w11]\n",
    "β   ","θ   ","X   ","Y   ","Z   ","L   ","M   ","N   ",
    "T   ","P   ","q   ","Time   ","Pj   ","Tj   ");

FmtFile(red,
"\n%s[w11] %s[w11] %s[w11] %s[w11] %s[w11] %s[w11] %s[w11] %s[w11] %s[w11]
%s[w11] %s[w11] %s[w11]\n",
    "β   ","θ   ","Cx   ","Cy   ","Cz   ","Cl   ","Cm   ","Cn   ","Uinf ","Vj   ","VRj  ","Cmuj ","Re  ");

for(j=0;j<numtheta;j++)
  {
  Fmt(msg,"Set theta to %f degrees, then hit any key.",theta[j]);
  GrfMsg(msg,4);
  getkey();

  for(i=0;i<numbeta;i++)
   {
   GrfMsg("Turn off tunnel to take data. Hit any key to continue.",4);
   getkey();
   Fmt(msg,"Set beta to %f degrees, then hit any key.",beta[i]);
   GrfMsg(msg,4);
   getkey();
   sub_setbeta (beta[i]);

   GrfMsg("Hit any Key to Take Tares.",4);
   getkey();
   GrfMsg("Taking Tares...",4);
   tunnel_tare ();
   GrfMsg("Done Taking Tares. Hit a key to view tares.",4);
   getkey();
   FmtFile(tare,"%f[w11e2p3] %f[w11e2p3] ",beta[i],theta[j]);
   FmtFile(tare,"TARES:\n");
   for(k=0;k<6;k++)
     {
     Fmt(msg,"%s tare: %f lbs. Hit any key.",Fname[k],tunnel_T[k]);
     GrfMsg(msg,4);
     FmtFile(tare,"%s tare: %f lbs.\n",Fname[k],tunnel_T[k]);
     getkey();
     RemovePlots(hand[k]);
     }

   GrfMsg("Ready to take data.  Turn on tunnel, then hit a key.",4);
   getkey();

   for(l=0;l<numVR;l++)
     {
     sub_setRe (4600000.0);
     sub_setVR (VRreq[l]);
     GrfMsg("Taking data...",4);
     tunnel_FandM ();
```

```
      q=tunnel_q ();
      T=tunnel_temp();
      p=tunnel_p();
      Re=tunnel_Re(cref);
      Uinf=tunnel_uinf();
      Vj=sub_jetspeed();
      Tj=sub_jettemp();
      Pj=sub_jetpres();
      VR=sub_jetVR();
      Cmu=sub_jetCmu();
      updateflow();
      GrfMsg("Done Taking Data. Turn off tunnel.",4);
      getkey();

      F[0][i][j][l]=-(tunnel_F[1]-tunnel_T[1]);
      F[1][i][j][l]=-(tunnel_F[0]-tunnel_T[0]);
      F[2][i][j][l]=-(tunnel_F[5]-tunnel_T[5]);
      F[3][i][j][l]=tunnel_F[3]-tunnel_T[3];
      F[4][i][j][l]=tunnel_F[4]-tunnel_T[4];
      F[5][i][j][l]=-(tunnel_F[2]-tunnel_T[2]);
      for(k=0;k<6;k++)
        {
        CF[k][i][j][l]=F[k][i][j][l]/q/Sref/144.0;
        if ((k==3)||(k==5))
          {
          CF[k][i][j][l]/=bref;
          }
        else if (k==4)
          {
          CF[k][i][j][l]/=cref;
          }
        SetActivePort(hand[k]);
        GrfCurv2D(VRreq,CF[k][i][j],l+1);
        }
      getkey();

      FmtFile(raw,
    "%f[w11e2p3] %f[w11e2p3] %f[w11e2p3] %f[w11e2p3] %f[w11e2p3] %f[w11e2p3] %f[w11e2p3]
%f[w11e2p3] %f[w11e2p3] "
    "%f[w11e2p3] %f[w11e2p3] %s[w11] %f[w11e2p3] %f[w11e2p3]\n",
        beta[i],theta[j],F[0][i][j][l],F[1][i][j][l],F[2][i][j][l],F[3][i][j][l],F[4][i][j][l],F[5][i][j][l],
        T,p,q,timestr(),Pj,Tj);

      FmtFile(red,
    "%f[w11e2p3] %f[w11e2p3] %f[w11e2p3] %f[w11e2p3] %f[w11e2p3] %f[w11e2p3] %f[w11e2p3]
%f[w11e2p3] %f[w11e2p3] "
    "%f[w11e2p3] %f[w11e2p3] %f[w11e2p3] %f[w11e2p3]\n",
        beta[i],theta[j],CF[0][i][j][l],CF[1][i][j][l],CF[2][i][j][l],CF[3][i][j][l],CF[4][i][j][l],CF[5][i][j][l],
        Uinf,Vj,VR,Cmu,Re);

    } /* Next VR*/
```

```
    FmtFile(raw,"\n");
    FmtFile(red,"\n");
    FmtFile(tare,"\n");

   } /* Next Beta */

  FmtFile(raw,"\n");
  FmtFile(red,"\n");
  FmtFile(tare,"\n");

  } /* Next Theta */

 CloseFile(raw);
 CloseFile(red);
 CloseFile(tare);

}
```

finbtswp.c

This program was used to get the fin forces and moments for different θ and β.

```
#include      "C:\lw\include\lwsystem.h"
#include      "C:\lw\include\gpib.h"
#include      "C:\lw\include\formatio.h"
#include      "C:\lw\include\graphics.h"
#include      "C:\LW\INSTR\tunnel.h"       /* Tunnel Instruments */
#include      "C:\LW\INSTR\sub.h"          /* sub */

/* This program sweeps through beta and theta. VG Fins. */
/* it uses VRreq as the constant jet parameter.       */

double F[6][7][7],CF[6][7][7],theta[7],beta[7];

char string[80],des[80];
int sub_config;
int hand[18];
int tunnel_err,tunnel_balid,tunnel_sweeps;
double tunnel_T[6],tunnel_F[6],tunnel_CF[6];
double tunnel_calvolt[8],tunnel_calalpha[8];
int hp3455a_err,hp3495a_err;

main()
{
 int i,j,k,numtheta,numbeta,raw,red,tare;
 double q,T,p,Re,Uinf;
 char *msg,*res;
 char *Fname[6];
```

```
msg="                                                    ";
res="                                          ";
Fname[0]="Axial    (X)";
Fname[1]="Normal   (Y)";
Fname[2]="Vertical (Z)";
Fname[3]="Roll     (L)";
Fname[4]="Pitch    (M)";
Fname[5]="Yaw      (N)";

theta[0]=75.0;        beta[0]=0.0;
theta[1]=60.0;        beta[1]=2.5;
theta[2]=45.0;        beta[2]=5.0;
theta[3]=30.0;        beta[3]=7.5;
theta[4]=15.0;        beta[4]=10.0;
                  beta[5]=12.5;
                  beta[6]=15.0;
numtheta=5;           numbeta=7;

sub_setupmodel (fin);
sub_setupgraphics ();

raw=0;
while (raw<=0)
  {
   sub_vidinput("Enter data filename prefix: ",msg);
   Fmt(res,"c:\\lw\\data\\%s.raw",msg);
   raw=OpenFile(res,2,1,1);
   Fmt(res,"c:\\lw\\data\\%s.red",msg);
   red=OpenFile(res,2,1,1);
   Fmt(res,"c:\\lw\\data\\%s.tar",msg);
   tare=OpenFile(res,2,1,1);
  }
sub_vidinput("Enter a description: ",des);
FmtFile(raw,"%s : %s\n\n",datestr(),des);
FmtFile(red,"%s : %s\n\n",datestr(),des);
FmtFile(tare,"%s : %s\n\n",datestr(),des);

/* File Header. */
FmtFile(raw,"UNITS:\n");
FmtFile(raw,"All pressures are in psi.\n");
FmtFile(raw,"All velocities are in ft/s.\n");
FmtFile(raw,"All temperatures are in ϕR.\n");
FmtFile(raw,"All forces are in lbs. \n");
FmtFile(raw,"All angles are in degrees. \n\n");

FmtFile(raw,
"\n%s[w11] %s[w11] %s[w11] %s[w11] %s[w11] %s[w11] %s[w11] %s[w11] %s[w11] %s[w11]
%s[w11] %s[w11]\n",
    "β   ","θ   ","X   ","Y   ","Z   ","L   ","M   ","N   ",
    "T   ","P   ","q   ","Time   ");
```

```
FmtFile(red,
"\n%s[w11] %s[w11] %s[w11] %s[w11] %s[w11] %s[w11] %s[w11] %s[w11] %s[w11]\n",
    "β   ","θ   ","Cx   ","Cy   ","Cz   ","Cl   ","Cm   ","Cn   ","Uinf ","Re  ");

for(j=0;j<numtheta;j++)
 {
 Fmt(msg,"Set theta to %f degrees, then hit any key.",theta[j]);
 GrfMsg(msg,4);
 getkey();

 for(i=0;i<numbeta;i++)
  {
  GrfMsg("Turn off tunnel to take data. Hit any key to continue.",4);
  getkey();
  Fmt(msg,"Set beta to %f degrees, then hit any key.",beta[i]);
  GrfMsg(msg,4);
  getkey();
  sub_setbeta (beta[i]);

  GrfMsg("Hit any Key to Take Tares.",4);
  getkey();
  GrfMsg("Taking Tares...",4);
  tunnel_tare ();
  GrfMsg("Done Taking Tares. Hit a key to view tares.",4);
  getkey();
  FmtFile(tare,"%f[w11e2p3] %f[w11e2p3] ",beta[i],theta[j]);
  FmtFile(tare,"TARES:\n");
  for(k=0;k<6;k++)
    {
    Fmt(msg,"%s tare: %f lbs. Hit any key.",Fname[k],tunnel_T[k]);
    GrfMsg(msg,4);
    FmtFile(tare,"%s tare: %f lbs.\n",Fname[k],tunnel_T[k]);
    getkey();
    RemovePlots(hand[k]);
    }

  GrfMsg("Ready to take data.  Turn on tunnel, then hit a key.",4);
  getkey();

  sub_setRe (6800000.0);
  GrfMsg("Taking data...",4);
  tunnel_FandM ();
  q=tunnel_q ();
  T=tunnel_temp();
  p=tunnel_p();
  Re=tunnel_Re(cref);
  Uinf=tunnel_uinf();
  updateflow();
  GrfMsg("Done Taking Data. Turn off tunnel.",4);
  getkey();
```

```
    F[0][j][i]=-(tunnel_F[1]-tunnel_T[1]);
    F[1][j][i]=-(tunnel_F[0]-tunnel_T[0]);
    F[2][j][i]=-(tunnel_F[5]-tunnel_T[5]);
    F[3][j][i]=tunnel_F[3]-tunnel_T[3];
    F[4][j][i]=tunnel_F[4]-tunnel_T[4];
    F[5][j][i]=-(tunnel_F[2]-tunnel_T[2]);
    for(k=0;k<6;k++)
      {
      CF[k][j][i]=F[k][j][i]/q/cref/cref;
      if ((k==3)||(k==5)||(k==4))
        {
        CF[k][j][i]/=cref;
        }
      SetActivePort(hand[k]);
      GrfCurv2D(beta,CF[k][j],i+1);
      }
    getkey();

      FmtFile(raw,
    "%f[w11e2p3] %f[w11e2p3] %f[w11e2p3] %f[w11e2p3] %f[w11e2p3] %f[w11e2p3] %f[w11e2p3]
%f[w11e2p3] %f[w11e2p3] "
    "%f[w11e2p3] %f[w11e2p3] %s[w11]\n",
        beta[i],theta[j],F[0][j][i],F[1][j][i],F[2][j][i],F[3][j][i],F[4][j][i],F[5][j][i],
        T,p,q,timestr());

      FmtFile(red,
    "%f[w11e2p3] %f[w11e2p3] %f[w11e2p3] %f[w11e2p3] %f[w11e2p3] %f[w11e2p3] %f[w11e2p3]
%f[w11e2p3] %f[w11e2p3] "
    "%f[w11e2p3]\n",
        beta[i],theta[j],CF[0][j][i],CF[1][j][i],CF[2][j][i],CF[3][j][i],CF[4][j][i],CF[5][j][i],
        Uinf,Re);


   } /* Next Beta */

  FmtFile(raw,"\n");
  FmtFile(red,"\n");
  FmtFile(tare,"\n");

  } /* Next Theta */

 CloseFile(raw);
 CloseFile(red);
 CloseFile(tare);

}
```

finnum.c

This program was used to collect the forces and moments versus number of fins for Series 2.

```
#include      "C:\lw\include\lwsystem.h"
#include      "C:\lw\include\gpib.h"
#include      "C:\lw\include\formatio.h"
#include      "C:\lw\include\graphics.h"
#include      "C:\LW\INSTR\tunnel.h"       /* Tunnel Instruments */
#include      "C:\LW\INSTR\sub.h"          /* sub */

/* This program sweeps through number of fins        */

double F[6][19],CF[6][19],num[19];

char string[80],des[80];
int sub_config;
int hand[18];
int tunnel_err,tunnel_balid,tunnel_sweeps;
double tunnel_T[6],tunnel_F[6],tunnel_CF[6];
double tunnel_calvolt[8],tunnel_calalpha[8];
int hp3455a_err,hp3495a_err;

main()
{
 int i,j,k,numnum,raw,red,tare;
 double q,T,p,Re,Uinf;
 char *msg,*res;
 char *Fname[6];

 msg="                                                    ";
 res="                                          ";
 Fname[0]="Axial   (X)";
 Fname[1]="Normal  (Y)";
 Fname[2]="Vertical (Z)";
 Fname[3]="Roll    (L)";
 Fname[4]="Pitch   (M)";
 Fname[5]="Yaw     (N)";

 num[0]=36;
 num[1]=34;
 num[2]=32;
 num[3]=30;
 num[4]=28;
 num[5]=26;
 num[6]=24;
 num[7]=22;
 num[8]=20;
 num[9]=18;
 num[10]=16;
 num[11]=14;
```

```
num[12]=12;
num[13]=11;
num[14]=10;
num[15]=8;
num[16]=6;
num[17]=4;
num[18]=2;

numnum=19;

sub_setupmodel (fin);
sub_setupgraphics ();

raw=0;
while (raw<=0)
  {
   sub_vidinput("Enter data filename prefix: ",msg);
   Fmt(res,"c:\\lw\\data\\%s.raw",msg);
   raw=OpenFile(res,2,1,1);
   Fmt(res,"c:\\lw\\data\\%s.red",msg);
   red=OpenFile(res,2,1,1);
   Fmt(res,"c:\\lw\\data\\%s.tar",msg);
   tare=OpenFile(res,2,1,1);
  }
sub_vidinput("Enter a description: ",des);
FmtFile(raw,"%s : %s\n\n",datestr(),des);
FmtFile(red,"%s : %s\n\n",datestr(),des);
FmtFile(tare,"%s : %s\n\n",datestr(),des);

/* File Header. */
FmtFile(raw,"UNITS:\n");
FmtFile(raw,"All pressures are in psi.\n");
FmtFile(raw,"All velocities are in ft/s.\n");
FmtFile(raw,"All temperatures are in ϕR.\n");
FmtFile(raw,"All forces are in lbs. \n");
FmtFile(raw,"All angles are in degrees. \n\n");

FmtFile(raw,
"\n%s[w11] %s[w11] %s[w11] %s[w11] %s[w11] %s[w11] %s[w11] %s[w11] %s[w11]
%s[w11] %s[w11]\n",
    "β   ","num ","X   ","Y   ","Z   ","L   ","M   ","N   ",
    "T   ","P   ","q   ","Time   ");

FmtFile(red,
"\n%s[w11] %s[w11] %s[w11] %s[w11] %s[w11] %s[w11] %s[w11] %s[w11] %s[w11]\n",
    "β   ","num ","Cx   ","Cy   ","Cz   ","Cl   ","Cm   ","Cn   ","Uinf ","Re  ");

GrfMsg("Turn off tunnel to take data. Hit any key to continue.",4);
getkey();
Fmt(msg,"Set beta to %f degrees, then hit any key.",15.0);
GrfMsg(msg,4);
```

```
getkey();
sub_setbeta (15.0);

GrfMsg("Hit any Key to Take Tares.",4);
getkey();
GrfMsg("Taking Tares...",4);
tunnel_tare ();
GrfMsg("Done Taking Tares. Hit a key to view tares.",4);
getkey();
FmtFile(tare,"%f[w11e2p3] %f[w11e2p3] ",15.0,55.0);
FmtFile(tare,"TARES:\n");
for(k=0;k<6;k++)
  {
  Fmt(msg,"%s tare: %f lbs. Hit any key.",Fname[k],tunnel_T[k]);
  GrfMsg(msg,4);
  FmtFile(tare,"%s tare: %f lbs.\n",Fname[k],tunnel_T[k]);
  getkey();
  RemovePlots(hand[k]);
  }

for(j=0;j<numnum;j++)
  {
  Fmt(msg,"Set number of fins to %f , then hit any key.",num[j]);
  GrfMsg(msg,4);
  getkey();

  GrfMsg("Ready to take data.  Turn on tunnel, then hit a key.",4);
  getkey();

  sub_setRe (6800000.0);
  GrfMsg("Taking data...",4);
  tunnel_FandM ();
  q=tunnel_q ();
  T=tunnel_temp();
  p=tunnel_p();
  Re=tunnel_Re(cref);
  Uinf=tunnel_uinf();
  updateflow();
  GrfMsg("Done Taking Data. Turn off tunnel.",4);
  getkey();

  F[0][j]=-(tunnel_F[1]-tunnel_T[1]);
  F[1][j]=-(tunnel_F[0]-tunnel_T[0]);
  F[2][j]=-(tunnel_F[5]-tunnel_T[5]);
  F[3][j]=tunnel_F[3]-tunnel_T[3];
  F[4][j]=tunnel_F[4]-tunnel_T[4];
  F[5][j]=-(tunnel_F[2]-tunnel_T[2]);
  for(k=0;k<6;k++)
    {
    CF[k][j]=F[k][j]/q/cref/cref;
    if ((k==3)||(k==5)||(k==4))
```

```
        {
        CF[k][j]/=cref;
        }
      SetActivePort(hand[k]);
      GrfCurv2D(num,CF[k],j+1);
      }
     getkey();

       FmtFile(raw,
     "%f[w11e2p3] %f[w11e2p3] %f[w11e2p3] %f[w11e2p3] %f[w11e2p3] %f[w11e2p3] %f[w11e2p3]
%f[w11e2p3] %f[w11e2p3] "
     "%f[w11e2p3] %f[w11e2p3] %s[w11]\n",
          15.0,num[j],F[0][j],F[1][j],F[2][j],F[3][j],F[4][j],F[5][j],
          T,p,q,timestr());

       FmtFile(red,
     "%f[w11e2p3] %f[w11e2p3] %f[w11e2p3] %f[w11e2p3] %f[w11e2p3] %f[w11e2p3] %f[w11e2p3]
%f[w11e2p3] %f[w11e2p3] "
     "%f[w11e2p3]\n",
          15.0,num[j],CF[0][j],CF[1][j],CF[2][j],CF[3][j],CF[4][j],CF[5][j],
          Uinf,Re);


    } /* Next Beta */

   FmtFile(raw,"\n");
   FmtFile(red,"\n");
   FmtFile(tare,"\n");

  CloseFile(raw);
  CloseFile(red);
  CloseFile(tare);

}
```

Vita

Todd Wetzel was born April 20, 1971, to Mr. Richard A. and Mrs. Janice E. Wetzel. He pursued a Bachelor of Science degree in Aerospace Engineering at Virginia Polytechnic Institute and State University, Blacksburg, Virginia, which he completed in May of 1992. He then entered graduate school in the Aerospace Engineering Department at Virginia Tech with the eventual goal of completing a Ph.D. in the field.